Electromagnetic Micropower generation - System Design and Analyses

A thesis submitted in fulfilment of the requirements for the degree of Master of engineering

Nibras Awaja
Bachelor of Engineering (Electrical & Electronic Engineering)

School of Electrical and Computer Engineering
Science, Engineering and Technology Portfolio
RMIT University

April 2010

Declaration

I certify that except where due acknowledgement has been made, the work is that of the author alone; the work has not been submitted previously, in whole or in part, to qualify for any other academic award; the content of the thesis is the result of work which has been carried out since the official commencement date of the approved research program; and, any editorial work, paid or unpaid, carried out by a third party is acknowledged.

Nibras Awaja

To Laith, Yousif and Ayser

Acknowledgements

I would like to thank my supervisor Prof. Andrew Jennings for providing me with the opportunity to conduct my MEng. Special thanks to Prof. Dinesh Sood for his support and guidance.

My thanks are also extended to RMIT University for giving me such a wonderful research environment and financial support. I would like to acknowledge the technical staff of the School of Electrical and Computer Engineering, Mr. Sinisa , Mr. Ivan Kiss and Mr. Chao for their great assistance. I also would like to thank Mr Peter Dale from the applied sciences for his great assistance in supplying vibration measurement equipments and his great technical support.

Thanks and appreciation to my colleague Simon Mutzenich, for his friendship and support. I would like to sincerely thank Sawsan, Nadia and Zuraini for their advice and encouragement.

I would like to thank my brother Firas Awaja for his unbelievable encouragement and academic support.

I am ever grateful to my parents Sahib and Fakhrea, my sister Eynas and my brother Mohannd for their constant love, confidence in me and caring of me and my family.

My most heart felt gratitude goes to my husband, Laith Al-Mashat for his understanding and unlimited support. For his support and partnership I will be always in debt.

I thank my wonderful children, Yousif and Ayser for their love and patience during my study.

Table of contents

List of figures

List of Tables

Abstract

Over the past few years, there has been a huge reduction in size and power consumption of MEMS devices like transducers and sensors. These devices are usually designed to run on batteries the replacement of batteries is not practical. The limited lifespan of batteries may induce costly maintenance, in the case of contaminated areas for instance. Moreover, batteries dying without warning cause serious problems in safety monitoring applications. That led to a surge of research in the area of energy harvesting. Sustainable power generation may be achieved in converting ambient energy into electrical energy. Some possible ambient energy sources are, for instance, thermal energy, light energy and mechanical energy. After an extensive survey of potential energy harvesting methods, the conversion of ambient vibrations to electricity was chosen as a method for further research. Since mechanical vibrations exist in most systems, many works focused on vibration-driven generators. In this field, the electromagnetic induction is well suited for the mechanical to electrical energy conversion. The design of the mechanical system that transmits the surrounding vibratory energy to the electromagnetic generator is a critical importance.

This thesis presents an optimization of an electromagnetic microgenerator. It describes the theory, design and simulation of an energy converter based on electromagnetic induction. The objectives of this research are designing, improving the performance and operational reliability of electromagnetic microgenerator. These have been achieved by identifying the desirable design features of the electromagnetic microgenerator. Extensive analytical investigation has been conducted to develop an efficient design of an electromagnetic microgenerator. An analytical model is developed and then used as a basis for optimization. Numerical analyses using Mat Lab software investigate the optimum design parameters to get maximum power output.

This thesis deals with the design and simulation of a number of flat springs to be used for supporting the moving magnet of an electromagnetic microgenerator. The flat spring and moving magnet are equivalent to a basic spring-mass system, in which the moving magnet is attached to a platform suspended by four beams. The theoretical models of such a beam-mass system are given to estimate its static and dynamic characteristics. These flat springs were designed by modelling and finite element method simulation using ANSYS 5.7. This helped in understanding the critical aspects of the design at the same time leading to the determination of the optimum parameters for the flat springs, such as static deflection, spring constant, resonant frequency, and dynamic range. A series of structural and vibration analyses were carried out using ANSYS to evaluate the flat spring characteristics and to choose the desirable mode of vibration.

Finite element method is also used for the analysis, evaluation and optimization of the electromagnetic design of the electromagnetic microgenerator. The objectives behind this analysis are to characterize the permanent magnet and to investigate the optimum position of the coil relative to the magnet. Output power is estimated using the ANSYS simulation results of the magnetic field induced on the coil. It is also found that the magnetic field of the permanent magnet in the vertical direction is higher in magnitude than the magnetic field in the horizontal direction. A coil model was mainly to calculate the length of wire, number of turns and coil resistance. Estimated power was calculated for different distance between the coil and the permanent magnet.

The methodology and findings in this research provided a number of contributing elements to the field of MEMS power generation, and provided an insight into the development of an

electromagnetic microgenerator. This thesis is concluded with a discussion on the performance of the proposed electromagnetic microgenerator and suggestions for further research.

Chapter 1. Introduction

1.1 Power MEMS

The advancements made in fabrication and micromachining techniques have enhanced the functionality of MEMS devices, which is one of the key reasons for the emergence of sustainable power sources. Power MEMS is one of the newest categories of MEMS, which encompasses microdevices and microsystems for power generation and energy conversion. The research and development of power MEMS have been promoted by the need for compact power sources with high energy and power density. Power MEMS has expanded to include not only various MEMS-based power generators but also small energy machines and microdevices for macro power generators. As various devices and systems, such as energy harvesting microdevices were presented in the literature. Their power levels vary from ten nanowatts to ten of microwatts.

1.2 Research Motivation

In the past few years the need for developing self-powered wireless sensing systems has increased. Wireless sensor networks are made of large numbers of small, low-cost sensor nodes working in collaboration to collect data and transmit them to a base station via a wireless network. Wireless sensing systems could potentially be used for a wide variety of applications. A few possible applications include: monitoring temperature, light, chemical pollution in big cities, and acceleration and pressure in vehicles. The power consumption of the wireless sensor network is 100μW for a lifetime [Vullers et.al., 2009]. Powering remote sensing systems becomes a problem due to the difficulty of battery replacement and the cost of wiring power to them. Therefore, many researchers focused on energy harvesting from the environment. In the field of MEMS power generation, electromagnetic, piezoelectric and electrostatic generators have been developed .Vibration-driven generators were very attractive due to the availability of the

vibration energy in the environment. This thesis is focused on using the principle of electromagnetic induction for the generation of electrical power from low frequency vibration in the environment (like vibration from bridges). Cantilevers have been used as a moving element in most generators to get a linear movement. The electromagnetic generator can be classified as a moving coil, moving magnet, micromachined or macro sized assembled generators. To the best of the author's knowledge there was no focus on the reduction of the parasitic damping of the generators to increase the power level. Therefore, the motivation in this thesis is to design an efficient power source with low damping ratio through the design of a compact suspension system.

1.3 Objectives of the thesis

The aim of this research is to investigate the methodology for designing and fabricating electromagnetic micropower generating devices at microlevel. Such micro generating device can be used to power wireless sensors network in remote or difficult to access applications.

This research consists of:

- Reviewing the literature about power generation for MEMS with particular emphasize on the principles of electromagnetic conversion devices at micro level.
- Describing the design of a new electromagnetic micropower generating device. This has been achieved by: (1) investigating and optimizing the mechanical and electrical properties of the materials employed. These properties have a direct effect on each part of the design. For example in the case of a spring design, material type and its properties limit the spring displacement which is needed to be as large as possible within the device volume, (2) Selecting patterns for each component in the design . The spring pattern

should be selected with low damping ratio, and (3) Using standard simulation software (ANSYS) to build the design.

- Developing an analytical model to carry a numerical analyses investigation for the optimum microgenerator design parameters.
- Developing an analytical finite element models for mechanical and magnetic characterization to optimize (comparison of a few flat spring designs and selecting the best) the proposed electromagnetic microgenerator.

1.4 Publications arising from this work

1. **Nibras Awaja**, Dinesh Sood, and Thurai Vinay, Design and Analyses of Electromagnetic Microgenerator, Sensors & Transducers Journal, Vol. 103, Issue 4, April 2009, pp. 109-121.
2. **Nibras Awaja**, and Thurai Vinay, Finite element analyses of a flat spring for use in an electromagnetic microgenerator, Sensors & Transducers Journal, Vol.107, Issue 8, August 2009,pp. 119-132.
3. **Nibras Awaja**, Zuraini Dahari, Thurai. Vinay and Dinesh Sood, Analytical Study of an Electromagnetic Micro- generator Based on Vibration to Electricity Conversion, in Proceedings of APCOT (Asia-Pacific Conference of Transducers and Micro-NanoTechnology), Singapore, 2006.
4. **Nibras Awaja**, Dinesh Sood, and Thurai Vinay, Modeling and simulation of a flat spring for use in an electromagnetic microgenerator, Smart Structures, Devices, and Systems II,Proceedings of SPIE Vol. 5649 ,361-372 ,2005.

1.5 Publications siting this research

Pei-Hong Wanga, Xu-Han Daia, Dong-Ming Fanga, and Xiao-Lin Zhaoa, Design, fabrication and performance of a new vibration- based electromagnetic micro power generator, Microelectronics Journal 38 (2007) 1175–1180

1.6 Thesis outline

Chapter 2, reviews the literature on the existing power sources particular for MEMS devices, with the focus on electromagnetic induction. Detailed descriptions of the ongoing research on electromagnetic microgenerators are given. The electromagnetic microgenerators that have been reported in the literature are broadly classified as the moving magnet, the moving coil type and or the spring type. A general vibration to electricity model, provided by Williams and Yates (Williams and Yates 1995), is presented and discussed. The major steps to improve the electromagnetic microgenerator are presented. Designs of the compact suspension system are presented. The design objectives and specifications of the flat spring to be used in the electromagnetic micro generator are discussed. A brief literature about the permanent magnet material selection and the coil configuration are given.

Chapter 3 presents the results of a study undertaken to characterize low-level vibrations from a small motor. This study aims to maximize the potential applicability of the electromagnetic microgenerator. Chapter 3 also presents an extensive analytical investigation to develop an efficient design of an electromagnetic microgenerator. A number of issues associated with the design of the microgenerator are addressed. A description of the basic operating principles of the electromagnetic microgenerator is presented. An analytical model is used for parametric study, optimization and reliability analysis of the microgenerator.

Chapter 4 presents details of the mechanical analyses performed on the proposed electromagnetic microgenerator. The basic theory of the static modelling of the micromechanical structures is presented. The key design parameters such as static deflection, spring constant, resonant frequency, and dynamic range are investigated. A linear analytical model is developed for the flat spring with deferent beam configurations. ANSYS finite element analysis software was used. A series of structural and vibration analyses were carried out using ANSYS to evaluate the flat spring characteristics. If the spring has movements in horizontal direction with rotation, rather than in vertical direction relative to the coil, the generator then will have more movements and it produces more power.

Chapter 5 provides details of the magnetic analyses performed on the proposed electromagnetic microgenerator. The objectives behind this are to characterize the permanent magnet and to investigate the optimum position of the coil relative to the magnet. An analytical model of the coil is reviewed. The coil dimensions are set according to the analytical model to be used for the magnetic analyses. The results were obtained using the finite element package ANSYS 2D for static magnetic simulation. Finite element model is developed for the electromagnetic microgenerator. Initially finite element analyses (FEA) of the permanent magnet and the coil are undertaken separately.

Chapter 6 summarizes the research outcomes. Useful conclusions drawn from the work carried out in this thesis are discussed and directions for future research are suggested.

Chapter 2: Literature review and background

2.1 Introduction

In this chapter, a review of the literature on the existing power sources that are applicable to MEMS devices is given. The basic principles of operation and the efficiency of the devices that convert the ambient energy to electricity are reviewed. Vibrations to electricity conversion devices are presented. Detailed descriptions of the ongoing research on electromagnetic microgenerator are given. The operating principles, the advantages and disadvantage of the various electromagnetic microgenerator designs that have been reported in the literature are discussed through a comparative study. A general model of the electromagnetic microgenerator is presented. A brief background about the history of the flat spring is given and a discussion the spring design objectives and considerations to be used in the electromagnetic microgenerator is provided. These points are important to help with the design later in chapter 4. A brief literature about the permanent magnet material selection and the coil configuration is given.

2.2 Overview of the existing power sources for MEMS

Most MEMS devices generally utilize macroscopic power sources and they greatly limit the main advantage of size reduction of MEMS devices. Batteries are commonly used for powering MEMS, however, they exhibit short lifetime, limited power storage and large weight and size in comparison with the device they power. Also chemicals contained in the batteries may be toxic. Moreover, in some applications the battery replacement is an expensive and difficult process or may be inconvenient for devices that are implanted in human patients like medical sensors. Therefore, spectacular efforts have been made by researchers to find alternative power supplies to cover the drawbacks of using batteries in MEMS applications. Some of these supplies can be specially designed to convert the ambient energy in the environment into electrical power.

2.2.1 Solar energy conversion

An abundant source of ambient energy is solar energy. A solar cell is a device that produces electrical energy directly from solar radiation. The power density of the solar radiation is about 1.4 kw/m^2 [Roundy et.al., 2003] and it changes slightly during the year by no more than 0.1%. The solar cells are fabricated from single crystal, polycrystalline and amorphous silicon. The basic device requirements of a solar cell are an electronic asymmetry, such as a p-n junction. When illuminated, photo generated electron-hole pairs are generated throughout the solar cell. If the cell is connected to a load, current will flow from one region of the cell, through the load, and back to the other region of the cell. Solar self powered devices such as calculator and watches are commonplace. Lee et al. [Lee, 2001] developed a thin solar cell that is specifically designed to produce the open circuit voltages which is required to supply MEMS electrostatic actuators. The array consists of 100 single solar cells connected in series, occupying a total area of only 1cm^3. Connecting the array to micro-mirror, a microsystem is produced that respond to the modulation of the applied light.

The efficiency of the solar cell varies from outdoor to indoor environments, depending on the light intensity and the differences of the incident light angle in both conditions. The efficiency is about 10-20 % and it depends on the silicon crystal type. A typical single crystal silicon PV cell of 100 cm^2 could produce about 1.5 watts of power at 0.5 volts DC and 3 amps under full summer sunlight. The power output of the cell is approximately proportional to the intensity of the sunlight. For example, if the intensity of the sunlight is halved the power will also be halved. This type of power generation is limited to the applications with access to light.

2.2.2 Thermal energy conversion

Temperature differences can also provide an ambient energy exploited to generate power. Thermoelectric generators are devices used to convert thermal energy directly to electrical

energy. Such devices are based on thermoelectric effects involving interactions between the flow of heat and of electricity through solid bodies. A typical thermoelectric module consists of an array of semiconductor pellets that have been “doped” so that one type of charge carrier– either positive or negative– carries the majority of current. The pairs of P/N pellets are configured so that they are connected electrically in series, but thermally in parallel. When a temperature gradient is created across the thermoelectric device, a DC voltage develops across the terminals. When a load is properly connected, electrical current flows. Starner [Starner, 1996] calculates the amount of energy that could be extracted from the skin temperature of a human being. The temperature difference between the skin and the surrounding atmosphere drives a flow of heat energy that could be captured. Using a simple model, Starner predicts that 2.4-4.8W of electrical power could be obtained if the entire body surface were covered. Stordeur and Stark [Stordeur and Stark, 1997] have presented a thermoelectric microgenerator based on thermocouples and it manly developed to MEMS powering. The device produces 20μW at temperature deference of 20K and it is capable to supply sufficiently microsystems.

The output power of the thermoelectric microgenerator has been developed by the improvement of the thermoelectronics [Castano et.al, 1997; Jacquot et.al. , 2002; Li et.al., 2003]. However, thermoelectric power generation still is considered as a low output power method and restricted by the temperature differences available.

2.2.3 Vibration energy conversion

Mechanical energy associated with the low amplitude vibration in the environment is another source of ambient energy that can be converted to electrical power. Low amplitude vibration is present in structures such us tall buildings, bridges, vehicles and industrial mechanics. The main design concept of the vibration based generator utilizes the free vibration available in the environment to produce movement and convert this movement of a suspended mass into

electrical power by an electromagnetic induction [Williams et.al., 1996; Shearwood et.al.,1997; Williams et.al, 2001; Amarithajah and Chandrakasan,1998; Amirtharajah R., 1999; Amirtharajah et.at.,2000; El-hami et.al., 2001; Ching et.al., 2002; Mizuno and Chetwynd, 2003; Kulah H. and Najafi K, 2004; Glynne-Jons et. al., 2004; Awaja et.al.,2005; Koukharenko et.al.,2006; Pan et.al., 2006; Wang et. al.,2007; Serre et. al.,2008; Saha et. al.,2008; Sari et. al.,2008; Kulkarni et. al.,2008] or piezoelectric material [Umeda et.al.,1997;Glynne-jones et.al.,2000 ; Ottman et.al.,2003] or an electrostatic material [Meninger et.al.,2001 ; Roundy S et.al.,2003]. More broad details about the vibration to electricity conversion generators will be presented in section 2.2. With the focus on electromagnetic to electricity conversion as it is the intention of this research.

2.2.4 Human body energy

Human body energy like breath movement, blood flow, walking, finger movement on a keyboard and body heat can be feasibly extracted and converted to electric power. Starner, and Shenck et.al. [Starner, 1996 and Shenck and Paradiso., 2001] examine the possibility of scavenging passive energy used and wasted by the human body for use by wearable electronic devices. They found that the highest power level was generated from human walking. The amount of power was about 5-8W. The conclusion of this research has led to the development of piezoelectric shoe inserts. The power density available from the shoe inserts can be useful for computing and communication devices. However, the issue of how to get the energy from the shoes to other places of the body still needs to be solved.

2.2.5 Gravitational fields

Seiko Kinetics wrist watch invented by Hayakawa [Hayakawa, 1991] is an example of converting the gravitational energy to electric energy. The ac generator works by connecting a weight with

an eccentric centre of rotation to a speed increasing gear train. As the wrist is moved, the centre of mass of the weight is raised relative to the axle. Gravity causes the weight to rotate until the centre of the mass again lies at its lowest position. The gear train supplies rotation to a dynamo at an increased rate of rotation. Power of 200 μW was estimated based on a weight of 2 grams falling through 1cm once a second.

2.3 Vibration to electricity conversion generators

2.3.1 Piezoelectric generators

A recent technique for generating power from vibration was presented by Glynne-jones et.al. and White et.al., [Glynne-jones et.al., 2001;White and Wenzel,2001]. A device is developed that consists of a thick-film piezoelectric layer (peizoceramic lead zirconate titanate, PZT) deposited on to a thin steel beam. As the beam oscillates and begins to resonate, the piezoelectric layer deforms. This deformation causes charge to be displaced across electrodes positioned on the top and bottom surfaces of the piezoelectric element. The resulting potential deference can be exploited to produce electrical energy. The device is designed to be easy to model rather than to be optimal for power generation. The size of the device is 23x10x0.2 mm. Initial results show that the prototype can generate up to 3 μW of power at 90Hz. However, order of magnitude improvements are shown to be possible by varying the material systems.

An optimal circuitry design for piezoelectric generator was published by Ottman et.al. [Ottman et.al., 2002; Ottman et.al., 2003]. The focus of their work has been on the optimal design of the power conditioning electronics for a piezoelectric generator driven by vibration. The circuit consists of an ac-dc rectifier with an output capacitor, an electrochemical battery, and a switch-mode dc-dc converter that controls the energy flow into the battery. The maximum power output

reported is 18 mw. The size of the piezoelectric converter is 19cm^2 at a driving vibration of 53.8 Hz.

Umeda et.al. [Umeda et.al., 1997] consider a different approach. Rather than having a resonant system, they examine the power that is generated when a steel ball strikes a piezoelectric membrane. It has been reported that a demonstrator was produced that supplied enough energy to power a digital watch unit when shaken up and down by hand.

The piezoelectric generators directly convert the vibration into a voltage output by using an electroded piezoelectric material. There is no requirement for having complex geometries. However, the piezoelectric materials are required to be strained directly and therefore their mechanical properties will limit the overall performance and lifetime. Also the transduction efficiency is ultimately limited by piezoelectric properties of materials employed.

The disadvantage of piezoelectric conversion is the difficulty of implementation on the micro-scale and integration with microelectronics. While it is true that piezoelectric thin films can be integrated into MEMS processing [Lee and White, 1995], the piezoelectric coupling is greatly reduced [Verardi et al, 1997]. Therefore, the potential for integration with microelectronics is less than that for electrostatic converters

2.3.2 Electrostatic generators

The electrostatic generator designed by Meninger et.al. and Roundy et.al. [Meninger et.al., 2001 and Roundy et.al.,2003] is based on converting of ambient mechanical vibration into electrical energy by using MEMS variable capacitor. By placing charge on the capacitor plates, the voltage will increase as the capacitance decreases. If the voltage is placed on the capacitor, charge will move from the capacitor as the capacitance decreases. In both cases, mechanical energy is converted into electrical energy which can be stored and utilized by a load.

The major problem associated with capacitive converters is that some method must be employed to hold the voltage, across the MEMS device, constant during the conversion process, which requires a separate voltage source. It is also not capable of converting sufficient power per unit volume. The maximum predicted output power from electrostatic generator is 8 μW. The output impedance of the devices is often very high and this makes them less suitable as a power supply. The output voltage produced by the devices is relatively high (>100 V) and often results in a limited current-supplying capability; this can lead to the requirement for custom circuit implementation processes for the realization of challenging circuit designs. Parasitic capacitances within the structure can sometimes lead to reduced generator efficiency and there is risk of capacitor electrodes shorting or of 'stiction' in wafer-scale implementations.

2.3.3 Electromagnetic microgenerators

Extracting electric power from vibration by electromagnetic induction has the interest of a group from Sheffield University [Williams et.al, 1996; Shearwood et.al., 1997; Williams et.al, 2001]. They have published an analysis of the vibration-based electromagnetic microgenerator. An electromagnetic micro generator is an inertial device that is anchored at one end and free at the other end. The microgenerator model consisting of a moving spring (k), rare earth permanent magnet, the mass of the spring (m) and an electrical coil represented by the dashpot (d) [Williams et.al, 1996]. The magnet is attached to the spring to form the spring mass system. When the generator is vibrating the magnet will move towards the electric coil. As a result, electric power will be induced across the coil according to Faraday's law of induction. The input to the generator is the vibration displacement, y (t) and this vibration produces a movement of the mass, x (t). The generator has the dimensions of 5x5x1mm and generates a maximum power of 0.3mW at an excitation of 4MHz. The generator was fabricated using GaAs bulk micromachining [Shearwood et.al.,1997]. It has two wafers bonded together with epoxy, the upper one is used to

form the mass spring system and the lower is used to pattern the coil. Samarium-cobalt permanent magnet is used in order to form the inertial mass. The magnet has a feature size of 1x1x0.3mm. A 2.5mm polyimide membrane is used to form the spring part and it has holes to allow vacuum operation. The polyimide membrane is chosen due to its robustness, ease of fabrication and possibility of large deflection. A planar gold coil is fabricated on the second wafer and joined to the spring-mass wafer. The coil fabricated by metallization and lift-off and form a 13 turn with a thickness of 2.5 μm. A square cavity was defined on the rear of the coil wafer to accommodate the movement of the magnet. Sheffield group report the maximum power for this generator but they did not report the output voltage. The input vibration was quite high in the range of 500nm over a frequency range of 4.4 kHz. This means that the generator works only in a very special environment with very high frequency and is not reliable in a common low frequency environment such as commonly found in buildings.

Another design of electromagnetic microgenerator is developed by a group of researchers [Amarithajah and Chandrakasan, 1998; Amirtharajah R., 1999; Amirtharajah et.al., 2000]. The generator is in a macro size and designed to work from vibrations induced by human walking, and is predicted to produce 400 μW of power from 2cm movement at frequency of 2Hz. The generator that consists of a wire coil l attached to a mass m connected to a spring k. The other end of the spring is attached to a rigid housing. A permanent magnet B is attached to the housing. As the housing is vibrated, the mass moves relative to the housing and energy is stored in the mass spring system. The moving coil through the field of a permanent magnet cuts the varying amount of magnetic flux, which in turn induces a voltage on the coil according to Faraday's Law of induction. Their simulation and measured result of the output voltage showed significant differences. The device was designed to have maximum power of 400 μW under ideal conditions without mechanical losses. The vibration source was 2cm and 2Hz to estimate the human

walking for their model. As they reported the measured output voltage which was 180mV, they did not report the output power. However, 180mV was still too small for their application and they needed a transformer to rectify the voltage and this one can vary both the electrical and mechanical parameters.

El-hami et.al.[El-hami et.al., 2001] presented a generator consisting of a magnetic core mounted at the tip of a planar steel beam. The design utilizes an electromagnetic transducer and its operating principal is based on the relative movement of a magnet pole with respect to a coil. As the device is vibrated, the resonant beam oscillates back and forth, moving past a coil of a few turns. The results show an output power of 0.53mW with an input vibration of amplitude 25 μm, and frequency 322Hz. Excluding the clamp at the base of the beam and the coil mounting, the device requires a volume of $0.24cm^{3.}$ It is clearly shown that device size is not in micro level and micromachining techniques were not used in its construction.

Ching et.al [Ching et.al., 2002] has developed a generator similar to the preposed generator by Li et al. [Li et.al., 2000]. It is micromachined generator that comprises a permanent magnet mounted on a laser-micromachined spiral spring structure next to PCB coil. A laser system was used to micromachined the resonating copper springs. The spring is designed to let the mass vibrate horizontally while the input vibration is applied vertically, and that this horizontal vibration increases the output voltage of the generator. This can be explained by faraday's law of induction which stated that the voltage output should be proportional to the rate of changing magnetic flux. The generator have an improved spiral spring resulted on a peak to peak output voltage of up to 4.4V and a maximum power of 830μw when driven by 200μm displacement at its resonant frequency of 110Hz. The generator total volume is $1cm^3$.

Another type of resonant microgenerator is described by Mizuno and Chetwynd [Mizuno and Chetwynd, 2003]. The proposed device comprises a beam with an integrated coil and a fixed

external magnet. The dimensions of the silicon cantilever beam were 500 μm × 100 μm × 20 μm and the size of the NdFeB magnet was 30 mm × 10 mm × 6 mm. The resonant frequency of the structure was 58 kHz. A power output of only 6 nW was predicted for a typical single-element electromagnetic microgenerator. The magnitude of the output voltage was estimated as being only 1.4mV. The authors fabricated a larger version of their proposed device for evaluation purposes. The actual size of the beam was increased to 25 mm × 10 mm × 1mmand the resulting resonant frequency was 700 Hz. For an input vibration of 0.64 μm, the output power was found to be 0.4nW. As a result of the low output power, the authors suggest that electromagnetic generators do not offer practical solutions for energy harvesting problems. They may have reached a different conclusion if they had chosen to evaluate a moving magnet approach as the additional seismic mass would have increased the electrical power available.

Kulah and Najafi [Kulah H.and Najafi K, 2004] describe a silicon-based generator, which comprises two separate chips combined together. Their device utilizes two resonant structures that are designed to achieve mechanical up-frequency conversion. The authors argue that because most silicon structures have relatively high resonant frequencies (several kHz) and a majority of ambient vibration frequencies are less 100 Hz, then a device that can perform mechanical up-frequency conversion will provide an efficient solution to energy harvesting problems. To demonstrate this, they have fabricated a silicon generator that has an upper diaphragm with a resonant frequency of 25 Hz. An NdFeB magnet on the upper diaphragm is used to excite a lower structure into resonance through magnetic attraction. The lower diaphragm has a resonant frequency of around 11 kHz. Integrated coils are fabricated on the lower structure. The authors quote the theoretical maximum power generated as being 2.5 μW, but they only measured 4nW from a millimetre-scale device. The level of input mechanical excitation is not quoted in the paper.

Glynne-jones et. al. [Glynne-jones et. al., 2004] present experimental results obtained from prototypes fabricated using batch micromachining and hand assembly with different magnet configurations. They followed the work of El-hami et.al.[El-hami et.al., 2001]. The initial prototype was based on moving magnets and had an overall volume of 0.83cm^3. The second device was a moving four-magnet generator (with a fixed coil), having an overall volume of 3.15 cm^3. The first prototype generated power levels up to 180 μW, for a free end beam displacement of 0.85mm. The second prototype was aimed at improving the magnitude of the output voltage by improving the magnetic coupling between the magnets and coil. For the same input vibration, the second generator produced more than twice the output voltage and four times the instantaneous power. The authors present the results showing the response from a generator mounted on the engine block of a car. An instantaneous power of 4nw was measured during a journey of 1.24 Km and the average power found to be 157 μW.

Koukharenko et.al. [Koukharenko et.al., 2006] present a silicon microgenerator. The generator consists of a cantilever paddle, four magnets and a coil. The coil is recessed in a silicon cantilevered paddle designed to vibrate laterally in the plane of the wafer. Discrete magnets are positioned within etched recesses in capping wafers that are bonded to each face of the middle wafer. Three sets of supporting paddle beam dimensions have been simulated, each 1 mm long and 500 μm thick. In model A the beam is 500 μm wide, model B 400 μm wide and C 300 μm wide. The resonance frequencies for the beams were 9.812, 7.149, 4.743 respectively, and the output power was found to be 2, 1.45, and 0.96 accordingly. The coil used in the initial simulation is a conventionally wound enameled copper coil with 600 turns of 25 μm wire. The outer diameter of the coil is 2.4 mm and the inner diameter is 0.6 mm. The separation between magnets and coil is 0.1 mm. The resulting mass of the silicon paddle plus coil is measured to be 2.8×10^{-5}Kg. The magnets used were sintered NdFeB with dimensions of 1×1×3 mm. the results

from a model A cantilever generator with a beam width of 500 μm. This was found to have a resonant frequency of 9.5 kHz and generated 122 nW into a 100 X load with a Q-factor of approximately 200.

Another electromagnetic microgenerator has been proposed by Pan et.al. [Pan et.al., 2006]. They fabricate and analyse an electromagnetic microgenerator using MEMS technology. The generator consists of a FePt permanent magnet sputtered on a silicon membrane and Cu planner coil. The spring pattern is 100μm in width, 40 μm in thickness and 100 μm in gap. The dimensions of the coil have the thickness of 15 μm, line width of 30 μm and 50 turns. Maximum power was 100 and voltage of 40mv at a resonance frequency of 60Hz.

Wang et. al. [Wang et. al., 2007] presents an electromagnetic micro power generator fabricated using microelectromechanical systems technology. The microgenerator consists of a permanent magnet of NdFeB, a copper planar spring and a two-layer copper coil. The structure is composed of an upper resonant structure on silicon wafer and a lower two-layer copper coil on glass substrate. The resonant structure is a vertically polarized NdFeB permanent magnet attached to the centre of a copper planar spring which consists of four spring beams and a platform. When the magnet is vibrating, it will move towards the coil and cause the change of the magnetic flux in the coil. The generator can generate 60mV ac peak–peak with an input frequency of 121.25Hz and at input acceleration of 14.7m/s^2.

Serre et. al. [Serre et.al., 2008] present a design of an electromagnetic microgenerator by using a moving magnet on a polyimide film and a fixed planar coil made of aluminium layer. A generator prototype has been fabricated with a modular manufacturing process in which the coil, the magnet and the polyimide film are manufactured separately, diced and then assembled. The device produced a power of 200nw at a resonant frequency of 360Hz for a displacement of 6.8μm.

Saha et.al. [Saha et. al. ,2008] develop a generator consist of axially magnetized permanent magnets placed vertically inside a tube so that facing surfaces have the same polarization. Thus the magnets repel one another. Two magnets are fixed at both ends of the generator tube housing. The middle is free to move but is suspended between fixed end magnets in the generator housing due to the repulsive force. A coil is wrapped around the outside of the tube. When the tube is vibrated the middle magnet vibrates up and down, and a voltage will be induced in the coil. There is no mechanical beam in this generator and suspended moving magnet works as magnetic spring constant. The generator millimeter prototype consists of two opposite polarity circular magnets tightly glued to a 3mm thick magnetic pole piece. This combination was inserted into a hollow Teflon tube so that it can move freely. After inserting, the two opposite polarity magnets were fixed on the both ends of the Teflon tube and 40μm copper wire with 1000 turns coil was wrapped around the tube at a point midway between the ends of the tube. The prototype generators generated 0.3–2.46mW when placed inside a rucksack which was worn during walking and slow running.

Sari et.al. [Sari et.al., 2008] present a generator covering a wide band of external vibration frequency by implementing serially connected parylene cantilevers in different lengths resulting in an array of cantilevers with varying natural frequencies. The simulation results showed that by utilizing 40 cantilevers and a length increment of 3μm, a frequency band of 1 KHz could be covered with a maximum steady power output of 0.4μw and a maximum voltage output of 50mV. The tests show that by utilizing 35 cantilevers, the fabricated device generates 10mV voltage and 0.4 μw power continuously within a frequency band of 800Hz.

Kulkarni et. al.[Kulkarni et. al.,2008] present three different designs of power generators which are partially micro-fabricated and assembled. Prototype A having a wire-wound copper coil, Prototype B, an electrodeposited copper coil both on a deep reactive ion etched (DRIE) silicon

beam and paddle. Both devices have a volume of 106mm^3. Prototype C uses moving NdFeB magnets in between two micro-fabricated coils. The integrated coil, paddle and beam were fabricated using standard micro-electro-mechanical systems (MEMS) processing techniques. The device volume was 150mm^3. For Prototype A, the maximum measured power output was 148nW at 8.08 kHz resonant frequency and 3.9 m/s2 acceleration. For Prototype B, the microgenerator gave a maximum load power of 23nW for an acceleration of 9.8 m/s2, at a resonant frequency of 9.83 kHz. Prototype C generates a maximum load power of 586nW across 110Ω load at 60 Hz for an acceleration of 8.829 m/s2.

2.4 Classification of electromagnetic microgenerators and comparison of their performances

A comparison of the various electromagnetic microgenerator designs discussed in Section 2.3.3 is presented in Table 2.1 - 2.3. The electromagnetic generators can be classified according to their moving element part, coil and magnet shapes, input vibration and /or the device volume.

The electromagnet generators can be discretely assembled generators with macro scale high-performance bulk magnets and multi-turn coils or micromachined generators with micromachined magnets, a planar coils and micromachined springs. Also there are some generators which are partially micromachined. The micromachined generators may have low output power and voltage compared to the assembled generators, due to the relatively poor properties of magnet, the limitations on the number of turns of the micro coil and the restricted .

Ref.(Year)	Moving element shape / material	Coil shape / material	Magnet shape / material	Resonance frequency (Hz)	Amplitude (ms^{-2})	Power (μw)	Device volume	Device features
shearwood et.al, (1997)	Circular/ Polyimide membrane	Gold (Au) planar coil	SmCo	440		0.3	$5\times5\times1$ mm^3	Moving magnet / micromachined device
Amarithajah and Chandrakasan (1998)		Wire coil		2		400 (simulated results)		Moving coil / discrete components/ o/p voltage =180mV
El-hami et.al. (2001)	Planar steel cantilever beam	Wire copper coil	NdFeB pole	322	25	530	240 mm^3	Moving magnet / Not a micromachined device
Ching et.al. (2002)	Laser micromachined spiral copper spring	PCB coil		110	200	830	1 cm^3	Moving magnet / same as Li et.al device/ spring vibrate horizontally with rotation
Mizuno and Chetwynd (2003)	Silicon cantilever	Integrated coil	NdFeB	58000 simulated results / 700	0.64	6nw simulated results / 0.4nw	2.1 cm^3	Moving coil

Table 2.1 Comparison of performance of various electromagnetic microgenerators

Ref. (Year)	Moving element shape / material	Coil shape / material	Magnet shape / material	Resonance frequency (Hz)	Amplitude (ms^{-2})	Power (μw)	Device volume	Device features
Kulah and Najafi (2004)	Silicon Diaphragm	Integrated coil	NdFeB	25, 11000		2.5 (simulated), 4nw	4 cm^3, 2 cm^3	Moving magnet
Glynne-Jones et.al .(2004)	Cantilever beam	Wound coil	NdFeB	322	2.7	180	0.84 cm^3	Moving magnet / partially micromachined device
Koukharenko et.al.(2006)	Silicon cantilever paddle	Wire wound coil	Four magnet of NdFeB	1615		104nw	100 mm^3	Moving coil/ micromachined device
Pan et.al.(2006)	Silicon membrane	Cu planner coil	Sputtered (FePt) magnet	60		100	0.45 cm^3	Moving magnet/microm achined gen.
Wang et. al.(2007)	Copper spring	2-layers copper coil	NdFeB	121.25	1.47			Moving magnet

Table 2.2 Comparison of performance of various electromagnetic microgenerators (continued)

Ref.(Year)	Moving element shape / material	Coil shape / material	Magnet shape / material	Resonance frequency (Hz)	Amplitude (ms^{-2})	Power (μw)	Device volume	Device features
Serre et. .al (2008)	Polyimide film	Aluminum planner coil	NdFeB	360		200nw		Moving magnet
Saha et.al. (2008)	No mechanical beam	Wound coil		8	0.38	300 to 2.5mw	12.7 cm^3	Moving magnet / not a micromachined
Sari et.al. (2008)	Parylene Cantilever	Sputtered Ti/Au coil	NdFeB	800		0.4		Moving coil
Kulkarni et.al. (2008)	Silicon paddle	Wire wound copper coil	NdFeB	8080	3.9	148nw	106 mm^3	Moving coil/ partially micromachined
	Silicon paddle	Electroplated coil	NdFeB	9837	9.81	23nw	106 mm^3	Moving coil/ fully micromachined
	Copper beam	Integrated coil	NdFeB	60	8.829	584nw	150 mm^3	Moving magnet/ assembled

Table 2.3 Comparison of performance of various electromagnetic microgenerators (continued)

amplitude of vibration, but they also have the advantage of micro size for easy integration of sensing systems Tables 2.1-2.3 summarize the works reported by researchers on developing the electromagnetic microgenerator. Williams et. al. [Williams et. al., 1996] presented a model for an electromagnetic microgenerator. The model was either for moving magnet or moving coil. Williams et. al. [Williams et. al., 1996] also established the main rules to design an efficient generator. Shearwood et.al. [Shearwood et.al., 1997] fabricated a micromachined moving magnet generator for remote microsensors systems based on Williams's model. They use a polyimide membrane as a moving element. This kind of spring has non linear starching characteristics at high amplitude of vibration therefore; using patterned spring will increased the linear movement of the spring over a large displacement range and the air damping and then increased the output power. Amarithajah and Chandrakasan [Amarithajah and Chandrakasan, 1998] modelled a moving coil generator. In their model they did not specify the moving element. They report a low output voltage from a macro size generator fabricated by discrete components. Therefore, their generator needs to be attached to a transformer to rectify the output. As it stated by Williams et. al. [Williams et. al., 1996] the moving magnet generator design has an advantage over the moving coil one as it is simple to fabricate by avoiding making electrical connection to the mass. Ching et.al. 2002 [Ching et.al.,2002] fabricate a moving magnet generator. They were successful in developing a spiral spring design with low resonant frequency and vibration horizontally with rotation. So they can increase the power output from 10μw to 830μw, El-hami et.al. [El-hami et.al., 2001] developed a moving magnet generator with a steel cantilever beam and wire copper coil. The generator was improved later by adding more magnets poles [Glynne-Jones et.al., 2004], but this come to the disadvantage of increasing the overall size from 240mm^3 to 830mm^3. Mizuno and Chetwynd [Mizuno and Chetwynd, 2003] present a moving coil generator. They used a silicon cantilever as a moving magnet. Their device did not offer a high output power even

after they scaled up the design dimensions. So if they want to get more electrical power they have to use a design with a moving magnet to increase the seismic mass. Kulah and Najafi [Kulah and Najafi, 2004] developed a moving magnet silicon diaphragm generator. The output power was first estimated through simulation work and then the millimetre scale device was fabricated and tested. The diaphragm has a low resonance frequency because it has array of beams and then the electrical power will be increased according to Williams' design rules. . Koukharenko et.al.[Koukharenko et.al., 2006] present a moving coil generator. There was a difference between the measured and simulated resonant frequencies. The difference was due to the influence of the assembly process and the bonding of the enamelled copper wires along the beam or across the meander. It is also clear from the measured results that mechanical damping mechanisms are dominating. These undesirable damping effects need to be substantially reduced in order to achieve the predicted power levels. Pan et.al. [Pan et.al., 2006] designed a moving magnet generator. The generator was fabricated by micromachining technology and has the silicon membrane as a moving element. The amount of output power is high. Although the generator is a micromachined device, the size of the generator is still large. Wang et. al. [Wang et. al., 2007] present a moving magnet micromachined generator. They used an electroplated Cu plannar spring. The spring has a long beam due to its configuration which keeps the spring constant smaller and the amplitude of vibration bigger which makes the generator gives more power. Serre et. .al. [Serre et. .al., 2007] present a moving magnet generator. They produced low output power due to the limited movement and the parasitic damping of the polymer film. Fabricating the spring from material with low mechanical losses like silicon will reduce the damping and increase the output power and this was in agree with the rule design suggested by Wiiliams et.al.[Williams et.al.,1996]. Saha et.al. [Saha et.al., 2008] present a moving magnet generator with no mechanical spring. The device is fabricated by assembling discrete components. The size

is on millimetres. This device has high damping losses because the moving magnet is directly touches the tube surface. This device has a low resonance frequency which makes the generator give low output power because the out put power is proportional to the cub of the frequency as it reported by Wiliiams et.al [Wiliiams et.al., 1996]. Sari et.al. [Sari et.al., 2008] presented a moving coil generator. The generator is fabricated by micromachining technology. parylene is used in this device as a structural material of the spring. The parylene spring gives large deflections and this will give larger generated power output. Kulkarni et.al. [Kulkarni et.al., 2008] present three generators with moving magnet. The device has a low output power due to the low amplitude of vibration of the paddle and the beam. The low amplitude of vibration is due to high parasitic damping.

The objective of the current research is to develop an efficient design of an electromagnetic microgenerator that can harvest a low amplitude of vibration and frequency and able to generate power enough for remote sensing systems around 100μw similar to the one proposed by Williams et. al. [Williams et. al., 1996]. Having considered the designs that have been reported in the literature to date, the author has come to the conclusion that the objective can be met only through a design that incorporates the following key features.

- Design a compact suspension system with low mechanical damping by using material with low mechanical hysteresis loss, such as Si.
- Design different spring configurations to get low natural frequency and low air damping with the aid of ANSYS modelling.
- Increasing the spring deflection and the linear movement by employing a cantilever spring. The spring should be designed so that the resonant frequency of the device matches the vibration frequency of the driving source.

- Increasing the electromagnetic coupling factor by increasing the magnetic flux density using higher remanence permanent magnet like NdFeB and making the magnet size as large as possible within the device size.
- Increasing the number of turns on the coil and that could be achieved by using narrower tracks in the planar coil or using 3D folded coil.

These key features for the proposed design will be used in Chapter 3, 4, and 5.

2.5 General model and design concept of an electromagnetic microgenerator

A simple model shown on the schematic diagram in Fig.2.1 has been proposed by Williams and Yates [Williams and Yates, 1995]. It is a general model for the conversion of the kinetic energy of the vibrating mass to electrical power based on linear system theory. It does not specify the mechanism by which the conversion takes place. The main design concept utilizes the free vibration available in the environment to produce movement and convert this movement of a suspended mass into electrical power by electromagnetic induction. The primary idea behind this model is that the conversion of energy from the oscillating mass to electricity looks like a linear damper to the mass spring system.

An electromagnetic micro generator is an inertial device that is anchored at one end and free at the other end. The system consists of a moving spring (k) supported by the housing, rare earth permanent magnet and the mass of the spring (m) and an electrical coil represented by the dashpot (d). The magnet is attached to the spring to form the spring-mass system. The model can be described by equation (2.1).

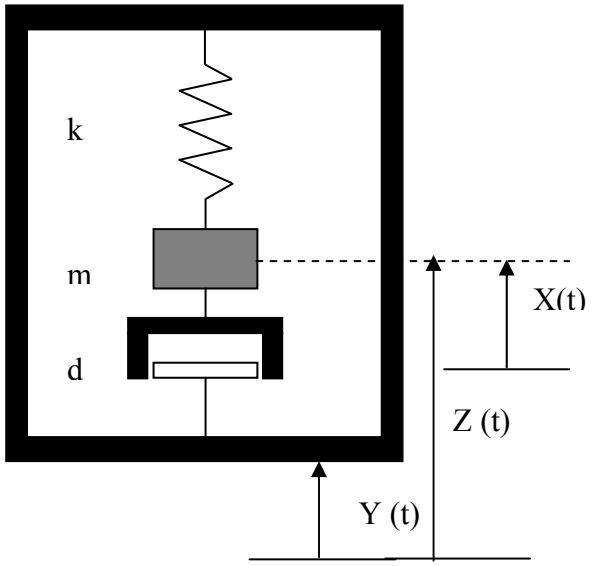

Fig.2.1 Schematic diagram of the vibration based microgenerator [Williams and Yates, 1995]

This design could be either for moving magnet or moving coil configuration. This is a fairly accurate model for certain types of electromagnetic converters like the one analysed by Williams and Yates [Williams and Yates, 1995] more than other types of converters like electrostatic and piezoelectric converters.

2.5.1 Steady state analysis

In order to determine and predict the practical performance of the device, steady state analysis has been undertaken. Consider the system in Fig.2.1 to consist of a point mass (m) mounted on the end of a beam providing a spring stiffness (K). The input to the generator is the vibration displacement, y (t) and this vibration produces a movement of the mass, x (t).

It can be assumed that the vibrating structure which is the source of mechanical energy is unaffected by the micro generator. The vibration frequency (ω) and vibration amplitude (Y_0) of

the source remain constant. The dynamic forces on the mass and its motion are described by applying Newton's Law of motion to the seismic mass:

$$m(\ddot{z}+\ddot{y}) = -kz - d\dot{z} \quad \text{..... (2.1)}$$

Where: z = spring deflection, y = input displacement, m = mass, d = damping coefficient,

k = spring constant.

The steady state response of the seismic mass to be,

$$z(t) = Z_0 \cos(\omega t - \phi) \quad \text{..... (2.2)}$$

Where

Z_0 is the vibration amplitude of the mass.

ω is the frequency of the driving vibrations.

ω = natural frequency of the mass spring system.

ϕ and Z_0 can be obtain from the equations (2.3) and (2.4)

$$\phi = \tan^{-1}\left(\frac{d\omega}{k - m\omega^2}\right) \quad \text{..... (2.3)}$$

$$Z_0 = \frac{m\omega^2}{\sqrt{\left(k - m\omega^2\right)^2 + \left(d\omega\right)^2}} Y_0 \quad \text{..... (2.4)}$$

$$= \frac{\frac{\omega^2}{\omega_n^2}}{\sqrt{\left(1 - \frac{\omega^2}{\omega_n^2}\right)^2 + \left(2\zeta\frac{\omega}{\omega_n}\right)^2}} Y_0 \quad \text{..... (2.5)}$$

Where $\omega_n = \sqrt{\frac{k}{m}}$ is the natural frequency, and $\zeta = \frac{d}{2\sqrt{mk}}$ the damping ratio of the seismic suspension.

The instantaneous mechanical power *p(t)* transferred from the source to the micro generator is given by,

$$p(t) = -\left[kz(t) + d\dot{z}(t)\right]\dot{y}(t) \quad \text{..... (2.6)}$$

$$= \left[kZ_0 \cos(\omega t - \phi) - \omega d Z_0 \sin(\omega t - \phi)\right]\omega Y_0 \sin \omega t \quad \text{..... (2.7)}$$

Integrating $p(t)$ over one complete cycle of vibration, we obtain the energy transferred during one cycle.

$$E_{Cycle} = \omega k Z_0 Y_0 \frac{\sin\phi}{2}\frac{2\pi}{\omega} - \omega^2 d Z_0 Y_0 \frac{\cos\phi}{2}\frac{2\pi}{\omega} \quad \text{..... (2.8)}$$

The average power is,

$$P_{average} = \omega k Z_0 Y_0 \frac{\sin\phi}{2} - \omega^2 d Z_0 Y_0 \frac{\cos\phi}{2} \quad \text{..... (2.9)}$$

By replacing Z_0 with its equivalent equation, the equation of power yields as below:

$$P_{average} = \frac{m Y_0^2 \zeta \frac{\omega^3}{\omega_n^3}\omega^3}{\left[\left(1 - \frac{\omega^2}{\omega_n^2}\right)^2 + \left(2\zeta\frac{\omega}{\omega_n}\right)^2\right]} \quad \text{..... (2.10)}$$

Equation (2.10) can be also written as:

$$\text{Power generated} = m Y_0^2 \omega^3 \left[\frac{\zeta r^3}{\left(1 - r^2\right)^2 + \left(2\zeta r\right)^2}\right] \quad \text{..... (2.11)}$$

Where $r = \frac{\omega}{\omega_n}$ is the ratio of source vibration frequency to micro generator natural frequency.

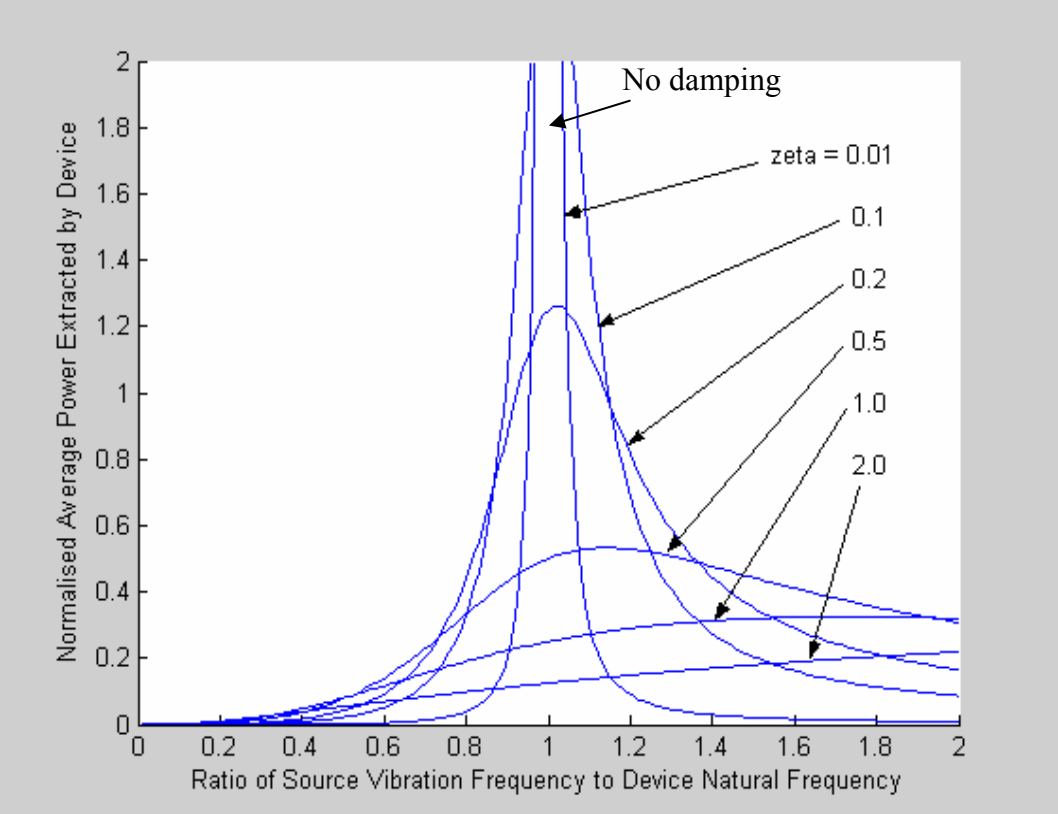

Fig 2.2 Average Power as a function of damping ratio and frequency ratio

Variation of the normalized average power, $\frac{P_{Average}}{mY_0^2\omega^3}$, as a function of the frequency ratio, *r*, for a range of values of ζ are shown in Fig. 2.2.

To maximize the power, the damping ratio should be very low and the natural frequency of the seismic suspension of the micro generator should be made equal to the frequency of vibration of the source. The damping factor controls the selectivity of the device. For applications where the frequencies of vibration are well defined and concentrated around one point, a low damping

factor would give more peaked response and increase power generation. Conversely, if the fundamental vibration frequency varies over time, a higher damping factor would be necessary to widen the bandwidth of the generator.

The following alternate expressions for the average power can also be obtained.

$$P_{Average} = mZ_0^2\omega^3\frac{\zeta}{r}$$

$$= \frac{1}{2}mY_0Z_0\omega^3 \quad \text{..... (2.12)}$$

Under resonance conditions, $z_0 = \frac{1}{2\zeta}y_0$, so the average equation can be formed as follows:

$$P_{\max} = \frac{mY_0^{\,2}\omega^3}{4\zeta} \quad \text{..... (2.13)}$$

The main fact gained from the steady state analysis is that the amount of power generated is proportional to the cube of the vibration frequency. This means that the generator will produce much more power in applications where there is a fairly high frequency of vibration, and low power at low frequencies.

2.5.2 Power generated in the electrical load

The maximum open circuit voltage across the coil is given by equation

$$V_{oc} = NBlz\dot{x}(t) \quad \text{..... (2.14)}$$

Where N is the number of turns in the coil, B is the strength of the magnetic field, l is the length of one coil ($2\pi r$), and z is the maximum distance of the magnet.

The voltage, e_c and current, i_c, generated within the system can be described by the following equations:

$$e_c = S\dot{x}(t) - i_c(R_c + jwL_c) \quad \text{(2.15)}$$

$$f_e = Si_c \quad \text{(2.16)}$$

Where f_e is the electromagnetic force generated by the electromechanical coupling, R_c and L_c are the resistance and inductance of the coil, respectively and the transformation factor S is:

$$S = NBl \quad \text{(2.17)}$$

If the current is driving a load of resistance R_L, the electrically generated force will be

$$f_e = \frac{S^2\dot{x}(t)}{R_L + R_c + jwL_c} \quad \text{(2.18)}$$

Hence the power converted to the electrical system is equal to the power removed from the mechanical system by d_e, the electrically induced damping. The electrically induced force is

$$f_e = d_e\dot{x}(t) \quad \text{(2.19)}$$

Then the electrically damping coefficient, d_e, will be:

$$d_e = \frac{S^2}{R_L + R_c + jwL_c} \quad \text{(2.20)}$$

Replacing the damping coefficients d_e the unitless damping ratios ζ_e according to the relationship $d_e = 2m\zeta\omega_n$ yields the following expression:

$$\zeta_e = \frac{de}{2mw_n} = \frac{S^2}{2mw_n(R_L + R_c + j\omega L_c)} \quad \text{(2.21)}$$

Maximum power is produced by the generator at resonance, which is the situation of most interest. At resonance, the impedance of the mass, spring and the coil inductance become infinite. The electrical generated damping ratio will be

$$\zeta_e = \frac{S^2}{2mw_n(R_L + R_c)} \quad \text{..... (2.22)}$$

Operating the device at resonance, where $\omega = \omega_n$ and substituting from equation (2.10) into equation (2.22) gives the power delivered to the load as:

$$P = \frac{Y_0^2 \omega^2 S^2}{8\zeta_T{}^2 (R_L + R_c)} \quad \text{..... (2.23)}$$

Where, ζ_T = combined damping ratio ($\zeta_T = \zeta_e + \zeta_m$)

And, ζ_m= mechanical damping ratio.

There is an equivalent electrically induced damping ratio, ζ_e, and the power output is maximized when that damping ratio is equal to the mechanical damping ζ_m in the system. Furthermore, it is better for ζ_e to be larger than ζ_m, rather than smaller than ζ_m. As shown in equation (2.23), P is a function of R, and can therefore be controlled by the selection of the load resistance.

2.5.3 Electromagnetic microgenerator design rules

The general guidelines for electromagnetic design that increase the output power can be formed (as stated by Williams et.al.[Williams et.al., 1996]) with more focus on the design of an electromagnetic generator at the micro level and more highlight on the spring and the magnetic

circuit as they are very critical points in term of the design. The design rules of an electromagnetic microgenerator are as follows:

- Characterize the load (remote wireless sensor).
- Characterize the input vibrations (frequency and amplitude).
- The seismic mass should be as large as possible within the available micro level volume of the device. The output power is proportional to the proof mass. This is obvious from the expression for power in equation (2.10).
- The maximum displacement of the seismic mass should be as large as possible in the space available. Employing a cantilever spring would result in increased linear movement, especially if a meandering spring design is employed.
- Estimate the power potential from the vibrations using the power expression given in equation (2.10). Determine how much volume, or mass, is necessary to supply the power needed for the load.
- Mechanical damping is a dominant limiting factor in the electromagnetic microgenerator and significant improvements in power output may be obtained through better spring linearity and vacuum operation.
- The spring should be designed so that the resonant frequency of the device matches the vibration frequency of the source. A meandering cantilever would allow the stiffness of the spring to be reduced, to get lower resonant frequencies, as the reduction in resonant frequency would result in a larger device.
- Increasing the electromagnetic coupling (S) which is proportional to the product of magnetic flux density and number of turns on the pick up coil, would also greatly improve the output. There is some scope for increasing the magnetic flux density by using a higher

remanence (The magnetization left behind in a medium after an external magnetic field is removed) permanent magnet, although the magnet is as large as practical for the size of the device. However, the number of turns on the coil could be increased significantly. This could be achieved either by using narrower tracks to increase the number of turns in the coil, which would require a corresponding increase in the thickness of the trucks to keep the coil resistance low, or by fabricating a multi-turn coil .

- The electrical load should be chosen so that the resulting amplitude of vibration of the seismic mass equals its limiting value (note that under resonance conditions, $z_0 = \frac{1}{2\zeta} y_0$).

2.6 Compact suspension system

Silicon micro beam mass structures are mechanical structures where linear elastic theory is generally applicable. However, to fabricate and use them as a functional system against a set design of specifications is extremely complicated due to their small sizes and the difficulties of using traditional mechanical performance and diagnostic methods [Bryzek et.al., 1994]. Finite Element-Analysis (FEA) CAD systems with sophisticated mechanical modelling capabilities allow designers to quantitatively predict the effects of process variations, and the optimise device performance. Thus, it has been a widely used tool in the design and modelling of mechanical structures. There are several commercially available software packages such as ANSYS, NASTRAN, COSMOS, and ABAQUS. A number of groups have reported the application of FEA for modelling the static and dynamic characteristics of microstructures [Tschan and Rooij,1991; Burrer et.al.,1993; Pures and Lapadatu,1994; Shearwood et.al.,1995; Gendron,1997 ; Vujanic et.al.,2000; Park et.al., 2002; Bhushan and Agrawal,2003].

2.6.1 Designs of the silicon flat spring in the literature

Silicon micromechanical structures with beam and mass have been utilised in micro sensors for almost two decades [Middelhoek and Audet, 1989]. Fig.2.3 shows the earliest silicon beam mass structures which was developed by Roylance and Angell [Roylance and Angell ,1979]. The beam mass structure is used in the design of the accelerometer. The silicon beam structure was a very thin cantilever beam surrounded by 2mmx3mmx200 μm thick rim which provided a rigid support for one end of the beam; a proof –mass was attached to the free end of the beam.

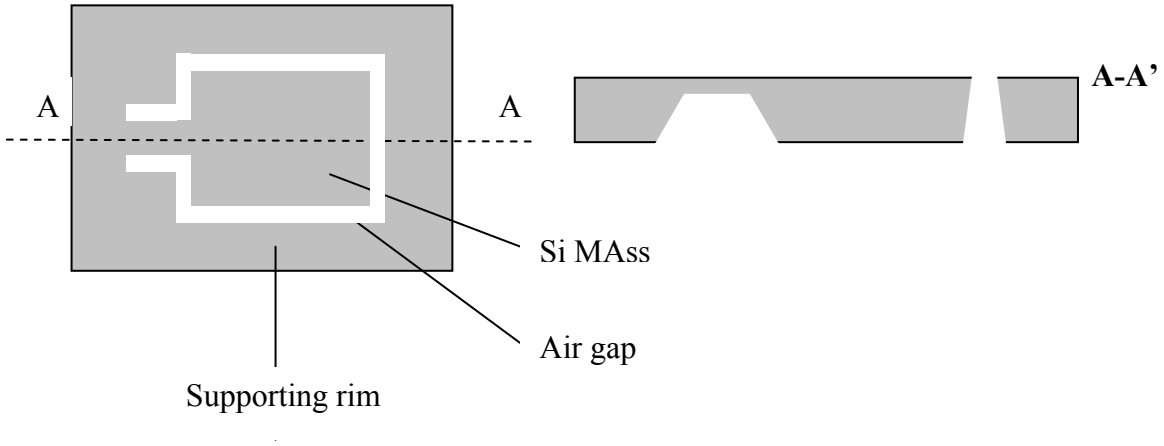

Fig.2.3Cantilever beam mass structure for accelerometer application [Roylance and Angell ,1979].

Tschan and Rooij [Tschan and Rooij ,1991] reported the characterisation and modelling of three different designs of beam-mass structures for piezoresistive accelerometer. Four and two beam

bridges and cantilever beams are shown in Fig.2.4 FEA were employed for the modelling of their vibration modes.

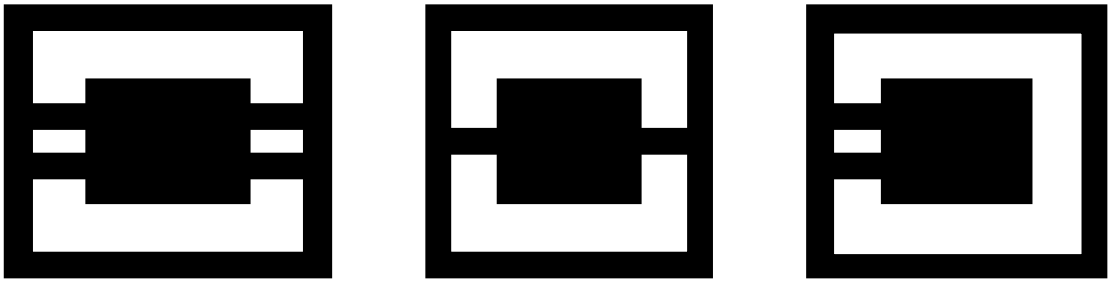

Four-beam bridge two beam bridge cantilever beam

Fig.2.4 Design of beam-mass structures [Tschan and Rooij ,1991].

The FEA of these designs revealed that the beam thickness is the most critical parameter among the structure dimensions; for example, a small variation of 0.5 μm was shown to change the sensitivity by 12% and the resonant frequency by 9%. The cantilever is the most sensitive structure, but its second and third modes are very easy to excite. For the four-beam bridge structure, the second mode is harder to excite when the distances between the two bridges are widened; consequently, the sensitivity along the y axis decreases. The opposite case occurs when the two bridges are brought together to form the two-beam bridge structure. Thus, the four-beam design is preferred over its two-beam counterpart due to its lower cross-axis sensitivity.

Puers and Lapadatu [Puers and Lapadatu ,1994] carried out an investigation of the characteristics of various beam mass structures as a suspension system. As shown in Fig.2.5, four different structures were proposed in their comparative study using FEA. The dimensions of the mass and the thickness of the beams are same for each structure.

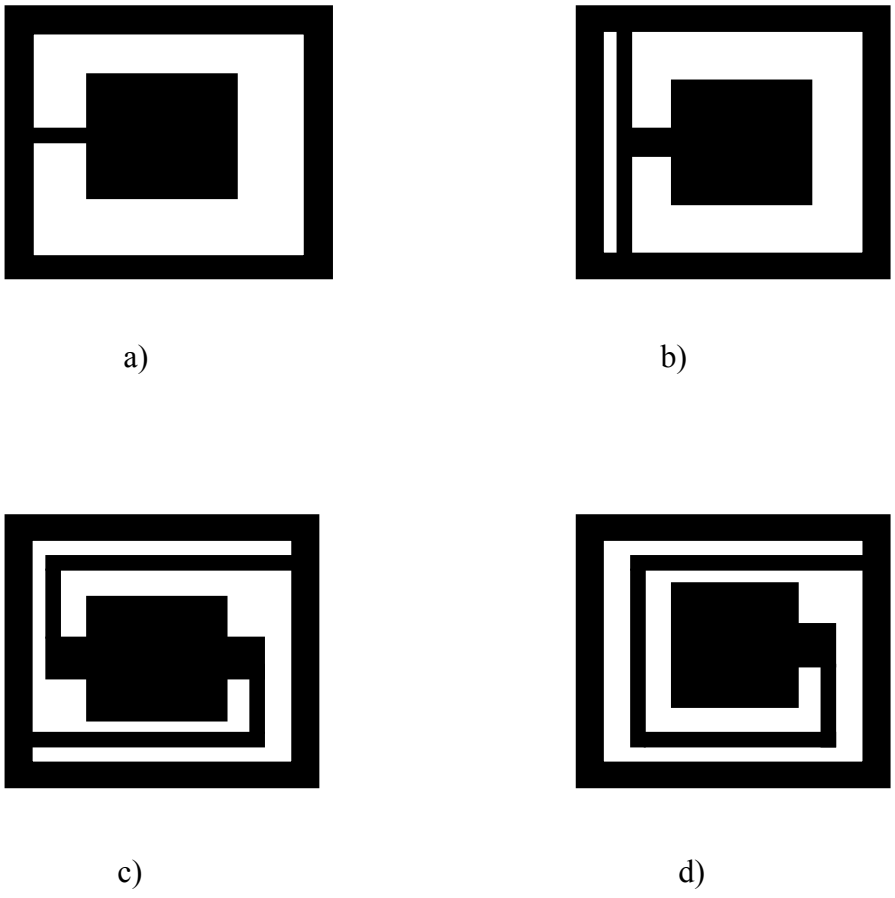

Fig.2.5 Different suspension structures: a) normal, b) torsional, c) meander-shaped, and d) spring beams [Puers and Lapadatu,1994].

Puers and Lapadatu [Puers and Lapadatu ,1994] presented the characteristics of each structure as follows: a) the normal structure, which is a cantilever beam, has a cross sensitivity as much as half of its main sensitivity, i.e. the sensitivity in Z direction; b) the torsional beam has the smallest main sensitivity and very high cross sensitivity; however, if the width of the arm is reduced to the value of its thickness, the cross sensitivity decreases significantly; c) the meander-shaped structure has a main sensitivity close to the value of normal beam, while it exhibits

extremely low cross sensitivity which can be further reduce by adding two more arms to the mass structure; d) the spring shaped structure is the most sensitive one; however, its cross sensitivity is 50% of the main. For all the structures above, the sensitivities can be modified by adjusting the physical parameter such as length, width and thickness of the beams, but the essential vibrational characteristics remain unaffected.

Wagner and Benecke [Wagner and Benecke ,1991] used a vertical DOF silicon structure to restrain the motion of a moving magnet in an electromagnetic micro actuator. As shown in Fig.2.6, in addition to the single vertical DOF, three new silicon structures were designed to achieve one, two and three DOF suspension. The structure in Fig.2.6b, which can be used as a torsional actuator, is the same as the two-beam bridge in Fig.2.4. Its second vibrational mode giving rotation along the y axis is easy to initiate. The structure studied had beams of length 1200 μm, width 400 μm, and thickness 8.5 μm.

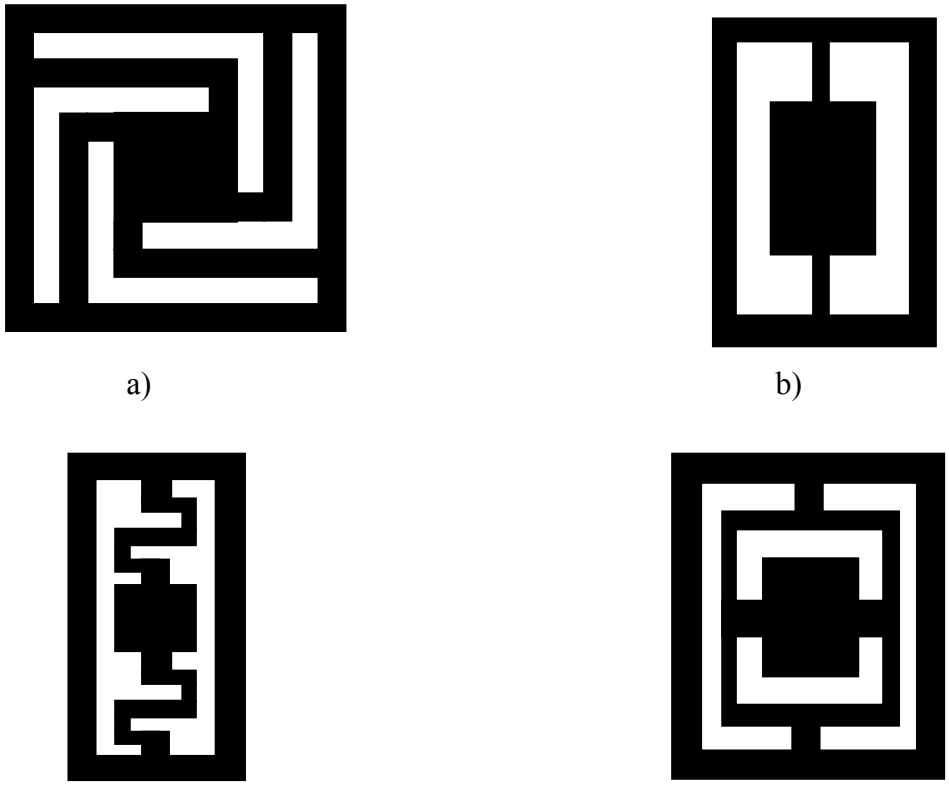

Fig.2.6 Suspension structures with deferent DOF, a) a vertical DOF, b) a torsional DOF,c) a vertical and torsional DOF, and d) a vertical and two torsional DOF[Wagner and Benecke ,1991].

Two other silicon beam-mass structures with multi-axis DOF were also proposed as seen in Fig.2.6 (c) and (d). The two DOF boss structure was suspended by two folded spring beams which ensured a high flexibility for vertical and torsional motion. The three DOF structure had two torsional rims inserted in to each other to create a suspension mechanism. As reported by Puers and Lapadatu [Puers and Lapadatu ,1994], the torsional beam has a low main sensitivity and high cross sensitivity. Therefore, the silicon boss could have two torsional motions around the outer and inner suspension rims and a vertical motion along Z direction.

Zhang [Zhang ,1997] and Bhansali et.al [Bhansali et.al , 2000] designed and developed four kinds of spring mass structures to be used in 1-DOF actuator. They intended to increase the mean beam length. As shown in Fig.2.7, each spring has mass in the middle and four beams. These springs are classified according to the shape of the beams. They are two L-shaped springs and two meander shaped. Zhang [Zhang ,1997] and Bhansali et.al [Bhansali et.al., 2000] achieved maximum large static deflection in the vertical direction with smallest real estate needed for the structure and maximum stiffness along the axes other than in vertical direction.

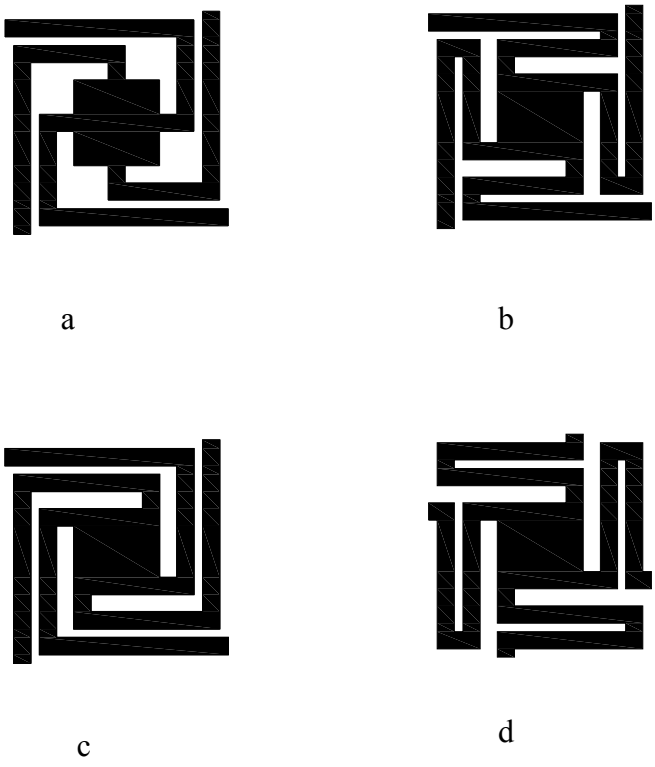

Fig.2.7 Designs of silicon beam-mass structures a, b, c, and d[Zhang ,1997 and Bhansali et.al ,2000].

2.6.2. Spring design objectives and considerations

One of the most significant improvements of the electromagnetic microgenerator efficiency is to optimize the spring design [Williams et.al., 1996; Shearwood et.al.,1997; Williams et.al, 2001]. According to the literature there are some limitations that should be considered when a spring is design to be used in the electromagnetic microgenerator:

- The mechanical damping should be reduced by using a spring fabricated from a material with a low mechanical hysteresis loss, such as Si. This would be a significant improvement on the previous use of polymide membrane spring.
- The deflection and the linear movement of the spring could be increased by employing a cantilever spring. Meandering spring design considered as the spring element in a meandering cantilever is longer than other designs allowing the spring to deflect further. The spring must have a maximum deflection within the generator size to make the magnet moves as close as possible to the coil to increase the induced flux.
- The spring should be designed so that the resonant frequency of the device matches the vibration frequency of the source.

Therefore, this research is investigating the spring designs for the use in power generating devices. Cantilever spring shape is considered to increase the linear movement. Different shapes of meandering and L-shaped springs with low resonance frequency are modelled and simulated with the aid of ANSYS finite element simulation software. Studying and investigating different materials to select the material with low mechanical losses.

2.7 Magnetic circuit

Magnetic circuit is the sum of the total number of paths the magnetic flux may follow as it passes from and returns to its point of origin [Moskowitz, 1995]. A magnetic circuit includes the magnetic flux source (basic permanent magnet) and any pole pieces or any ferromagnetic parts that are carrying some portion of the flux.

2.7.1 Permanent magnet

Due to the increasing availability of high energy permanent magnet materials, there has been much interest and studies in electromagnetic generators with permanent magnet excitation [Williams et.al., 1996; Shearwood et.al.,1997; Williams et.al, 2001; Amirtharajah et.at.,1998; Amirtharajah R., 1999; Amirtharajah et.at.,2000; Li etal.,2000; El-hami et.al., 2001; Ching et.al., 2002; Mizuno and Chetwynd, 2003; Kulah H. and Najafi K, 2004; Huang et. al., 2003; Awaja et.al.,2005; P´erez-Rodr´ıguez et. al.,2005 ; Scherrer et. al.,2005; Beeby et. al.,2005; Kulkarni et. al.,2006; Wang et. al.,2007]. Using the recently developed powerful permanent magnet material, Neodymium-Iron-Boron, further enhances the reliability and effectiveness of the generator. The permanent magnet establishes the flux in the coil. The coil should be located as close as possible to the magnet to minimize the amount of magnet flux leakage.

It is important to choose a type of magnet that will produce a strong flux density. Rare earth magnets are ideal for the electromagnetic microgenerator, and offer up to five times the magnetic energy density of conventional Alnico magnets which is an alloy of aluminium (Al), nickel (Ni) and cobalt (CO). Much of the recent progress made in the development of permanent magnet machines can be attributed to remarkable improvement of the properties of magnet materials. Following the successful development of samarium cobalt ($SmCo_5$ and then Sm_2Co_{17}) in 70s, there was some concern that the cost and availability of the principal constituents might limit the commercial success of these magnets. Attention was drawn to find new magnetic materials with

superior properties to existing ferrite and alnico types. Earlier investigations involved using iron in place of cobalt with a variety of rare earth elements, but all the R_2Fe_{17} compounds have very low operating temperature [Strnat, 1970]. A technical term, 'Curie temperature' (T_c), is introduced to describe fundamental characteristic of magnetic materials. The term T_c expresses the temperature above, which spontaneous magnetization will not exist. The practical operating temperature for a magnet is well below T_c and yet T_c itself is only around125ºC for Sm_2Fe_{17} and around 60 ºC for Nd_2Fe_{17} .

Important progress was made in early 1980s. R_2Fe_{17} was modified to the ternary compound $R_2Fe_{17}B$ which has tetragonal crystal symmetry and strong uniaxial magnetocrystalline anisotropy. The Curie temperature for $R_2Fe_{17}B$ is some 200-300 ºC higher than those of the corresponding R_2Fe_{17} compounds. Then, development quickly focussed on $Nd_2Fe_{17}B$. This new alloy offers the highest saturation magnetization, and its T_c is over 300 ºC [Strnat, 1987]. The most compelling attribute of this compound, however, is that neodymium is considerably more abundant in the nature than samarium. It promises a significant saving in raw material cost by coupling neodymium with the use of iron as the transition metal. $Nd_2Fe_{17}B$ is the basic compound for the modern family magnets known as neodymium-iron-boron, but various partial substations and modifications are commonly made to adjust the magnetic properties to suit practical applications.

It is known that the required magnet volume is inversely proportional to the energy product, i.e. B-H for a given air gap volume being magnetized to a certain flux density. Contours of constant energy product are rectangular hysteresis curve, usually drawn from property data sheet provided by magnet suppliers. The maximum energy product or (BH)max of a given magnet occurs where the magnetization characteristic is tangent to BH hysteresis curve. As Nd-Fe-B has a large energy density than most of permanent materials, it has widely used in various types of electric

machines. NdFeB magnets, also known as a rare earth iron magnets, are produced by a sintering process called rubber isostatic pressing (RIP). These high performance magnets are being used in both the electronics and power industries.

Fig.2.8 shows a typical BH or hysteresis loop. The flux density *B* is displayed on the vertical axis and the magnetizing force *H* is on the horizontal axis. Note that positive and negative values of both parameters are utilized. One variation of the BH loop is the demagnetization curve commonly used to display the properties of permanent magnetic materials. The "demag" curve only represents the second quadrant of the full BH loop. This is where the material has been magnetized.

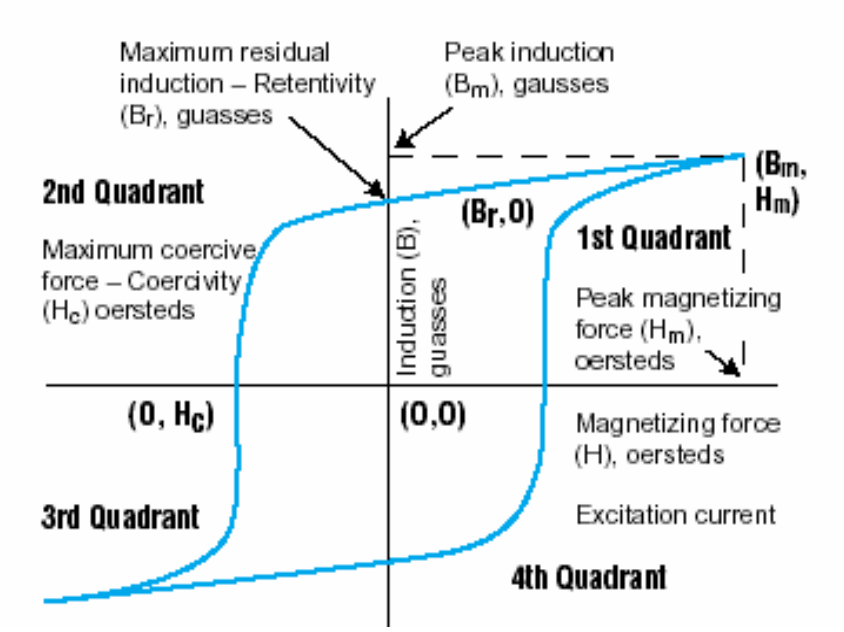

Fig.2.8 BH loop (Arnold, 2003)

2.7.2 Coil configuration design

It has been established that a greater output can be achieved from the electromagnetic microgenerator by increasing the number of coil windings and reducing the impedance of the coil [Williams et.al, 2001]. One of the improvements that have been suggested is to employ a wire wound coil. Coil parameters like coil configuration, diameter, wire material, number of winding

turns and the shape of wire folding are studied. There are two main types of coil in the literature. Firstly, the circular wire wound coil such as, solenoidal and spiral [Grant et.al.,2001; Kruusing,2002] as shown in Fig.2.9 a),b) and c), and secondly, the planar coil [Neagu et.al.,1997 ;Holmes et.al.,2005] that is fabricated by micromachining process as shown in Fig.2.9 d). The wound wire coils take advantage of reduced coil diameter. Coils with large inductance are difficult to implement in planar forms since many turns are required, resulting in large areas and large series of resistance. The planar coil is 2D coil while the folded coil is a 3D that makes the magnetic flux of the permanent magnet more accommodated by the folded coil.

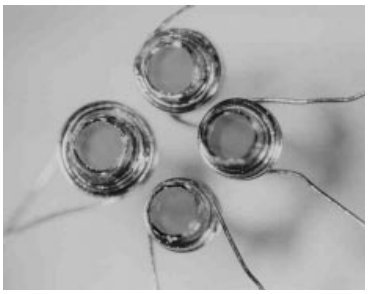

a)

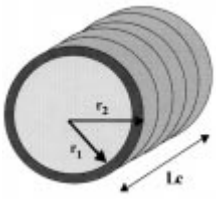

b)

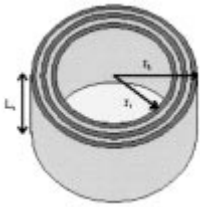

c)

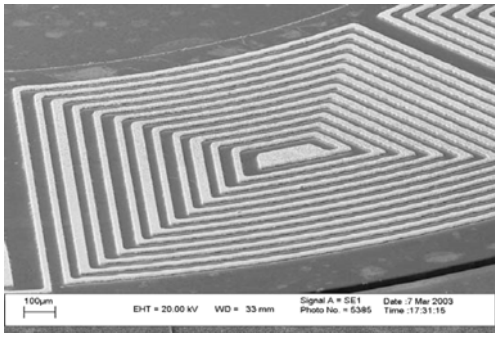

d)

Fig.2.9 Coil types in MEMS, a) Multilayer wire microcoils. b) Idealized solenoidal coil geometry. c) Idealized multilayer coil geometry. d)SEM photograph showing top layer of a stator coil.

2.8 Summary

Vibration-to-electricity conversion offers the potential for MEMS and microelectronics devices to be self-powered in many environments. Low level vibrations occur in many environments including: large commercial buildings, automobiles, aircraft, ships, trains, and industrial environments. Electromagnetic microgenerators offer a well-established technique of electrical power generation over the piezoelectric and electrostatic generators.

A comparison of the various electromagnetic microgenerator designs has been discussed. The electromagnetic generators can be classified according to their moving element part, coil and magnet shapes, input vibration and or the device volume. The generators are also classified as macro size and micro size generators. A wide variety of spring/mass configurations with various types of material are used in the design of the electromagnetic microgenerator. High-performance bulk magnets and multi-turn, macro-scale coils are used in the macro size electromagnetic generators. Micromachined coils and micromachined magnet are used in the micromachined electromagnetic generators.

The general guide lines for efficient electromagnetic microgenerator design (as stated by Williams et.al.[Williams et.al., 1996]) has been formed. These guidelines will be described in chapter 3 for further study of the generator model through analytical investigations and parametric study.

A brief review about the springs design in the literature was presented. It was focused on improving the beam deflection of the spring from the first design with one cantilever beam to the design of a spring with a platform and four cantilever beams. It was found that a spring with four

cantilever beams can achieve maximum large static deflection in the vertical direction and maximum stiffness to be along the axes other than in vertical direction.

A brief background of the permanent magnet and coil was given in this chapter to justify the selection of the NdFeB as a magnetic material and a 3D coil for the electromagnetic microgenerator.

Chapter 3: Analysis of an electromagnetic microgenerator design

A qualitative study of the general vibration to electricity model, provided by Williams and Yates (Williams and Yates 1995), was presented in Chapter 2. In Chapter 3 an extensive analytical investigation develops an efficient design of an electromagnetic microgenerator. An analytical model is developed and then used for investigating the optimum design parameters to get maximum power output. A magnetic circuit concept is used in the analytical study. A description of the basic operating principles of the electromagnetic microgenerator is presented.

3.1 Introduction

As discussed previously, our approach is to drive electromechanical converters from the ambient vibration. Vibration driven generators are presented in chapter 2. This chapter focuses on the development of the electromagnetic generator. Two research groups [Williams's et. al., 2001, Amirtharajah & Chandrakasan, 1998] created and developed the electromagnetic generators. These references from chapter 2 are repeated here for convenience. The device developed by Williams et. al. [Williams et. al., 2001], consists of a moving magnetic mass mounted on a flexure which allows a change of flux linkage with a coil deposited beneath the moving mass. For this case the EMF is given by the following equation:

$$\varepsilon = -N\frac{d\Phi}{dt} \quad \text{..... (3.1)}$$

Where, ε is the electromotive force (EMF) in volt, Φ is the magnetic flux, N is the coil number of turns. The electromagnetic microgenerator was built and tested by Amirtharajah and Chandrakasan [Amirtharajah & Chandrakasan, 1998] but they focused their design on moving coil rather than moving magnet. In this case, the conductor is wound in a coil to make an inductor. The relative motion between the coil and magnetic field causes a current to flow in the coil. In the simple case of a coil moving through a perpendicular magnetic field of constant strength, the maximum EMF across the coil is given by equation 3.2.

$$\varepsilon = NBl\nu \quad \text{..... (3.2)}$$

where:

N is the number of turns in the coil ,B is the strength of the magnetic field ,l is the length of one coil ($2\pi r$) ,ν is the velocity of the coil through the magnetic field

In practice a moving magnet design is simpler to fabricate as it avoids making electrical connection to the mass [Williams et. al., 1996].There are two significant strengths to electromagnetic implementation. First, no separate voltage source is needed to get the process

started. Second, the system can be easily designed without the necessity of mechanical contact between any parts, which improve reliability and reduce mechanical damping. The moving magnet being attached with the spring will increase the seismic mass of the system and then increase the electrical power. This type of converter could be designed to have very little mechanical damping.

3.2 Characterization of Vibration Source

In order to determine how much power can be converted from vibrations, the details of the particular vibration source must be considered. This chapter presents the results of a study undertaken to characterize low-level vibrations from a small motor. Electromagnetic generator design has been established based on the measured vibration out of a small motor. Power output is obtained by using the input vibration. 100 Hz is available in a second story floor of a wood frame office building as measured by Roundy [Roundy ,2003].

I use 100Hz as a practical amount of vibration to prove the generator principle of design and to prove that the proposed generator can generate practical amount of power based on a practical amount of vibration. While frequency of 13.98 Hz in chapter 4 is a result of using selected dimension of the spring and silicon material and a result of modelling the generator design under the free vibration This study aims to maximize the potential applicability of the project.

3.2.1 Characteristics of Vibrations Measured

In this case, to get a practical amount of input vibration, a commercial 1hp motor is used. The measurement of the frequency has been made by attaching a standard piezoelectric accelerometer on the top cover of the motor by a magnet while it is running and then connect the accelerometer to an oscilloscope. The acceleration sensor is attached to the cover of the motor to measure the vibration of the cover caused by the motor rotation**.** A few representative vibration spectrums are

shown in Fig.3.1. Data were acquired with a Fast Fourier Transform (FFT) based digital oscilloscope at a sample rate of 10 kHz. Only the first 1000 Hz of the spectra are shown because all phenomena of interest occur below that frequency. Above 1000 Hz, the acceleration magnitude is essentially flat with no harmonic peaks. Fig.3.1.a shows acceleration vs. time for the cover of the motor. The sinusoidal nature of the vibrations can also be seen in this figure. This sharp, low frequency peak is representative of virtually all of the vibrations measured. Second, fundamental vibration frequency of the cover of the motor is 100 Hz.

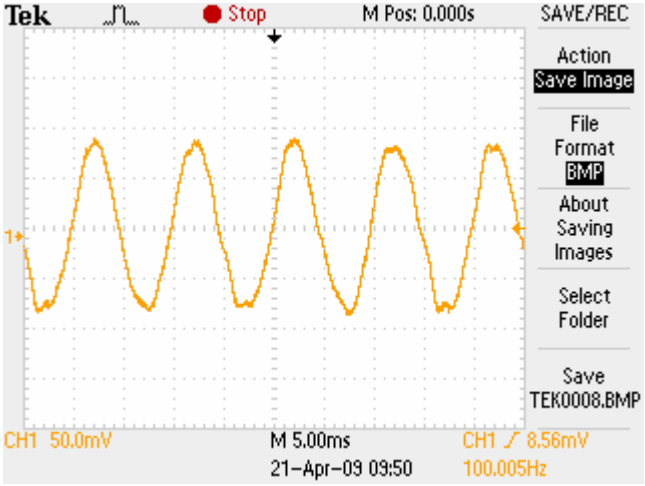

a)

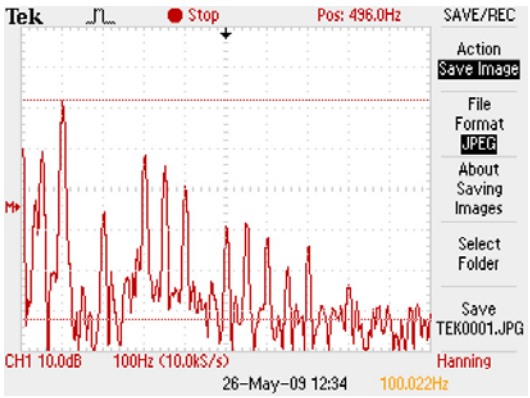

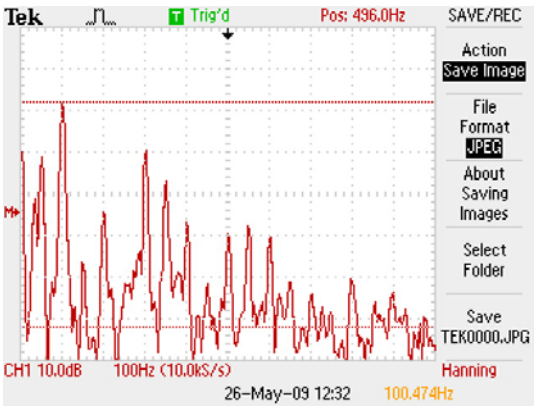

b) **c)**

Fig. 3.1 Acceleration vs. time for the cover of the motor case showing the sinusoidal nature of the vibrations. b) and c) Acceleration vs. Frequency at different points of the cover of the motor.

In Fig3.1 b and c, vibration spectrums out of the cover of the motor have several key aspects. First, there is a sharp peak in magnitude at a fairly low frequency with a few higher frequency harmonics. Fig 3.1 b,c shows a peak of 100 Hz frequency and other signals. These signals are due to that the vibration was measured in a room affected by 50Hz noise signal**.** This low frequency peak will be referred to as the fundamental vibration frequency hereafter. The height and narrowness of the magnitude peaks are an indication that the sources are fairly sinusoidal in character, and that most of the vibration energy is concentrated at a few discrete frequencies.

Given the characteristics of the measured vibrations described above, it is reasonable to characterize a vibration source by the acceleration magnitude and frequency of the fundamental vibration mode. The frequency of the fundamental vibration mode is about 100 Hz, which is very close to that of many sources [Roundy,2003]. For these reasons, the small motor will be taken as a baseline when designing the electromagnetic generator. The voltage and power will be presented using the vibration source of 0.58m/s^2 at 100 Hz. this frequency value will be used in section 3.3.

3.3 Analytical model proposed

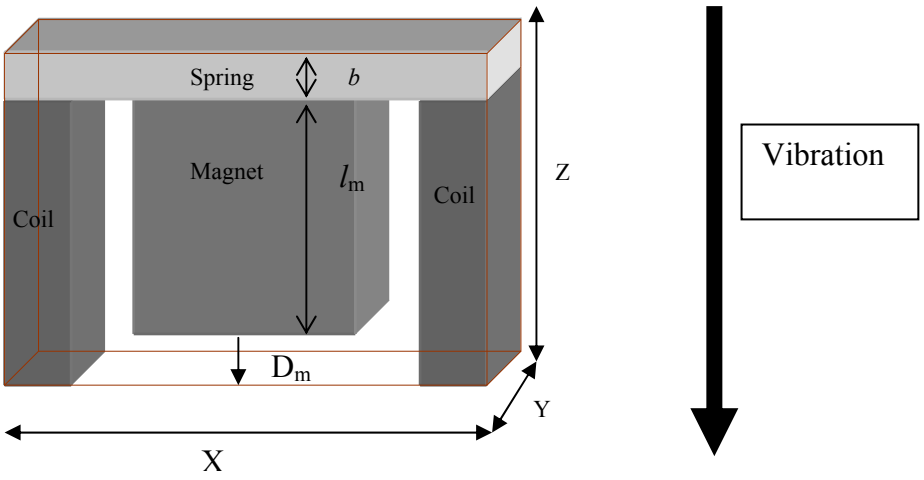

Fig 3.2 Schematic of an electromagnetic generator

A schematic of the electromagnetic generator is shown in Fig.3.2. The intention in this stage is not to go into details of MEMS fabrication steps for such a device, but to consider the operation principles and to understand the various design constraints. In this structure it is assumed that the coil remains fixed while the magnet moves in response to the vibration. Since the magnet has greater mass than the coil, movement of the magnet has more beneficial than movement of the coil. For the purpose of the analysis the system is assumed to be mass-spring system [Williams et.al., 2001]. The available mechanical energy will depend on the level of vibrations and acceleration to which the device is subjected. However, the maximum displacement D_m is given by the difference between the external dimension of the generator, Z, the spring thickness b and the magnet length l_m. Assuming a sinusoidal vibration and expressing the peak displacement of the mass as $D_m = (Z\text{-}b\text{-}l_m)$, the velocity, v of the mass can be expressed in terms of the input vibration and the mass displacement:

$$v = \omega D_m \quad \text{(3.3)}$$

$$v = \omega(Z - b - l_m) \quad \text{(3.4)}$$

The power delivered to the resistive load, R_L, can then be obtained from,

$$P = \frac{1}{2} i^2 R_L \quad \text{(3.5)}$$

Where i is the induced current through the circuit and R_L is the load resistance. The expression of the induced current, i is given by,

$$i = \frac{\varepsilon}{R_L + R_c} \quad \text{..... (3.6)}$$

In this equation, Rc is the coil resistance and ε is induced electromotive force (emf) on the coil defined by,

$$\varepsilon = -\frac{d\phi}{dt} \quad \text{..... (3.7)}$$

As, $\phi = BA$, $dA = lds$, $d\phi = BdA = Blds$,

Therefore, $\varepsilon = (\frac{ds}{dt})Bl = vBl = \omega\ D_m Bl$, and the power equation will be:

$$P = \frac{R_L}{2}\left(\frac{\varepsilon}{R_C + R_L}\right)^2 \quad \text{..... (3.8)}$$

$$P = \frac{R_L (vBl)^2}{2(R_c + R_L)^2} \quad \text{..... (3.9)}$$

The dimension of the generator was based on a proposed overall size of the generator and the proposed model in this section. Typically, for a structure with an overall size of 5000μm x 5000μm x 2000μm=5 x 10^{10} μm^3, the generator external dimension is, Z= 5000μm, the spring thickness b=250 μm, the magnet length l_m=1500 μm and the coil length $l_c = 2\ \pi\ \frac{d_1}{2}$ =785.398 μm. Where d_1, is the coil diameter and is equal to 0.25 mm. The input frequency is assumed to be 100Hz. The resistance of the coil can be calculated from:

$$\text{Rc} = \frac{l_c \rho}{\frac{1}{4}\pi\ d_1^2} \quad \text{..... (3.10)}$$

ρ is the density of the coil material and for copper material it is equal to $16.78 \times 10^{-6}\Omega.mm$. So Rc will be equal to $0.26845\times 10^{-3}\Omega$ and $0.3\times 10^{-3}\ \Omega$ load resistance is chosen.

3.4 modelling of the magnetic field of the electromagnetic microgenerator

The magnetic circuit concept of the electromagnetic generator is shown in Fig. 3.3. It consists of the permanent magnet which is attached to the spring and the coil.

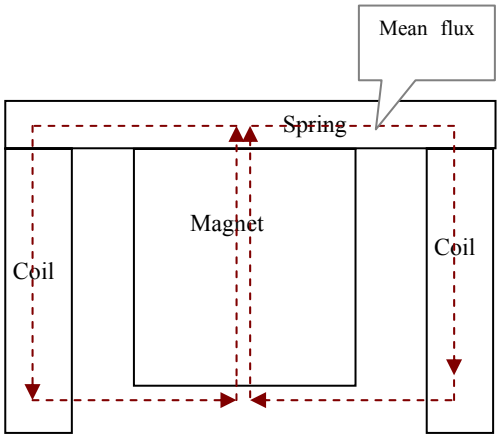

Fig.3.3 Magnetic flux path in the electromagnetic generator

The magnetic field density (B) is chosen to be obtained from a numerical approach including 3D magnetic modelling. The permanent magnet is modelled using the current model [Furlani, 2001]. The coordinate system is centred with respect to the magnet. Let (x_1, x_2), (y_1,y_2), and (z_1,z_2) be the positions of the edges of the magnet with respect to x-,y-,z-axes as shown in figures 3.4,and 3.5 .

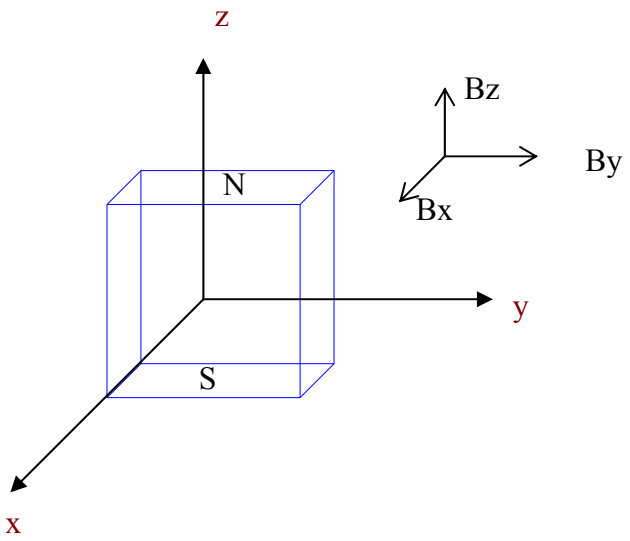

Fig .3.4 Rectangular magnet geometry and polarization with reference frame [Furlani, 2001].

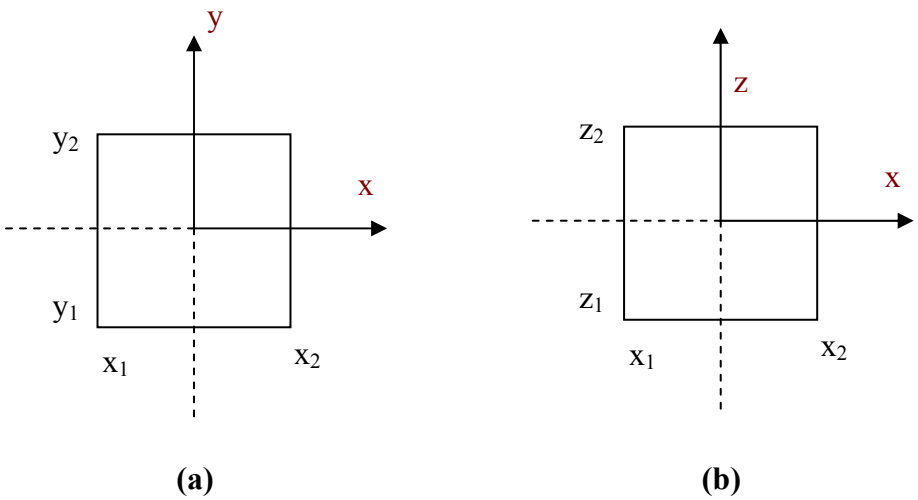

Fig. 3.5 Cross-sectional views of a bar magnet with reference frame: (a)x-y plane; and (b) x-z plane[Furlani, 2001].

The permanent magnet is proposed to move in z-direction, so the magnetic flux will be cut by the coil in the x-y plane. Therefore, the components of the magnetic flux density vector of the rectangular magnet at a general surface outside the magnet are B_x and B_y and they are given by the following equations [Furlani, 2001]:

The X-component is:

$$B_x(x,y,z) = \frac{\mu_0 M_s}{4\pi} \sum_{k=1}^{2} \sum_{m=1}^{2} (-1)^{k+m} \ln[F(x,y,z,x_m,y_1,y_2,z_k)] \quad (3.11)$$

Where

$$F(x,y,z,x_m,y_1,y_2,z_k) = \frac{(y-y_1)+[(x-x_m)^2+(y-y_1)^2+(z-z_k)^2]^{1/2}}{(y-y_2)+[(x-x_m)^2+(y-y_2)^2+(z-z_k)^2]^{1/2}} \quad (3.12)$$

And the Y-component is:

$$B_y(x,y,z) = \frac{\mu_0 M_s}{4\pi} \sum_{k=1}^{2} \sum_{m=1}^{2} (-1)^{k+m} \ln[H(x,y,z,x_1,x_2,y_m,z_k)] \quad (3.13)$$

Where

$$H(x,y,z,x_1,x_2,y_m,z_k) = \frac{(x-x_1)+[(x-x_1)^2+(y-y_m)^2+(z-z_k)^2]^{1/2}}{(x-x_2)+[(x-x_2)^2+(y-y_m)^2+(z-z_k)^2]^{1/2}} \quad (3.14)$$

The theory of equations 3.6and 3.6 is applied to a cubic magnet with limited dimensions of x_1=-1.5, x_2=1.5, y_1=-1.5, y_2=1.5, z_1=-1.5, z_2=1.5. The magnet is chosen to be neodymium iron boron (NdFeB) for its hight flux density of 1.4 Tesla. The coordinate system is located at the centre of the magnet. Distributions of the magnetic field in x and y direction, B_x and B_y were obtained and the computed data are illustrated in Fig. 3.6 and 3.7.

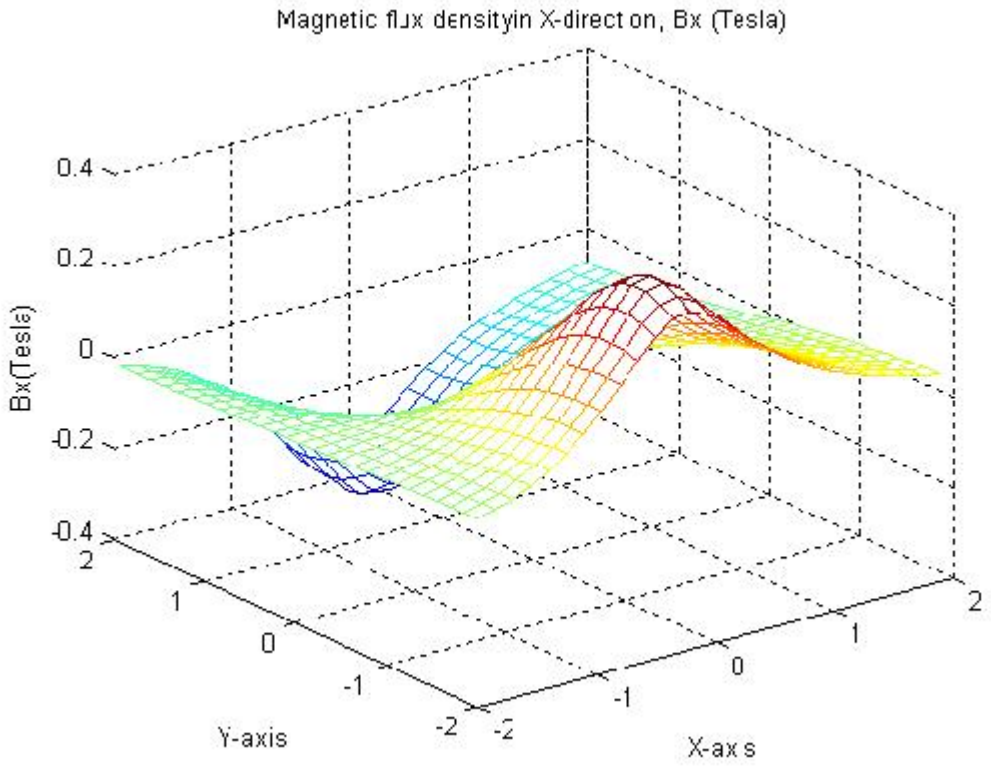

Fig.3.6 Magnetic field component in x-direction.

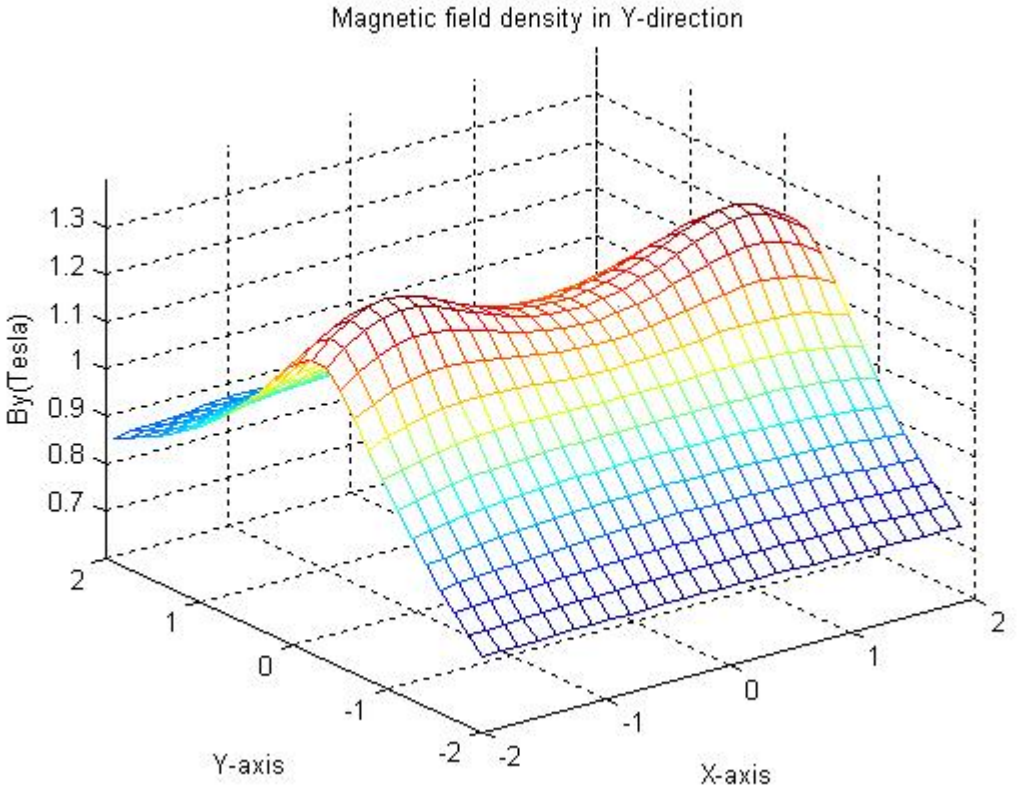

Fig.3.7 Magnetic field component in Y-direction

It is observed from the figures 3.6, 3.7 that the magnetic field components B_x and B_y dip near the centre of the magnet and peak near the edges. The B_y component is significantly higher in magnitude than the B_x component. Since our interest in this particular design is to generate magnetic field at x-y plane, it would be desirable to maximize the B_x and B_y component of the permanent magnet in the regions close to the magnet edges.

Fig.3.8 shows the averaged magnetic field density $B = \sqrt{(B_x)^2 + (B_y)^2}$ as a function of the x-y axes. Fig.3.8 also shows that the magnetic field density peaks near the edges of the magnet.

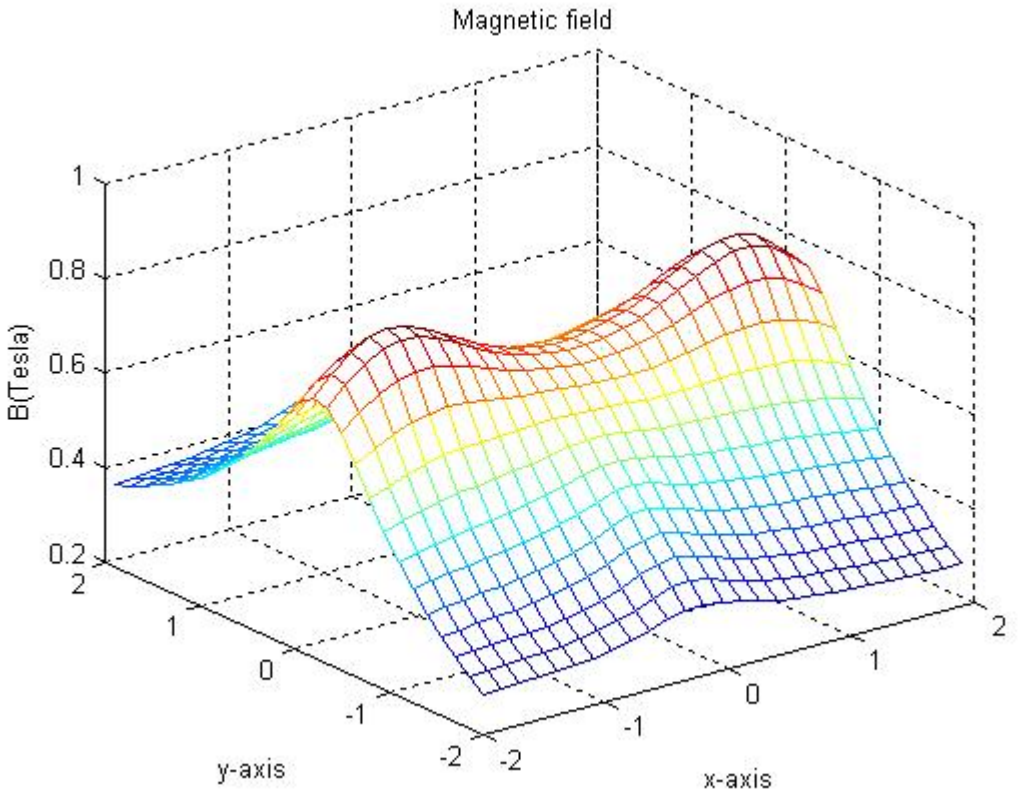

Fig.3.8 Magnetic field of a permanent magnet.

As the magnetic field density of the permanent magnet become available, the output power can be obtained now using the equation (3.9). Fig3.9 shows the output power which is computed taking the values of R_L , Rc, *v* and l from section 3.2.

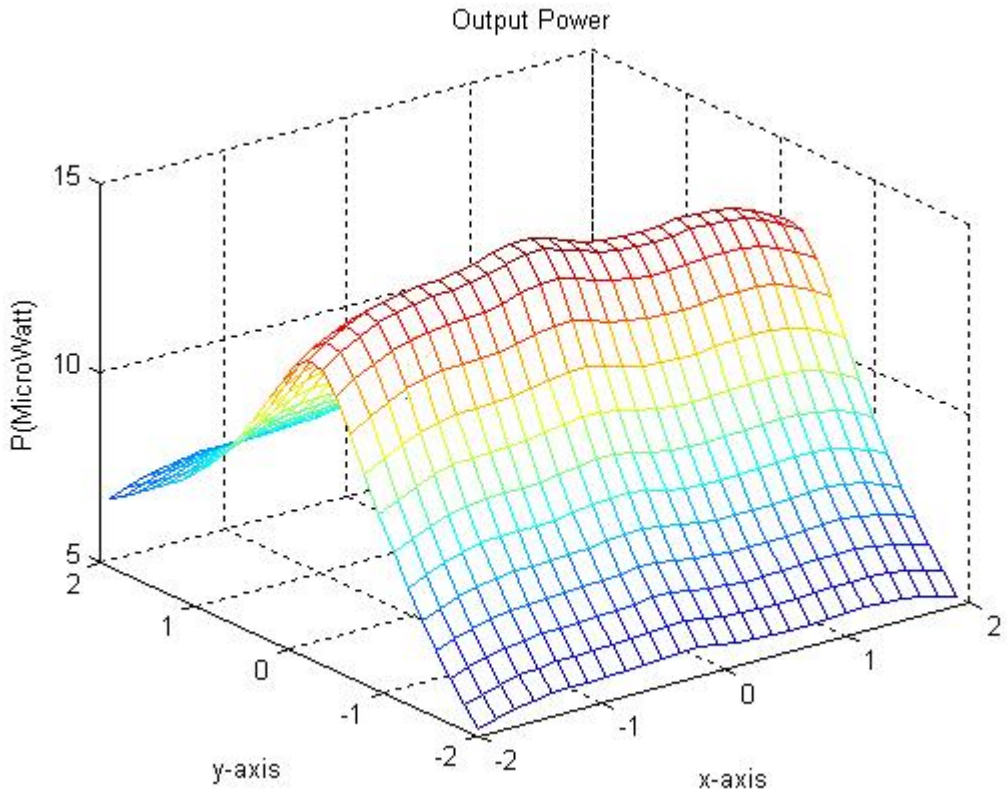

Fig 3.9 Output power of proposed model of electromagnetic microgenerator.

3.5 Effect of the magnet size on the out put power

Analyses are performed to obtain the magnetic field density and the output power in term of variation of the size of the permanent magnet. Results are shown as in Fig. 3.10 and 3.11.

Fig.3.10 shows the influence of the size of the permanent magnet on the magnetic field distribution. The maximum magnetic field densities (B) in Fig.3.10, a, b, c, d again occur near the edges of the permanent magnet. These magnetic field densities are close in magnitudes but the distribution of the magnetic field becomes flatter with increasing the magnet size.

a)

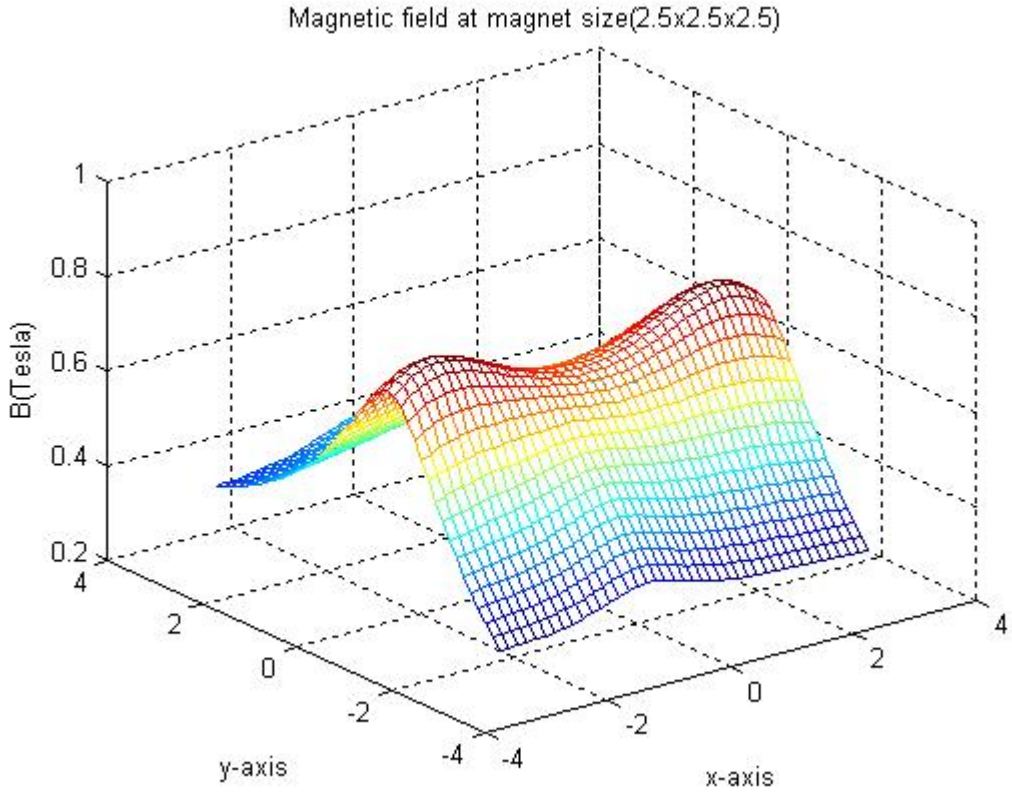
Magnetic field at magnet size(2.5x2.5x2.5)
B(Tesla)
1
0.8
0.6
0.4
0.2
4
2
0
-2
-4
y-axis
-4
-2
0
2
4
x-axis

b)

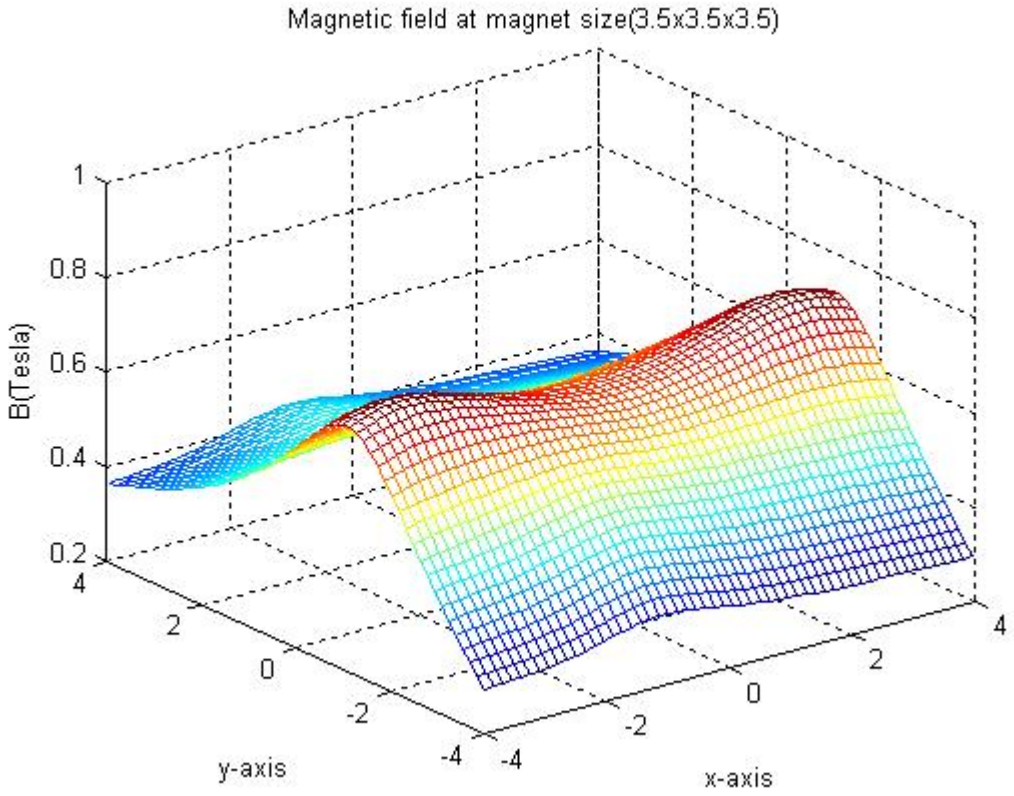
Magnetic field at magnet size(3.5x3.5x3.5)
B(Tesla)
1
0.8
0.6
0.4
0.2
4
2
0
-2
-4
y-axis
-4
-2
0
2
4
x-axis

c)

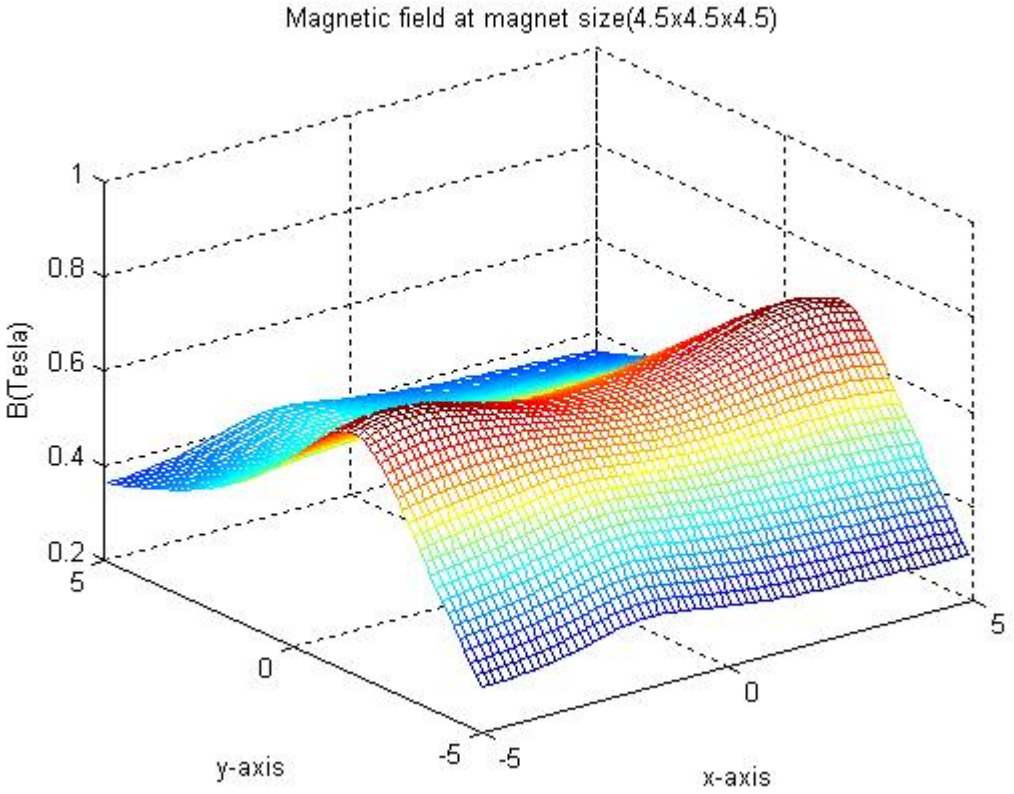

d)

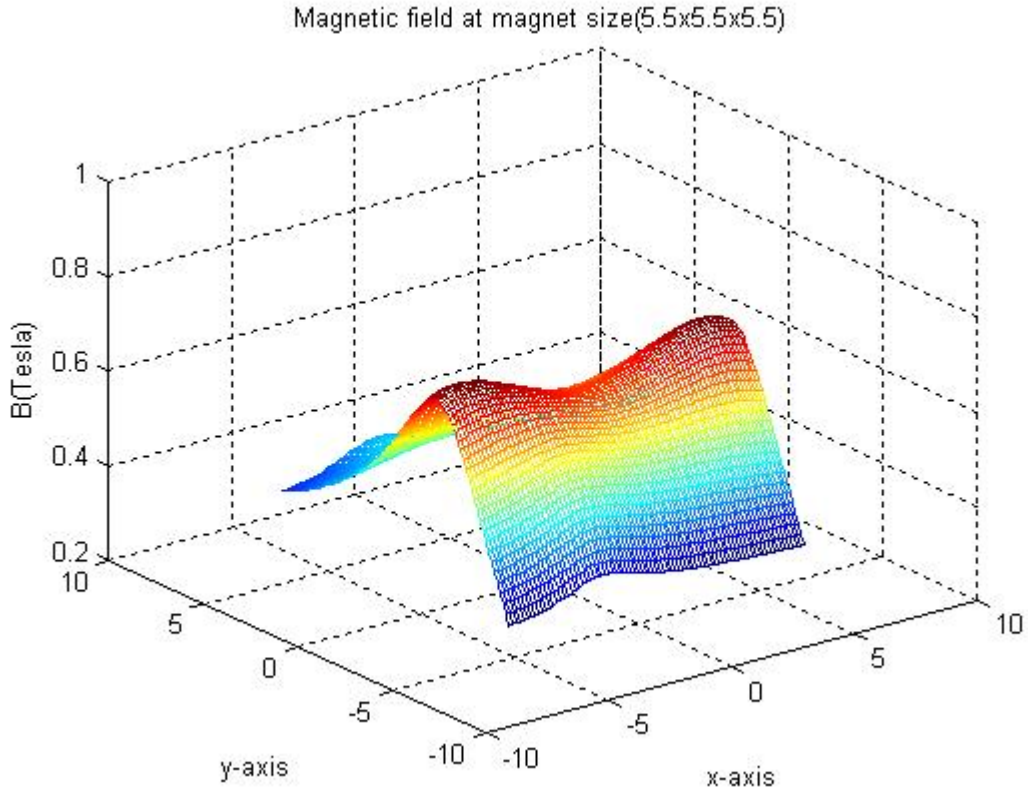

Fig.3.10 3D plot of the output power versus magnet size a)2.5×2.5×2.5 ,b)3.5×3.5×3.5, c)4.5×4.5×4.5, d)5.5×5.5×5.5mm

Fig.3.11a, b, c, d shows the effect of the permanent magnet size on the output power. As can be seen from the graph, it is desirable to have as big magnet as possible according to the available volume of the microgenerator. At higher sizes of the permanent magnet of (5.5×5.5×5.5) mm^3, the output power reaches maximum value of 35.76 µw.

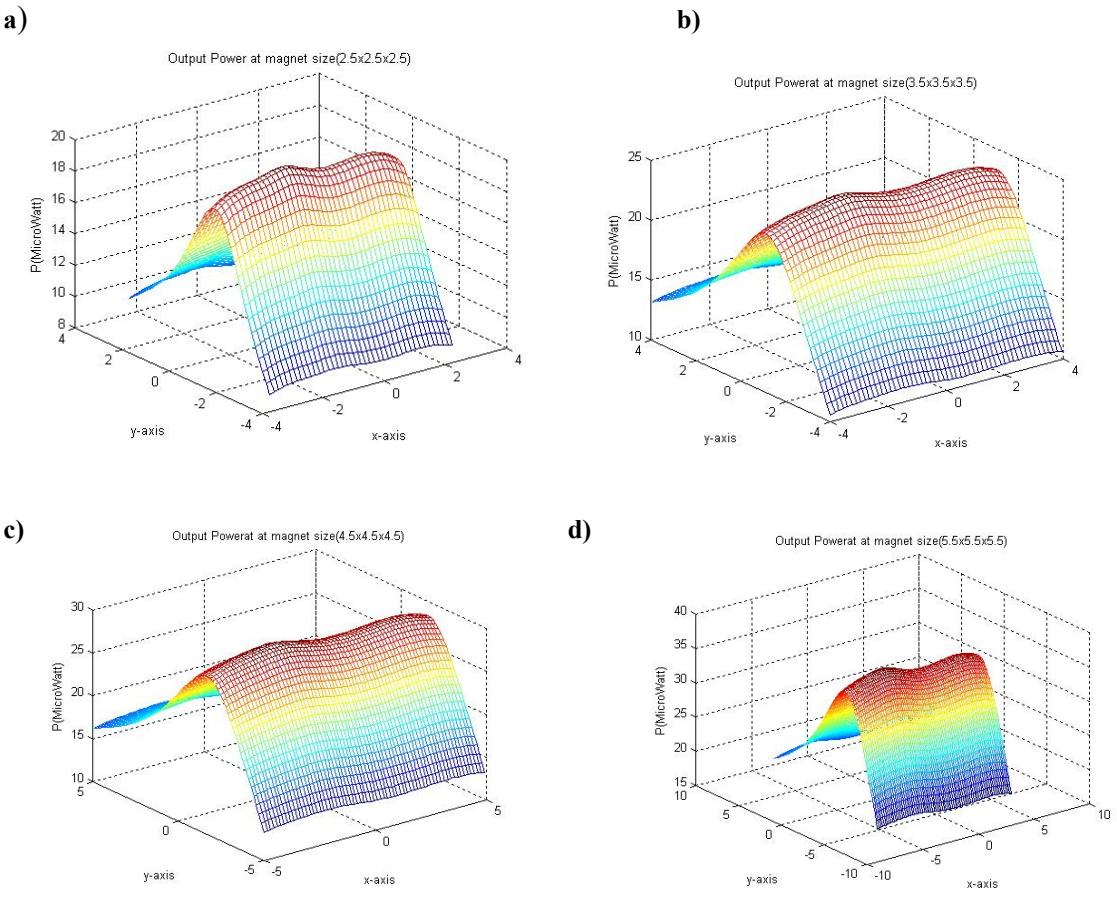

Fig.3.11 3D plot of the output power versus magnet size a)2.5×2.5×2.5 ,b)3.5×3.5×3.5, c)4.5×4.5×4.5, d)5.5×5.5×5.5mm

3.6 Effect of the coil parameters on the out put power

Analysis is performed to obtain the output power in term of variation of the length and resistance of the electric coil or the electromagnet part of the electromagnetic generator. Equation 3.9 used for this analysis and the values of *v* and l are computed from section 3.3. Rc is calculated using equation 3.10 and R_L is chosen to match the Rc. Results are shown as in Fig. 3.12 and 3.13.

Fig.3.12 shows the influence of the coil length on the output power. The maximum output power occurs when the coil length is 1.57mm and that close in magnitude to the proposed length of the magnet.

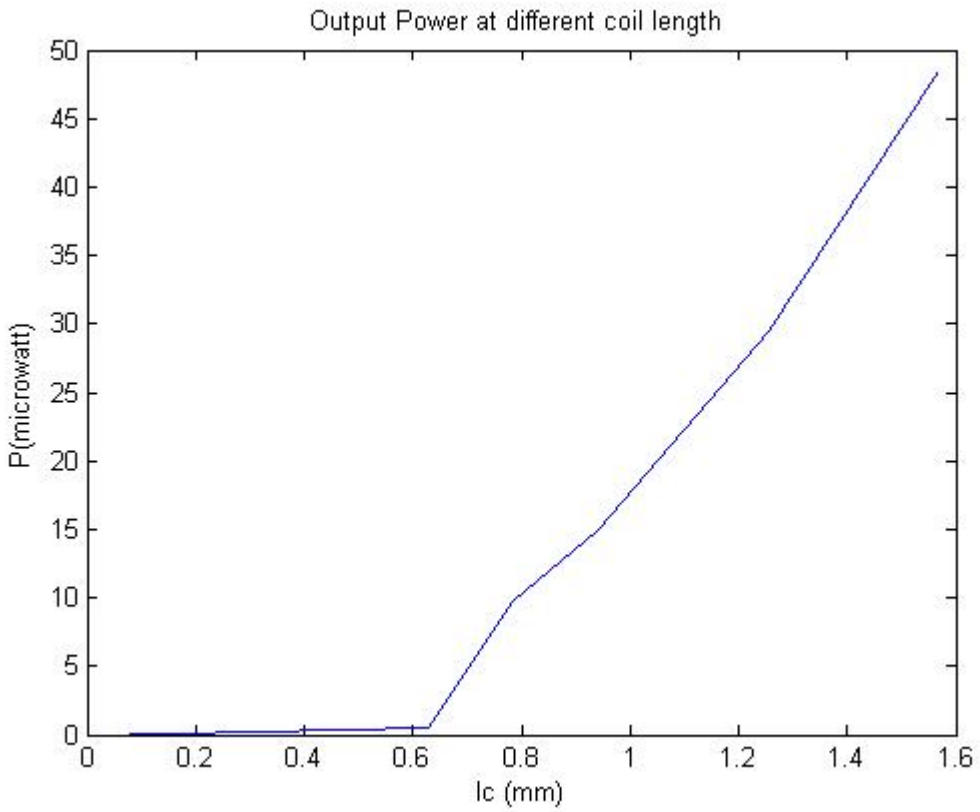

Fig.3.12 Output power Vs coil length

Equation (3.10) has been used to study the effect of varying the coil resistance on the output power. Fig.3.13 shows the calculated power output vs. coil resistance. It is observed that the

output power is increased when the coil resistance is decreased. Therefore, the coil resistance should be kept less than 0.35μΩ.

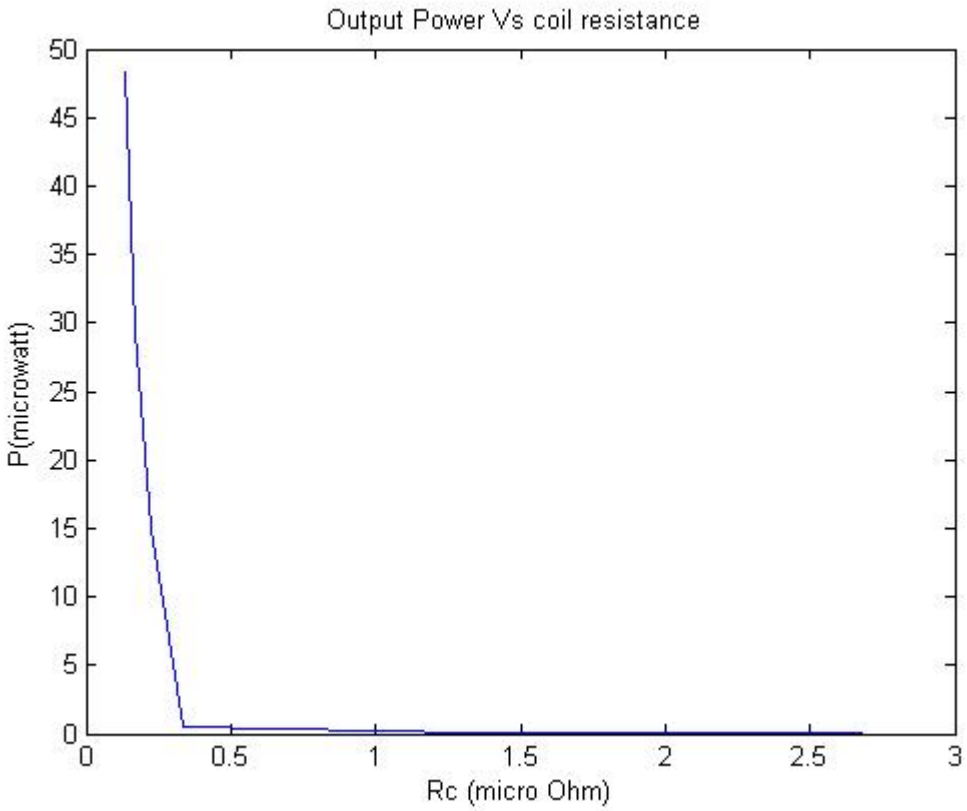

Fig. 3.13 Output power Vs coil resistance

Fig.3.14a, b shows the influence of the coil number of turns on the output voltage and the output power. It is clearly observed that increasing the coil turns increase both the voltage and the power. The maximum values for the voltage and the power are 150.9mV and 1.754×10^{5}.

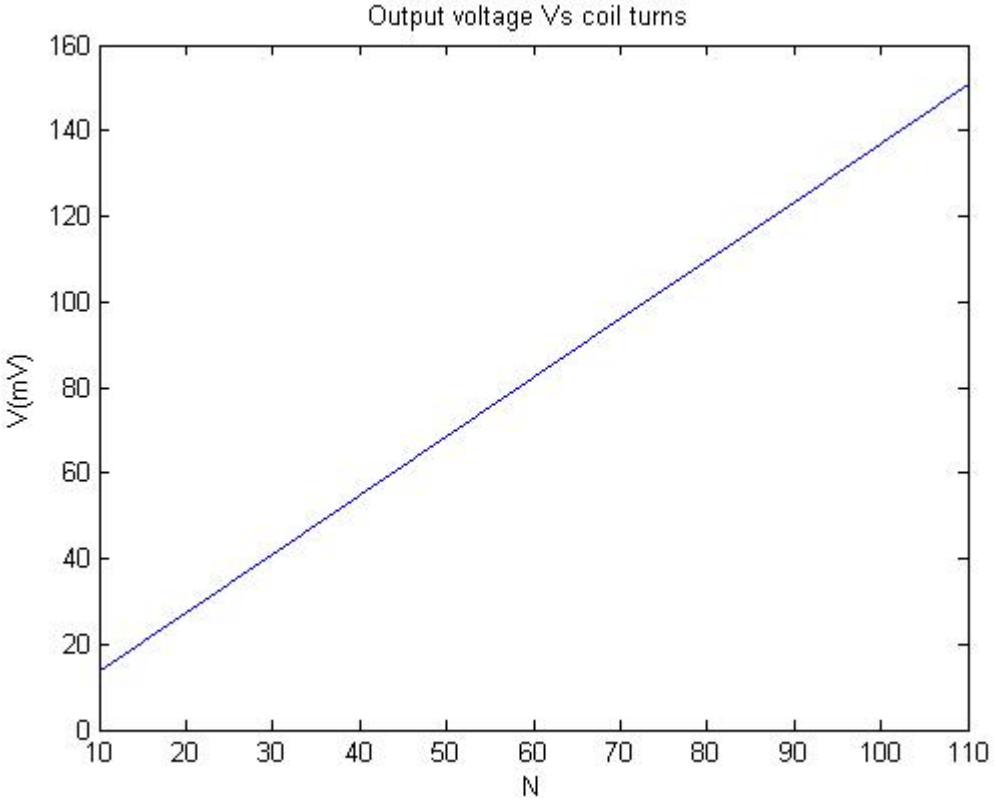

(a)

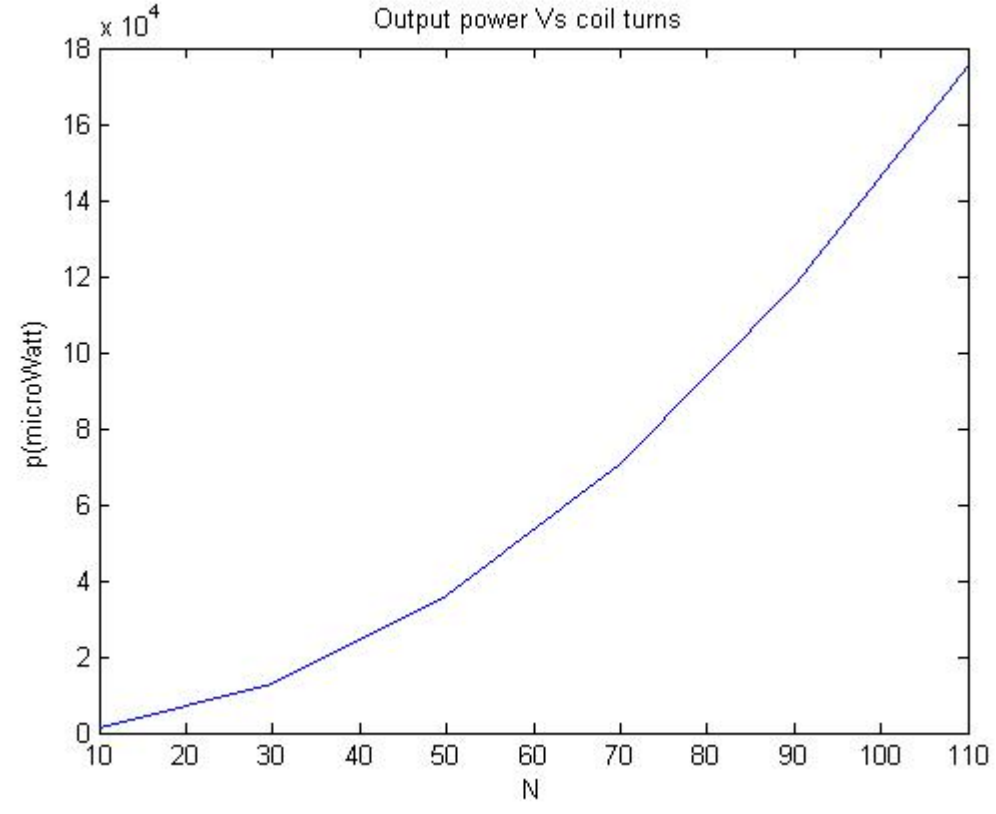

(b)

Fig.3.14 a) Output voltage VS coil turns,b) Output power Vs coil turns.

3.7 Limitations of the electromagnetic microgenerator design

Design analyses carried out in previous sections of the electromagnetic microgenerator have revealed a number of limitations.

1. The output power is proportional to the proof mass. This is not immediately obvious from the expression for power in equation 3.9. However, increasing the magnet mass will increase the magnetic field density (B) and this would significantly increase the predicted power output and can be clearly seen in Fig.3.10,a,b,c,d.
2. The power output is proportional to the square of the frequency of the driving vibrations. This follows directly from equation 3.9 because the input frequency is included in calculating the generator velocity (v) as it can be seen from equation 3.4.
3. The power output is proportional to the square of the coil length. This follows from equation 3.9. It can be observed from Fig.3.12 that increasing the coil length will increase the output power.
4. The power output is inversely related to the square of the coil resistance. Again, this follows from equation 3.9. This clearly can be seen from Fig.3.13. As the increasing of the coil resistance occur decreasing of the output power.

3.8 Design configuration of the proposed electromagnetic microgenerator

Fig.3.14 shows a schematic diagram of the proposed electromagnetic microgenerator. The system consists of two parts: an upper mass-spring system and a lower wounded coil. Vertically polarized permanent magnet forms the inertial mass and is attached to the centre of the spring. A wound coil is made up of a number of copper wires and wound around a plastic capillary. The coil is joined to the spring-mass system.

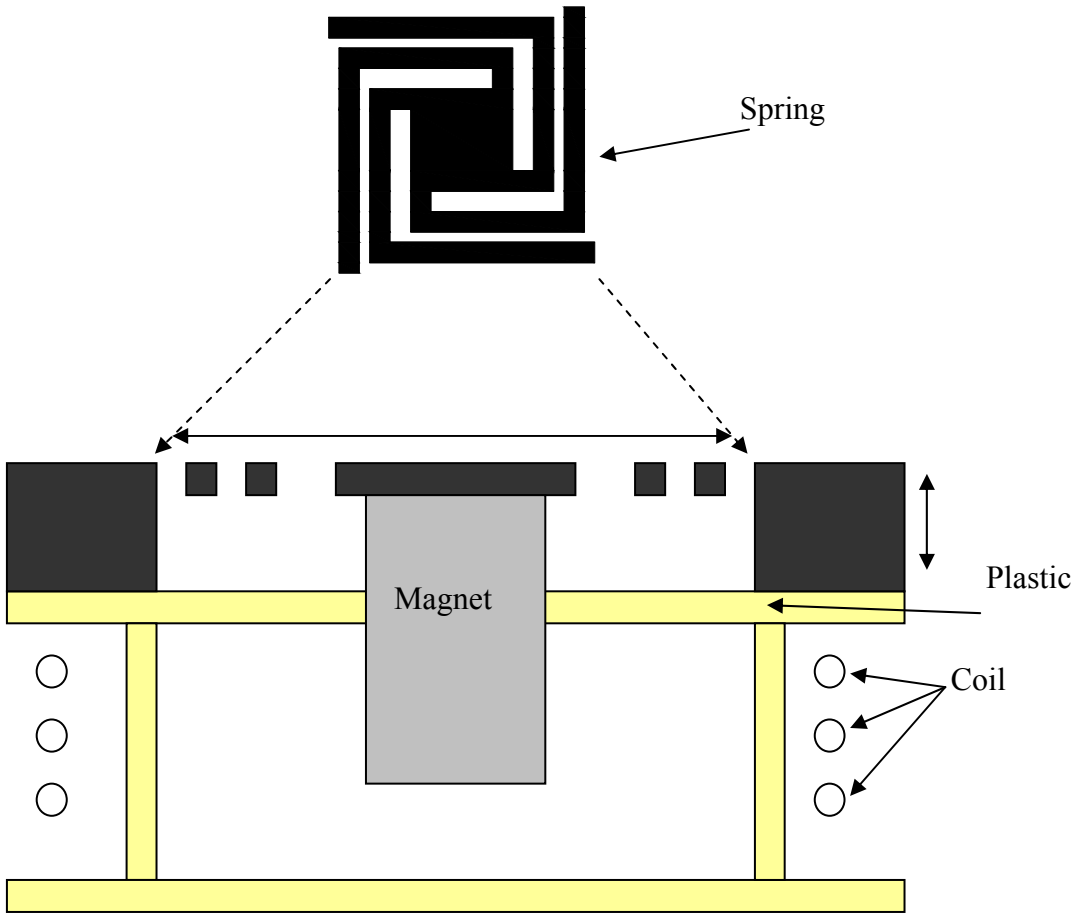

Fig.3.14 Cut view diagram of the microgenerator

It is proposed that the over all size of the generator of 5mm x 5mm x 2mm. the spring is assumed to be a flat with a four beams and middle platform. A detailed study and mechanical analysis of the flat spring will be presented in chapter 4. The coil is assumed to be wire wound coil. Magnetic analysis of the coil will be presented in chapter 5. The magnet is a rare earth permanent magnet.

Potential advantages of this design are:

1. The spring is selected to be a cantilever type to increase the mass deflection and the linear movement of the spring and then reduce the mechanical damping.
2. The magnet is decided to be a moving magnet and attached to the middle of the spring to increase the inertial mass of the generator.

3. The coil is decided to be a wound coil to get large number of turns to accommodate the magnetic field.

3.9 General Principal of operation

The operating principle of the device is as follows: when the housing is vibrated, a mechanical input force feeds into a second order mechanical system, the mass moves relative to the housing and energy is stored in the mass-spring system. This relative displacement, which is sinusoidal in amplitude, causes the magnetic flux to cut the coil. This in turn induces a voltage on the coil due to the varying flux linkage within the motion between the magnet and the coil as stated by Faraday's law of induction. The electrical system involved is simply a first-order LR circuit with the inductance of the coil (L) in series with the load resistance and parasitic resistance of the coil (R). In the former case, the amount of electricity generated depends upon the strength of the magnetic field, the velocity of the relative motion and the number of turns of the coil.

The voltage on the coil is determined by Faraday's Law given in equation 3.14.

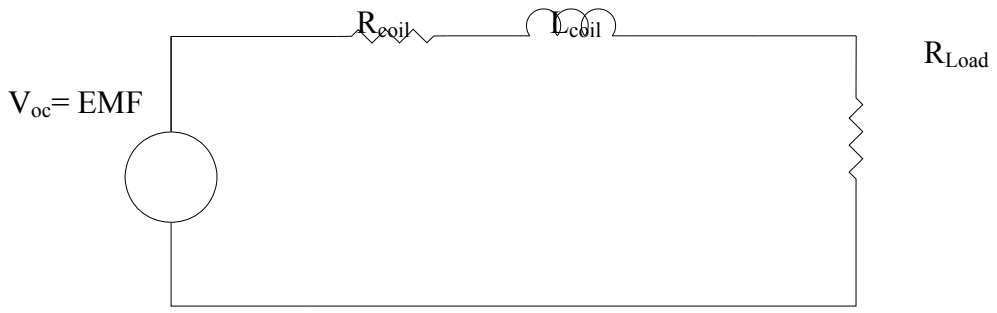

Fig. 3.15 Simplified equivalent circuit model of electromagnetic microgenerator

If a simple resistive load is attached to the electromagnetic microgenerator as shown in Fig. 3.15, an AC voltage (V_{load}) will appear across the load. The average power delivered to the load is then simply $P = V_{load}^{2} / 2R_{load}$. In reality, a simple resistor is not a very useful load. The voltage

should be rectified and conditioned by power electronics. However, the circuit shown in Fig 3.15 gives an easy and useful calculation of power generation.

3.9 Summary

The magnetic circuit concept was applied to obtain an analytical model and carry out an extensive investigation of the electromagnetic microgenerator. The analytical model was used for parametric study; optimization and reliability analysis of the electromagnetic microgenerator. Numerical analyses were preformed using MatLab software to obtain the magnetic field density and the output power in term of variation of the magnet size. The effect of changing the coil parameters like, coil length and resistance has been studied. Limitations of the proposed electromagnetic microgenerator design have been set according to the numerical analyses results. An electromagnetic microgenerator whose operating principle is based on the relative movements of a permanent magnet with respect to a coil has been proposed.

Chapter 4: Modelling and Simulation of flat spring designs

The numerical technique has been recognized as a practical and accurate method of field computation to aid the design of electromagnetic microgenerator. This chapter presents the different designs of the flat spring. The basic theory of the static and dynamic modelling of the micromechanical structures were studied and presented. The design objectives and specifications of the flat spring to be used in the electromagnetic micro generator were discussed. The key design parameters such as static deflection, spring constant, resonant frequency, and dynamic range were investigated. Cantilever spring shape is considered to increase the linear movement. Different shapes of meandering and L-shaped springs with low frequency resonating springs are modelled and simulated with the aid of ANSYS finite element simulation software. Studying and investigating different materials to select the material with low mechanical losses is presented.

4.1 Theoretical considerations of the flat spring design

4.1.1 Static considerations

The cantilever beam in the flat spring is assumed to be straight and have a rectangular cross section. As shown in Fig.4.1, the beam is assumed to be long in proportion to its thickness and is not excessively wide. All loads and reactions are to be perpendicular to the axis of the beam and lie in the longitudinal pane of symmetry of the beam.

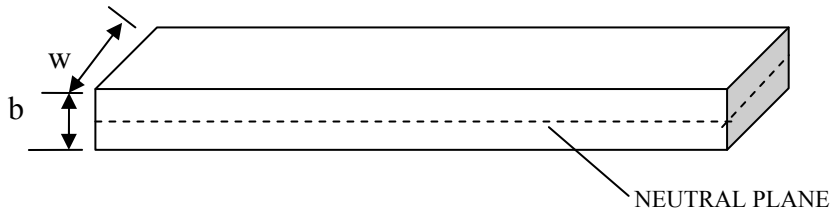

Fig.4.1 Cantilever beam in the original position

4.1.1.1 Stress and strain

The stress on a cantilever beam is $Stress(T) = F / A$ where, F = Applied force and, A = cross-sectional area of the beam and the strain result of an applied force and it is expressed as $Strain(\varepsilon) = \Delta l / l$ where, Δl = extension and, l = original length of the beam. So the relationship of the strain and the stress of a cantilever beam can be expressed as $E = T / \varepsilon$, where E is the elasticity or the young's modules of the beam material [Timoshenko, 1940]. As shown in Fig.4.1, for a beam with rectangular cross section and with a width of w and a thickness of b the moment of inertia is $I = wb^3 / 12$.

4.1.1.2 Deflection of the flat spring

The static deflection D is given by the basic expression of an undamped spring-mass system:

$$D = F / k \quad \text{..... (4.1)}$$

Where F is the applied force and k is the spring constant.

The deflection of the cantilever beam for the case of a concentrated force F applied at the free end of the beam as shown in Fig.4.2 is given by Equation (4.2):

$$D = \frac{Fl^3}{3EI} \quad \text{..... (4.2)}$$

Where l is the length of the beam, I is the second moment of area of the cross section of the beam, and E is Young Modulus of the material of the beam.

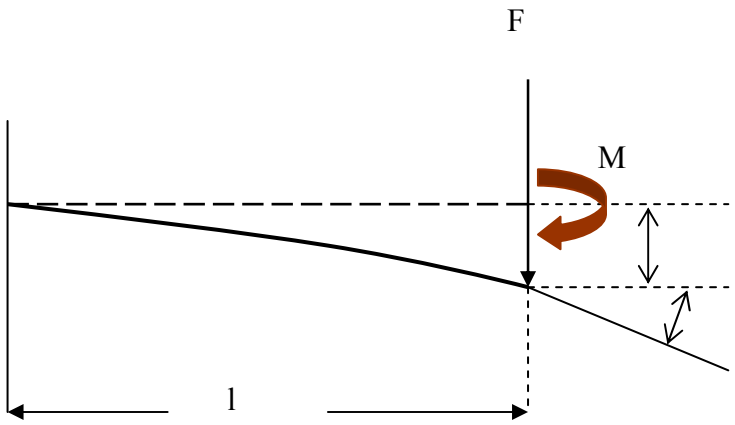

Fig. 4.2 Basic diagram of the deflection of cantilever beam with concentrated force F applied at the free end of the beam and Moment M applied at the free end of the beam

For a four beams spring, the spring constant can be given by [Blevins,1979;Wagner and Benecke ,1991]:

$$k = \frac{4Eb^3w}{l^3} \quad \text{..... (4.3)}$$

Where b, w and l are the thickness, width and mean length of the spring beam and E is the modulus of elasticity of the spring material. By substituting equation (4.3) in equation (4.1) gives the static deflection for the four beams mass springs.

$$D = Fl^3 / 4Eb^3 w \quad \text{..... (4.4)}$$

4.1. 2 Dynamic considerations

4.1. 2.1 Vibration of a spring mass system

Fig. 4.3 shows a typical spring mass system which consists of a mass m restrained by a spring of stiffness k and a damper having viscous damping coefficient c. the mass is assumed to be constrained to move in the x direction, and the mass of the spring is assumed negligible compared with m. If the mass is excited by the external force $F(t)$, Newton's second law of motion can be applied to the system [Thomson,1972].

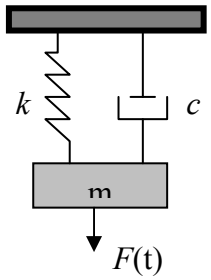

Fig.4.3 Spring mass system with single degree of freedom

The flat spring-mass structure is equivalent to an undamped spring-mass system if it operates in vacuum, or the damping caused by air is neglected. Without the external force $F(t)$, free vibrations will occur in the system when the mass is subject to an initial displacement or velocity. The natural frequency or resonant frequency of the suspension system is:

$$f = \frac{1}{2\pi}\sqrt{\frac{k}{m}} \quad \text{..... (4.5)}$$

4.2 Flat spring design suitable for electromagnetic microgenerator

4.2.1 Design parameters and limitations

In addition to the design consideration of the flat spring mentioned in chapter two, there are other important design parameters to be considered, which include the static displacement of the platform after the magnet is attached, the spring constant and the resonant frequency of the spring. Four different patterns of mechanical springs have selected for further analyses based on the earlier work of Zhang [Zhang, 1997] and Bhansali et.al [Bhansali et.al , 2000].

4.2.2 Initial structural design of the flat spring

Fig.4.4 shows the flat spring with a central platform. The flat spring is formed by four L-shaped beams where each beam is fixed to the spring edge and attached to the spring platform in the other end. The permanent magnet mass is on the platform. The outer dimensions of the springs were chosen to be 2600μm× 2600μm to have a 100μm as a gap between the beams and 200μm between the beams and the rectangular platform. The platform dimension is fixed to be 1000μm ×1000μm, which is enough to accommodate an 800μm ×800μm ×1200μm permanent magnet. The beam mean length is varying from 3800μm to 4300μm according to the spring type and the beams configuration.

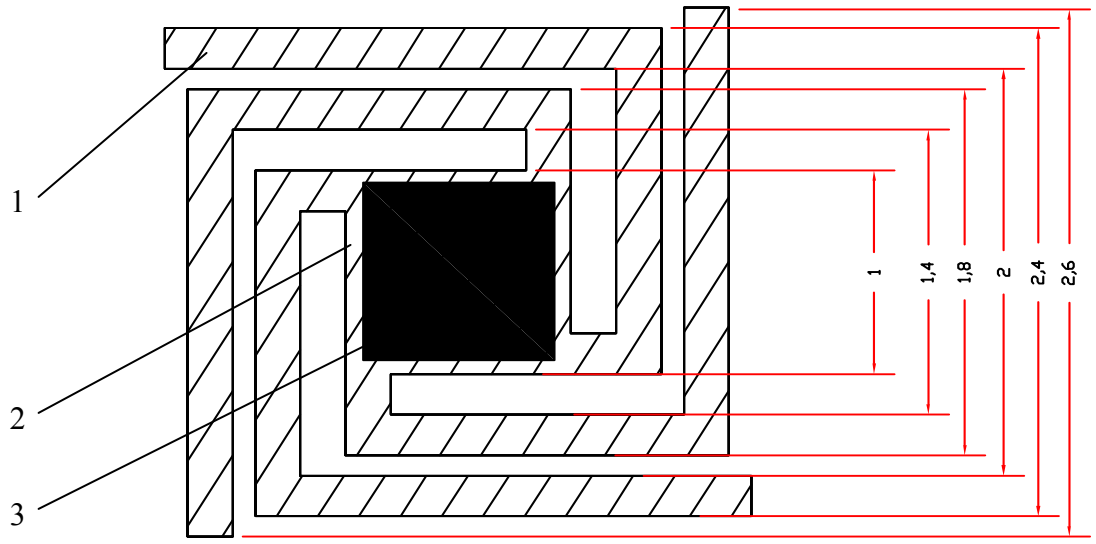

1. Spring beam. 2. Platform. 3. Permanent magnet.

Fig.4.4 Schematic diagram of microspring

Fig.4.5 shows the four spring shapes which were selected for more study and investigation using the finite elements analysis software ANSYS. In Fig.4.5.a and b the springs have a platform and four L-shaped beams while, Fig.4.5.c and d the springs have a platform with four meander shaped beams. The idea behind changing the beams configuration is to get longer beam in a limited area.

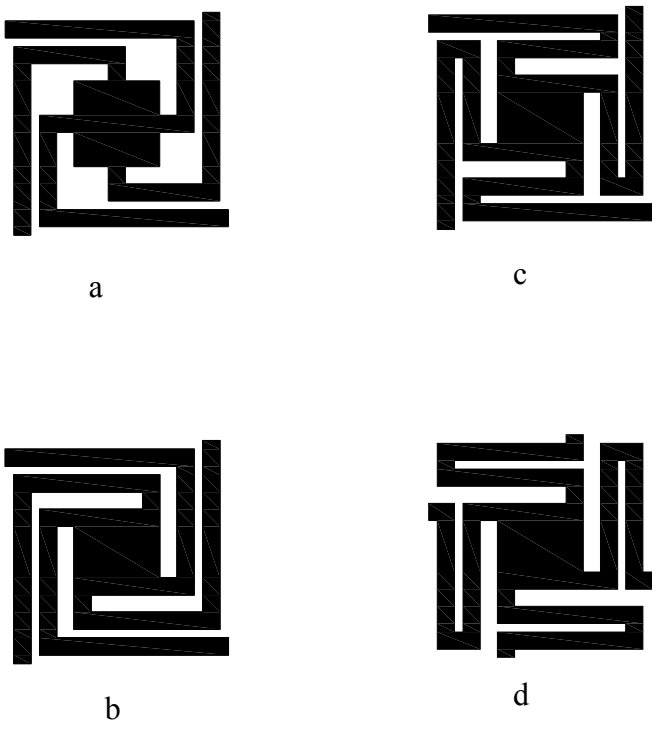

Fig.4.5 Four springs: a) L-shaped1, b) L-shaped2,c)meander1 d) meander 2

4.2.3 Material selection

Large mass deflection and high resonance frequency of the flat spring are the goals of designing the spring and it is highly dependent on the material properties. In comparing different materials a few fundamental material properties are important like Young's modulus (E) which decides the stiffness of the spring. To achieve this, different materials have been considered. Their relevant properties are summarized in table 4.1 [Madou, 1997, Seidemann et.al., 2002]. SU-8, Gallium Arsenide (GaAs) and copper (Cu) have lower young's modulus than silicon that make the spring able to give larger deflection with the same applied force. However, these materials have very low yield strength in comparison to the silicon yield strength. GaAs is an expensive material and requires a very difficult fabrication processes and SU-8 has the problem of removal after

fabrication. Therefore, silicon was chosen as the preferred material for the spring as it has good mechanical properties such as high yield strength and low mechanical losses. At room temperature and under applied load, silicon can only be elastically deformed. Moreover silicon is relatively inexpensive material and has available standard processes of fabrication [Petersen, 1982; Madou,1997].

Table 4.1 Properties of materials considered for the mechanical springs

Material	Young's modulus (GPa)	Poisson's Ratio	Density (g/cm^3)	Yield Strength (MPa)
Silicon	190	0.22	2.30	7000
Gallium Arsenide	75	0.31	5.3	2000
Copper	110	0.35	8.94	69
SU-8	3	0.22	1.19	179.4

4.3 Finite-Element Modelling

Much work has been dedicated to analytical and numerical modelling techniques for mechanical structures. Finite-element modelling is a very powerful tool for understanding the behaviour of the mechanical springs. The modelling was accomplished by utilising a commercial available finite-element software package, ANSYS 5.7. The first step in a finite-element procedure is to divide the domain of interest into number of smaller subdomain that contain of elements and nodes. The nodes are points at the intersection of the element boundaries. The finite element method uses an integral formulation at each point to create a system of algebraic equations. An approximate continuous function is assumed to represent the solution for each element. The complete solution is then generated by connecting or assembling the individual solutions [Moaveni,1999]. In general finite-element program for modelling should contain these steps:

- The meshing of the problem (subdivide the geometry of the model into regions that can be represented by nodes and elements).
- The selection of the appropriate shape functions to represent the physical behaviour of the elements. In ANSYS, this is done by selecting the element type which is responsible for the approximate continuous function representing the solution for each element.
- The assembly of the elements (constructing the global stiffness matrix to represent the entire problem).
- The application of the boundary and initial conditions (i.e. mechanical or electrical loading).
- To solve the set of algebraic equations simultaneously to obtain nodal results.
- The extraction of the important information such as displacement and electric potential.

Analytical example:

A cantilever beam has been used as an analytical example to investigate the mechanical behaviour of the flat spring. The flat spring is considered as a platform with a four cantilever beams with tip loading. The basic formula for the cantilever beam deflection is presented [Timoshenko, 1940].

Fig.4.6 shows a cantilever spring with rectangular cross section (0.5mm * 7μm) , length L=2.5mm and the attached mass is 2.4 mg. equation 4.2 is used to calculate the deflection mathematically and compared with the finite element analysis result .

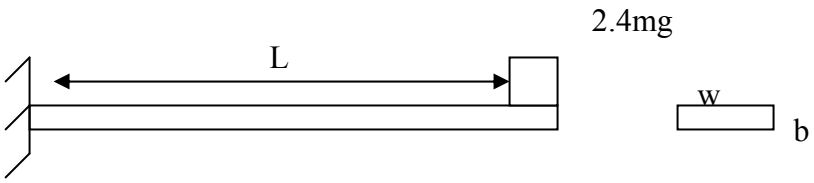

Fig.4.6 Cantilever beam with E silicon= 190 GPa and F= 23.5 µN where F=m(mass)x g (gravitational force)

Finite element analysis is carried out a 2D modelling of a cantilever using ANSYS software. Fig.4.7 shows the deflection of the cantilever due to the mass pressure on the tip of the cantilever. Table 4.2 presents the mathematical results and the simulation results of the static deflection in Z_direction. The results show a significant agreement. That was a step to check the accuracy ratio between the mathematical and finite element analysis result.

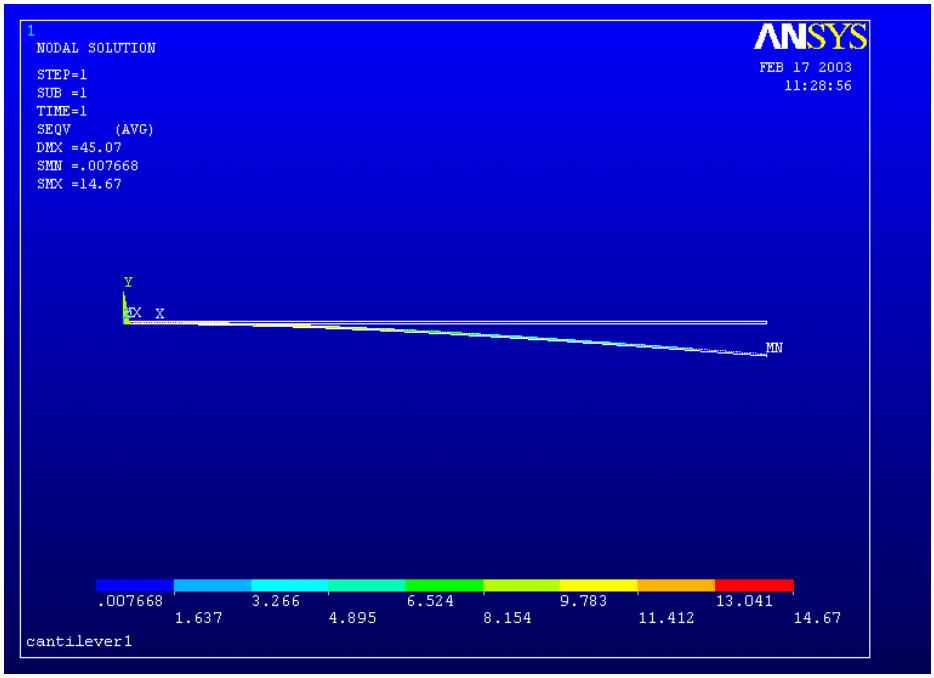

Fig.4.7 Deflection of a cantilever beam

Table 4.2 Deflection results of a cantilever

Beam length (mm)	Mathematical deflection (μm)	Modelling deflection (μm)
2.5	45.07	45.07
3	77.8	77.8
3.5	123.6	123.6
4	184.6	184.6
4.5	262.8	262.8

4.4 Characterisation of the spring deflection using finite element analysis:

4.4.1 Spring model definition in ANSYS

The aim of using the finite-element method is to gain a deeper understanding of flat spring mechanical characteristics. To achieve this aim, a 2D finite-element model was prepared using the same specification as described in section 4.2.2 All finite-element simulations performed were conducted using two different analyses firstly, structural analysis; this technique is used to determine the displacement and the deflection of a structure under the gravitational force. Secondly, frequency analysis is used to determine the vibration modes under free vibration.

Fig.4.8 shows ANSYS model where the model is solved to find the simulation results of the maximum static deflection of the four springs. The flat spring has a cantilever beam configuration with a platform in the middle. A rectangular magnet is attached to that platform.

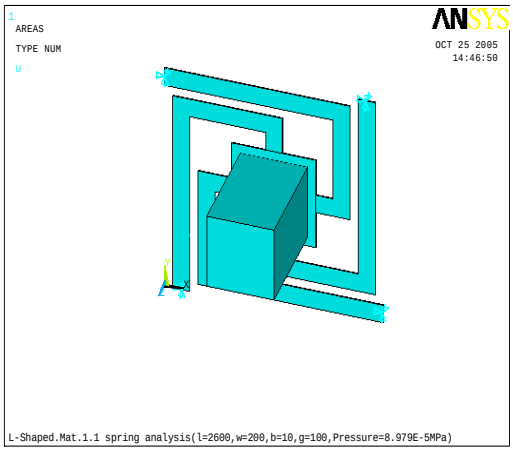

a)

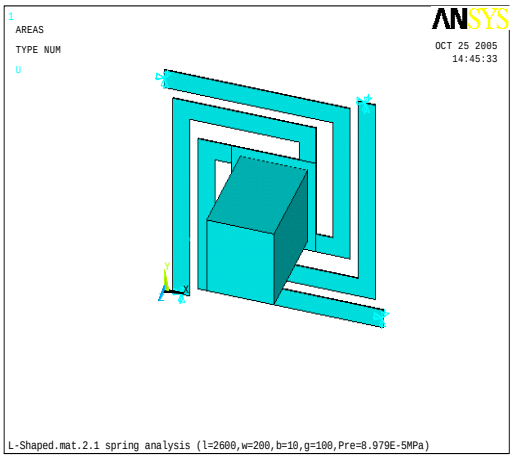

(b)

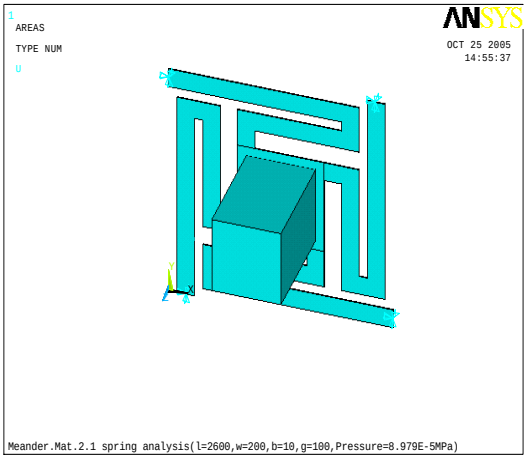

(c)

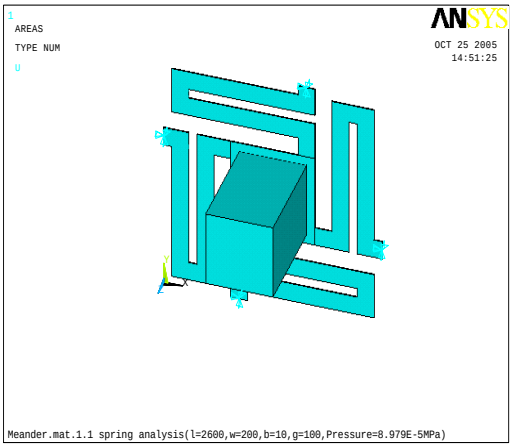

(d)

Fig.4.8 ANSYS finite element models for the flat spring, a) L-shaped1,b)L-shaped2, c)meander1 and d)meander2

4.4.2 Structural analyses and ANSYS results

ANSYS structural static analyses were preformed on the four spring shapes. The maximum static deflection under gravitational force was determined. In the first set of the structural analysis, the four springs have the same outer dimensions and same platform size but different beam length and configuration. It is assumed that the type of material is fixed to silicon and applied to all spring's shapes. SOLID92 element type was chosen to represent the finite elements in the model. SOLID92 is a structural element which also has plasticity, creep, swelling, stress stiffening, large deflection, and large strain capabilities. This element may be used for spars and beam. The element has ten nodes having three degree of freedom at each node: translations in the nodal x, y and z directions. SOLID92 is very effective for MEMS devices because it can significantly reduce the number of element, and therefore save precious computer resources such as memory size and CPU time. Fig.4.9 shows the mesh created spring-mass structure. The area representing spring consists of approximately 45,000 nodes forming over 90,000 elements. An additional 2,000 nodes represent the magnet. The mesh was created so that the highest density of nodes was on the beams and in the centre of the structure. The units used in the ANSYS software are in the "μmks" system where μm is used everywhere in place of m (meter) meaning that N (Newton) becomes μN (Kg. μ m/s^2)and P (Pascal Pressure) becomes MPa (Kg / μ m.s^2).

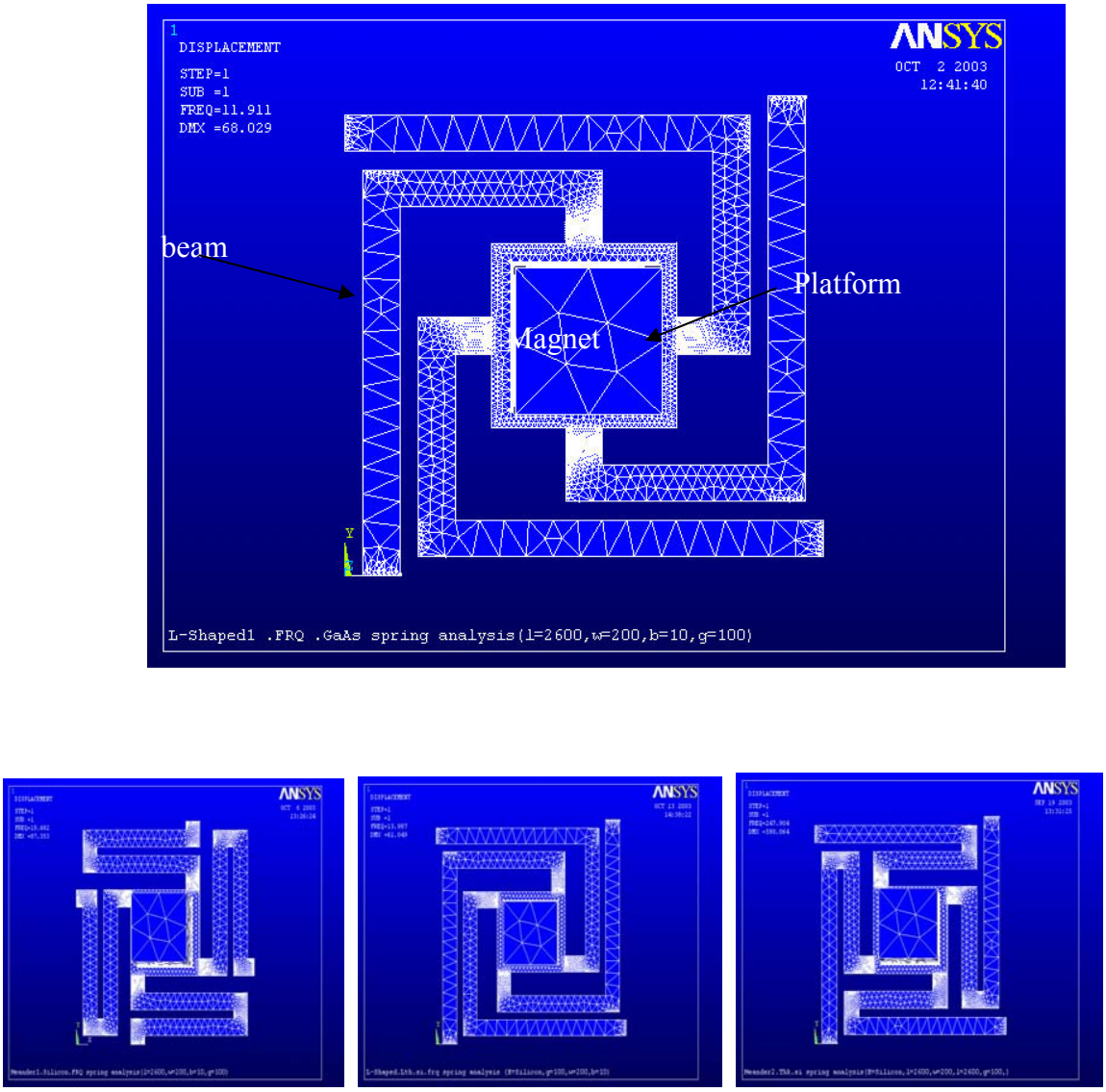

Fig.4.9 Three dimensional mesh size of the four spring mass structure

The displacement on the ends of the model is constrained to be zero. The gravitational force due to the magnet weight is represented by a pressure ($8.979E^{-5}$ MPa) in the Z-direction. An example of an input file written by the author used for determining a spring deflection, developed for finite element analysis package ANSYS, is shown in Appendix A1. Each model is solved to find the simulation result of the maximum static deflection of the four springs. Fig.4.10 shows the simulation results of the spring static deflection. The spring deflection is represented by a

deformed area of each spring in the z-direction and it is clearly shown from the side view of each spring. Fig.4.10,a and b represent the deflection of the springs with L-shaped beam configuration (as shown in Fig.4.8 a,b), while Fig.4.10.c and d represent the deflection of the springs with meander shaped beams(as shown in Fig.4.8.c and d). It is clearly observed that changing the beams configuration from L-shaped to meander has a great effect on the beam length and then on the output deflection. Therefore, Fig.4.10.a along with table 4.3 represent that the spring with longer beam length which is L-shaped2 (as shown in Fig.4.8. b) has the maximum deflection over the other springs. The resulted deflection is found to match with theory shown in equation 4.4.

(a)

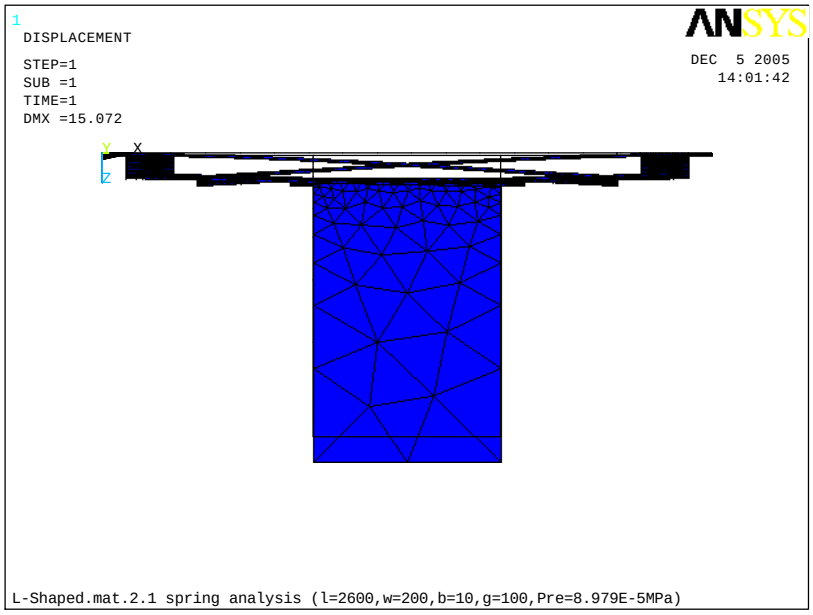
1
DISPLACEMENT
STEP=1
SUB =1
TIME=1
DMX =15.072
ANSYS
DEC 5 2005
14:01:42
L-Shaped.mat.2.1 spring analysis (l=2600,w=200,b=10,g=100,Pre=8.979E-5MPa)

(b)

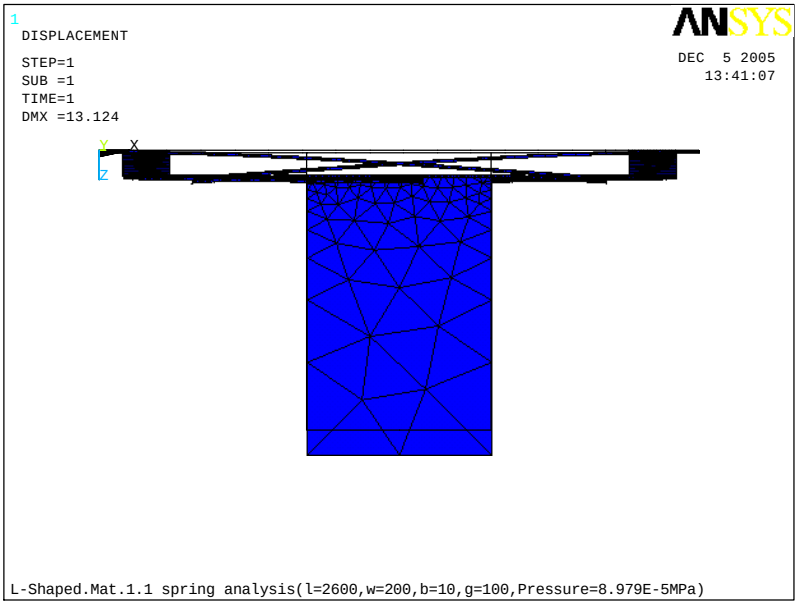
1
DISPLACEMENT
STEP=1
SUB =1
TIME=1
DMX =13.124
ANSYS
DEC 5 2005
13:41:07
L-Shaped.Mat.1.1 spring analysis(l=2600,w=200,b=10,g=100,Pressure=8.979E-5MPa)

(c)

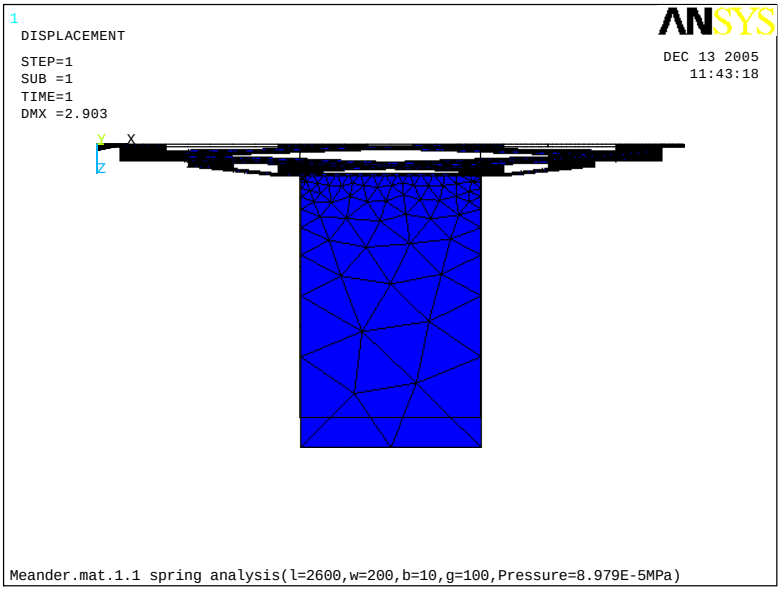

(d)

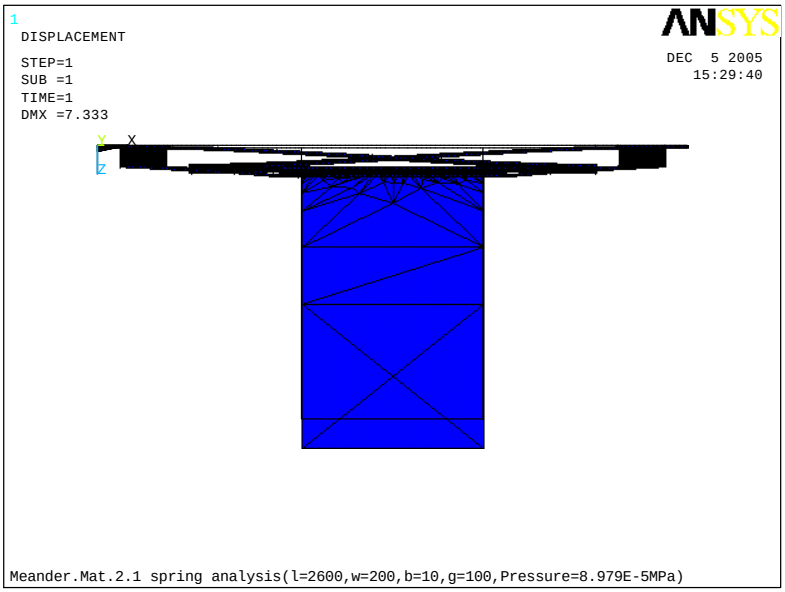

Fig.4.10 ANSYS Analysis of the deflection of the flat spring (side view): a) L-shaped1, b) L-shaped2, c) meander1 d) meander 2

Table 4.3 ANSYS results of maximum deflection in z-direction

Spring shape	L-Shaped1	L-Shaped2	Meander1	Meander2
Deflection(μm)	11.66	13.43	5.11	7.34

The same initial model of the four springs (as shown in Fig.4.4) is then used for the second set of structural static analysis. Table 4.1 shows different materials selected which are the most common materials used for mechanical structures in MEMS. These materials [Silicon, Gallium Arsenide, Copper and SU-8] are applied to all spring shapes. Each material has a Young's Modulus (E) which has a great effect on the stiffness of the spring. A third set structural static analysis has been done to find the most influential parameters on the spring deflection. Fig.4.11 shows the simulation results of static analysis of the four shapes of the flat springs by varying the young's modulus (E) of materials, length, width, thickness of the beam and the gaps between the beams. The analysis output is the maximum deflection in Z-direction of the flat spring under the gravitational force. Fig.4.11.a shows the spring deflection in Z-direction by using different young's modulus (E) of materials. It can be seen that the spring with L_shaped beams has the maximum deflection among other types of springs. It is clearly observed from Fig.4.11.b that using springs with different beam length varied from 2600 μm to 3000 μm gives a great increase in the spring deflection. Fig.4.11.c shows the deflection of the four springs, by increasing the thickness of the spring beam the deflection start to drop as it reached the value of less than 2 μm with beam thickness of 25 μm. Fig.4.11.d presents the deflection of the springs by selecting spring's beam widths start from 100 to 250. The deflection of the spring has the highest value at 32 μm when the beam width is 100 μm. Fig.4.11.e shows that the deflection of the spring reached its highest value when the gap between the beams is the minimum. Fig.4.11 shows that the

simulation results are in agreement with the equations 4.3 and 4.4 of spring constant and deflection. Therefore, Young's modulus, the thickness, length and the width of the beams are the dominant factors to determine the deflection.

The results in Fig.410 and Fig.4.11 conclude that the largest mass displacement could be obtained from L-Shaped2 spring (as shown in Fig.4.8.b). To satisfy the requirement of the spring mask design and the fabrication process limitations (silicon bulk etching), the beam thickness was chosen to be 10μm and the beam width was chosen to be 200 μm so the maximum deflection is 13.43μm. That is because L-Shaped2 has the longest beam length among the other springs due to the way its beam folding. Based on the work of Williams et. al. [Williams et. al, 1996], the amount of the power generated is proportional to the square of the peak mass displacement. Therefore, L-Shaped2 configuration was chosen to study the spring vibrational behaviour.

(a)

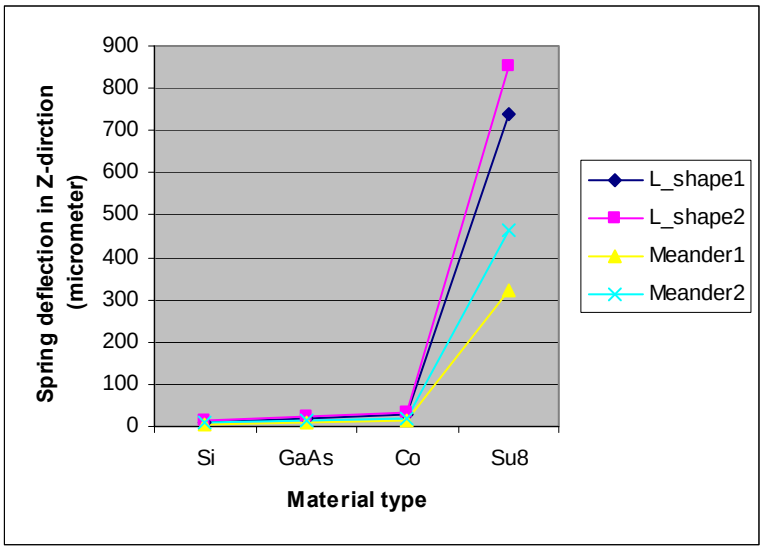
Spring deflection in Z-dirction (micrometer)
900
800
700
600
500
400
300
200
100
0
Si
GaAs
Co
Su8
Material type
L_shape1
L_shape2
Meander1
Meander2

(b)

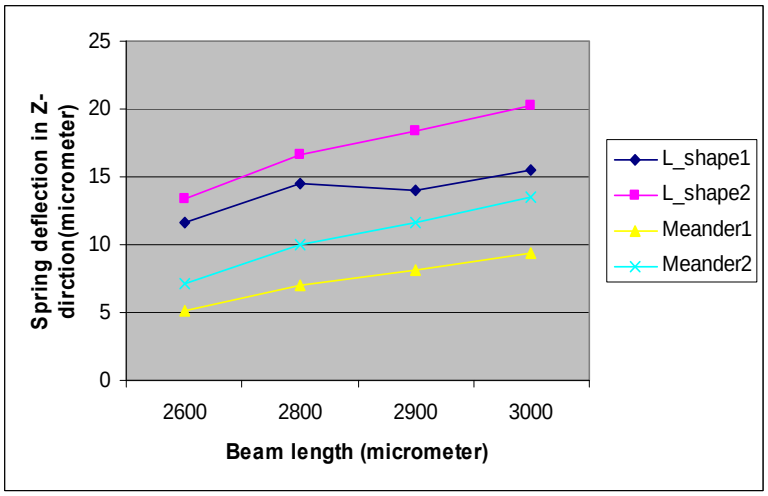
Spring deflection in Z-dirction(micrometer)
25
20
15
10
5
0
2600
2800
2900
3000
Beam length (micrometer)
L_shape1
L_shape2
Meander1
Meander2

(c)

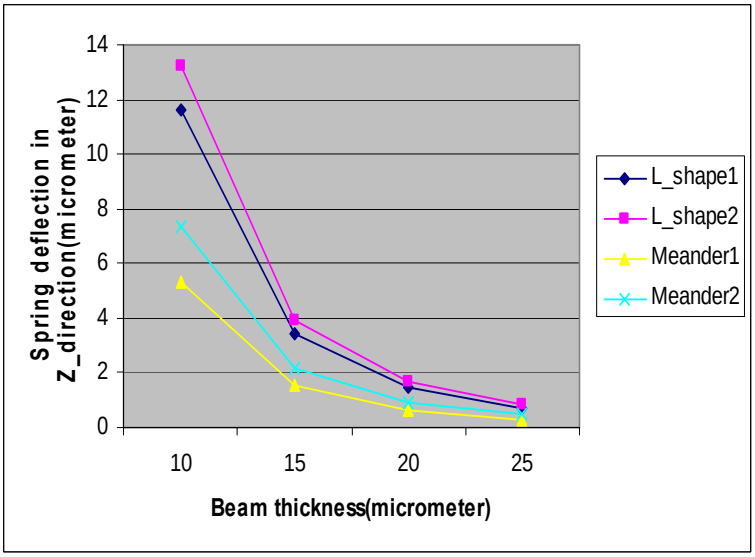
Spring deflection in Z_direction(micrometer)
14
12
10
8
6
4
2
0
10
15
20
25
Beam thickness(micrometer)
L_shape1
L_shape2
Meander1
Meander2

(d)

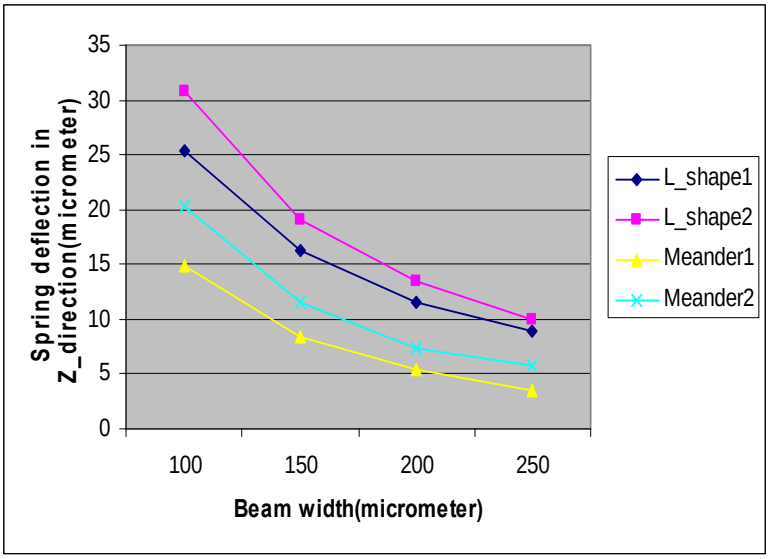

(e)

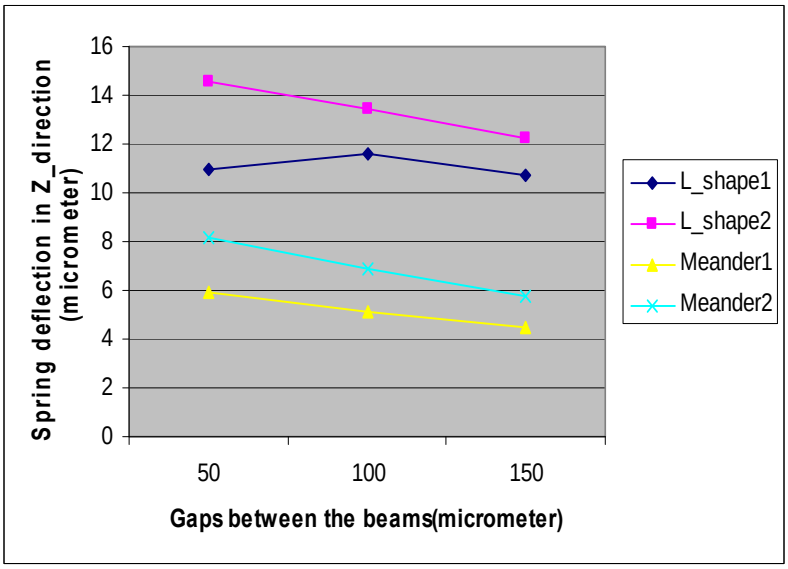

Fig.4.11 ANSYS simulation results of spring deflection in Z_direction versus: (a)spring Material,(b)Beam length,(c) beam thickness (d) beam width (e)Gaps between beams.

4.5 Vibration characteristics of the flat spring

The degree of freedom of a freely vibrating body may be defined by the number of independent coordinates that are required to identify its displacement configuration during vibration. For example, a rigid block supported by a linear spring of stiffness k can vibrate in six different ways; it can have six degrees of freedom. It can translate in the direction of its three x, y, and z principal axes, and it can also rotate about the same three axes. Therefore, we need three displacement coordinates associated with the x, y, and z directions and angular displacements with respect to the axes in order to be able to define the position of the mass at any time t during vibration. Each of these possibilities of a free vibration is defined as a mode of vibration, and the natural frequency associated with each mode is dependent on the frequency of the other modes. On this basis, it can be stated that the natural frequencies of a freely vibrating body are equal in number to its degrees of freedom and that there is a mode shape associated with each frequency.

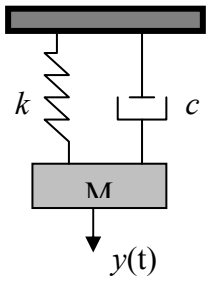

Fig.4.12 Spring mass system(Thomson,1972)

If the mass of the spring-mass system in Fig.4.12 is restricted to move in the vertical direction only, then this system has one degree of freedom, and the single coordinate y(t) shown in the Fig.4.12 is sufficient to define completely the position of the mass m during vertical vibration.

The vibration behaviour of the flat spring has been studied theoretically. It is found that classical formulae describing the dependence of mechanical resonance frequency on geometrical and material properties are valid for all modelled designs using finite element analysis.

4.5.1 Resonant frequency modes

The flat spring (simply supported beam) has three modes of vibration in the transverse direction. The lowest frequency of vibration is the fundamental frequency, and the higher frequencies, such as the second and the third modes are termed harmonics. In many problems, especially those dealing with structures, the fundamental mode of vibration is of particular importance because the amplitudes of vibration would be the largest, and it is often used to define the flexibility of the structure. The rigidity of the structure is a function of its free frequency of vibration. The larger the frequency the stiffer the structure would be. ANSYS Modal Analysis was used to study the free vibration characteristics of the flat spring and to select the desired mode of vibration. This analysis aimed to know the resonance situation of the spring where the electric power generation will be the maximum [Williams et.al, 2001]. The studied model is L_ shaped 2 with length (2600μm), beam width (200μm), and thickness (10μm). The resonant frequencies of the beam structured are calculated using Block Lanczos method, which is used as a mode extraction method to solve the eigenvalues. The flat spring material is silicon. ANSYS files written by the author with all the modal analysis commands is presented in Appendix A2.

(a)

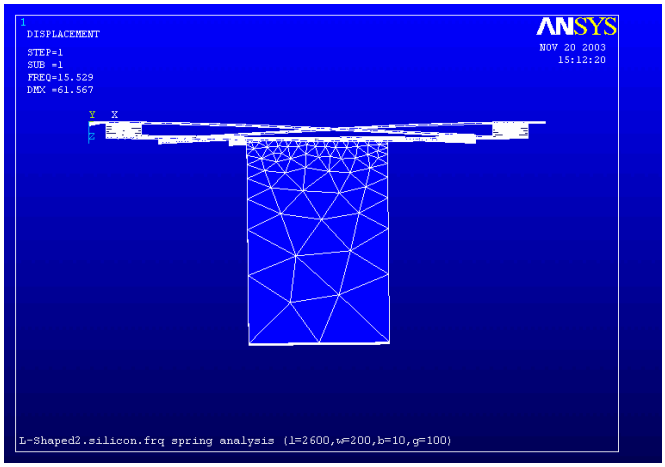

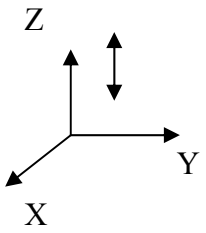

(b)

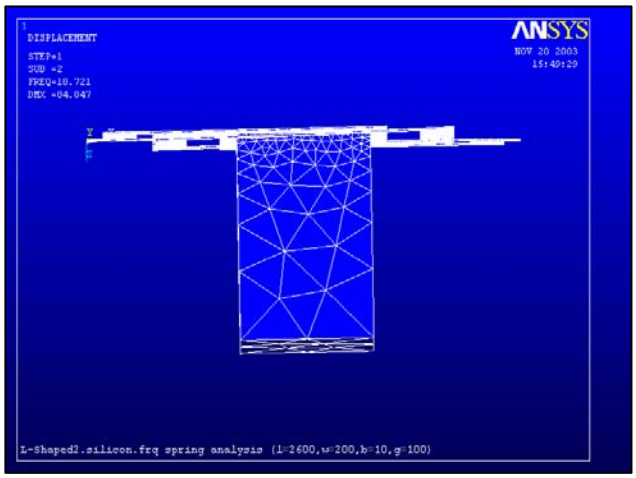

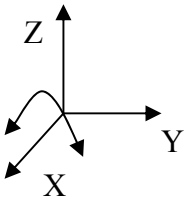

(c)

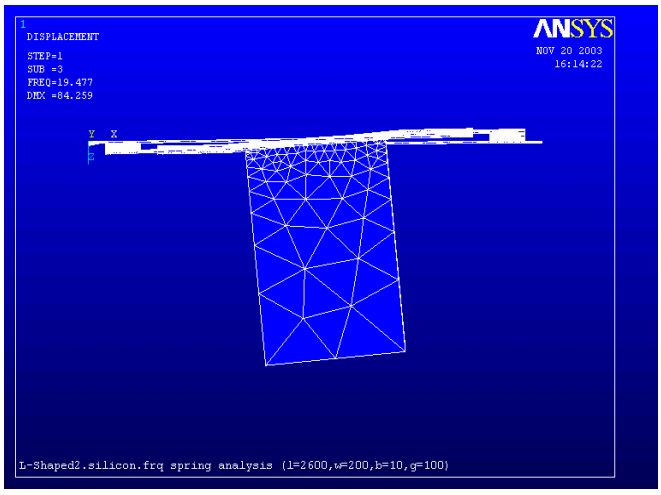

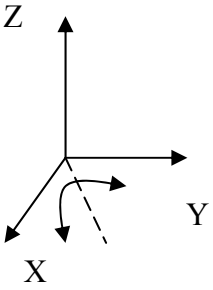

Fig.4.13 Simulation results of modal analysis of the L-shaped spring (a) first mode shape, (b) second mode shape, (c) third mode shape

Table 4.4 ANSYS results of L-Shaped2 modal analysis.

No. Of modes	Natural frequency (Hz)
Mode1	13.98
Mode2	17.79
Mode3	18.56

The ANSYS simulation results in Fig.4.13 show that the motion of the spring mass system (represented by the flat spring and the magnet) has three different resonant vibrations. Fig.4.13.a shows the first resonance mode where the spring and the mass move in vertical direction while in Fig.4.13 b,c it was observed that the spring mass system rotate and has second and third mode where the movement of the spring mass system is in horizontal direction. Table 4.4, shows the values of spring natural frequencies for the first three modes. It is clearly shown that the value of spring natural frequency in mode1 is less than its values in mode2 and mode3. The vibration results are in agreement with what was reported by Ching et al. [Ching et al., 2002]. If a spring is designed to have movements in horizontal direction with rotation, rather than in vertical direction relative to the coil, the generator will have more movements and then it produces more power. This can be explained by Faraday's law of induction which indicates that the voltage output should be proportional to the rate of changing magnetic of flux.

4.6 Power generation

Estimated output power has been calculated using the resonance frequencies of the L-Shaped2 spring. Theoretical model of electromagnetic micro generator and the power generating equation are given in chapter3.

Fig.4.14 shows the output power generation as a function of resonance frequencies of the selected spring. The spring resonance frequency of L-Shaped2 is applied to equation 2.10 at input vibration frequency of 3kHz with amplitude of 5μm. The spring mass system is assumed to be underdamped so the damping ratio is assumed to be 0.3. It was observed that the output power in the first mode is less than the output power in the second and third modes. It shows clearly that the electromagnetic microgenerator will produce more power when the input vibration matches the spring resonance frequencies in the horizontal direction

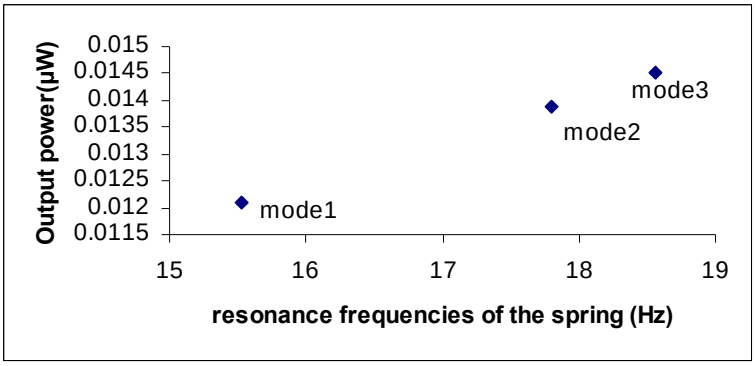

Fig.4.14 Calculated output power of three different resonant frequency modes.

The out put power can be optimized by:

1) Increase the mass size within the device size.

2) Adjust the spring constant to make the generator resonance frequency match the frequency of the vibration source.

4.7 Summary

Theoretical static and dynamic considerations were presented to characterize the mechanical behaviour of the spring. The spring design objectives and considerations were presented which are suitable for the use in the electromagnetic microgenerator. Finite element analysis was used to determine the deflection and the maximum displacement in Z- direction. The static and dynamic equations can be used to provide initial design parameters for each beam in the spring. These can be fed into the finite element model to more accurately assess the results. The graphs from the early finite element analyses can be used to assess which design parameters can be changed to provide the design with the deflection required. Once a final design has been assessed, a second finite element analysis should be preformed to validate the final design.

From the finite element model, it is found that each design parameter effects the deflection achievable from the gravitational force. That was in agreement with simple cantilever beam theory. It is found that decreasing or increasing the young's modulus (E), beam thickness; beam width and gaps between the beams can increase or decrease the deflection and the stiffness.

Model analysis was conducted to characterize the vibration behaviour of the spring and to choose the desirable mode of vibration. It was found that the motion of the spring mass system has three different resonant vibrations. The first resonance modes where the spring and the mass move in vertical direction while rotate in the second and third mode and have movement in horizontal direction. It is also observed that the value of natural frequency in vertical direction is less than its values in the horizontal direction and the natural frequencies in horizontal direction are very close on values. That leads to make the generator have more movements and then it produces

more power. This can be explained by Faraday's law of induction which indicates that the voltage output should be proportional to the rate of change of magnetic flux.

Chapter 5: Finite element modelling and analysis of magnetic behaviour of electromagnetic microgenerator

Finite element method has been used in this chapter for the analysis, and evaluation of the electromagnetic design of the microgenerator. The objectives of the magnetic analyses are to characterize the permanent magnet and to investigate the optimum position of the coil relative to the magnet. Output power is estimated using the ANSYS simulation results of the magnetic field induced on the coil. A comparison of the output power between the electromagnetic generators in the literature and the electromagnetic generator in this thesis is presented.

5.1 Electromagnet (coil)

Considering high inductance, low resistance and small size, in this research the coil is decided to be a wire wound coil. Coil design has been selected according to the mathematical model for a 3D coil in ref. [Wilson, 1948]. For a given dimensions of a coil, a mathematical model of calculating the number of turns and length of wire is used. In this mathematical model, a wound coil is considered.

There are two methods of calculating the number of turns and length of wire in a coil of given dimensions. Either the number of layers or turns per layer may be worked out from first principles the diameter of the wire being known. In this mathematical model a round wound coils will be assumed.

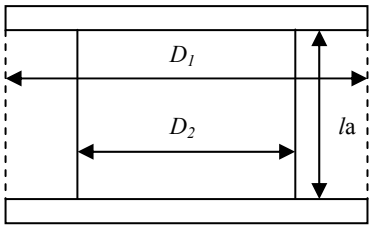

Fig. 5.1 Dimension of the coil

Fig.5.1 shows the schematic diagram of the coil. Assuming that the outside diameter D1, the inside diameter *D2*, and axial length *la* , are given; the following relationships could be derived. The winding depth and the sectional area of winding are given in Eq. (5.1) and Eq. (5.2) respectively.

$$\text{Winding depth} = \frac{1}{2}(D_1 - D_2) \quad \text{..... (5.1)}$$

Sectional area of winding $= \frac{1}{2} l_a (D_1 - D_2)$ …….…….…. (5.2)

The diameter and the length of mean turn can be derived as in equation (5.3) and equation (5.4). From these equations, the length of wire can be derived as in equation (5.5).

Diameter of mean turn $= \frac{1}{2}(D_1 + D_2)$ …….……. (5.3)

Length of mean turn $= \frac{1}{2}\pi(D_1 + D_2)$ …….…….. (5.4)

Length of wire = $n \times$ length of mean turn

$= \frac{1}{2}\pi n(D_1 + D_2)$ …….……..……..…..……. (5.5)

Where n= total number of turns of wire

Equation (5.5) provides the method of finding n depends on several conditions, such as the thickness of insulation and the method of winding and needs to be found by actual practice for each set of conditions. Calculation from first principles is quite an accurate method, and does not require any experimental work. By assuming:

Turns per layer = $\frac{l_a}{d_1}$ …….…….. ..(5.6)

Where d_1 = covered diameter of wire

Number of layers = $\frac{depth}{d_1}$

$$= \frac{\frac{1}{2}(D_1 - D_2)}{d_1} \quad \text{..... (5.7)}$$

Total turns $= n = \frac{l_a}{d_1} \times \frac{\frac{1}{2}(D_1 - D_2)}{d_1}$

$$= \frac{\frac{1}{2} l_a (D_1 - D_2)}{d_1^{\,2}} \quad \text{..... (5.8)}$$

Or $$d_1 = \sqrt{\frac{l_a (D_1 - D_2)}{2n}} \quad \text{..... (5.9)}$$

This method assumes, first, that the successive layers ride over one another, and secondly, that the work of winding is accomplished neatly, that is, without waste of space.

By combining equation (5.5) and equation(5.8), the length of wire could be derived as,

Length of wire $l_c = \frac{\frac{1}{2}\pi(D_1 + D_2) \times \frac{1}{2} l_a (D_1 - D_2)}{d_1^{\,2}}$

$$= \frac{\frac{1}{2}\pi l_a (D^2{}_1 - D^2{}_2)}{d_1^{\,2}} \quad \text{..... (5.10)}$$

As regards the proportions of the coil itself, it is found that for general purposes the most efficient shape is one n which D1=about 3D2, and l =D1 approximately.

To calculate the resistance of the wire:

$$R= \rho.\frac{l_c}{A} \quad \text{..... (5.11)}$$

Where l_c = total length of wire, and ρ = resistively of copper, A= is the wire cross sectional area.

$$R= \frac{l_c \rho}{\frac{1}{4}\pi d_1^2} \quad \text{..... (5.12)}$$

The selected parameters for the coil are as in table 5.1. In the proposed generator design the coil is attached to the outer frame of the spring, therefore, the coil dimensions were selected to be as close as possible to the outer dimension of the spring and then the coil will be close to the moving magnet. Also the coil material was selected according to the availability in RMIT University

Table 5.1 Coil parameters

Inner diameter, D2	2.6mm
Outer diameter,D1	3mm
Wire material	Copper
Resistance, ρ	1.72 X 10-8Ω
Wire diameter, d1	0.025mm
Axial length, la	0.15mm

The coil dimensions that will be used for the magnetic analysis is listed in table 5.2

Table 5.2 Calculation of coil dimensions

Sectional area of coil winding	0.03 mm^2	Equation (5.2)
Coil resistance	14.7 Ω	Equation (5.12)
No. of coil turn	48	Equation (5.8)
coil wire length	422.016mm	Equation (5.10)
length of the mean turn	8.792mm	Equation (5.4)

5.2 Finite element model

The schematic configuration of the electromagnetic microgenerator is illustrated in Fig.5.2.

This electromagnetic microgenerator mainly consists of a flat spring with an attached permanent magnet and copper coil wound around the magnet. When the flat spring is deflected, the magnet will have a displacement and will move towards the coil. An induced voltage will be generated across the coil due to the varying of magnet flux lines by the coil. The Finite Element Analysis will calculate the magnetic flux density on the coil. As shown in Fig.5.3, the FEA model is represented by the magnet and the coil.

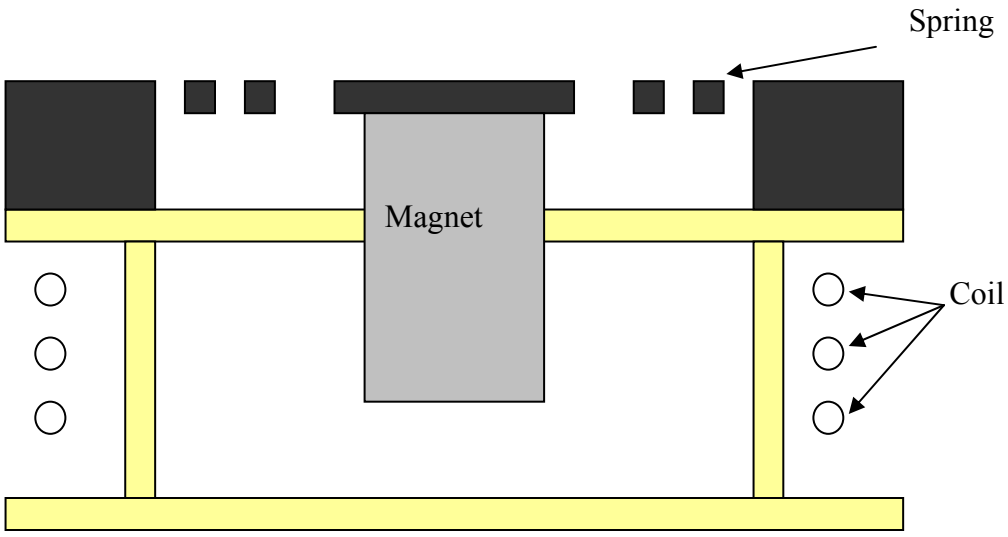

Fig.5.2 Schematic diagram showing the electromagnetic microgenerator

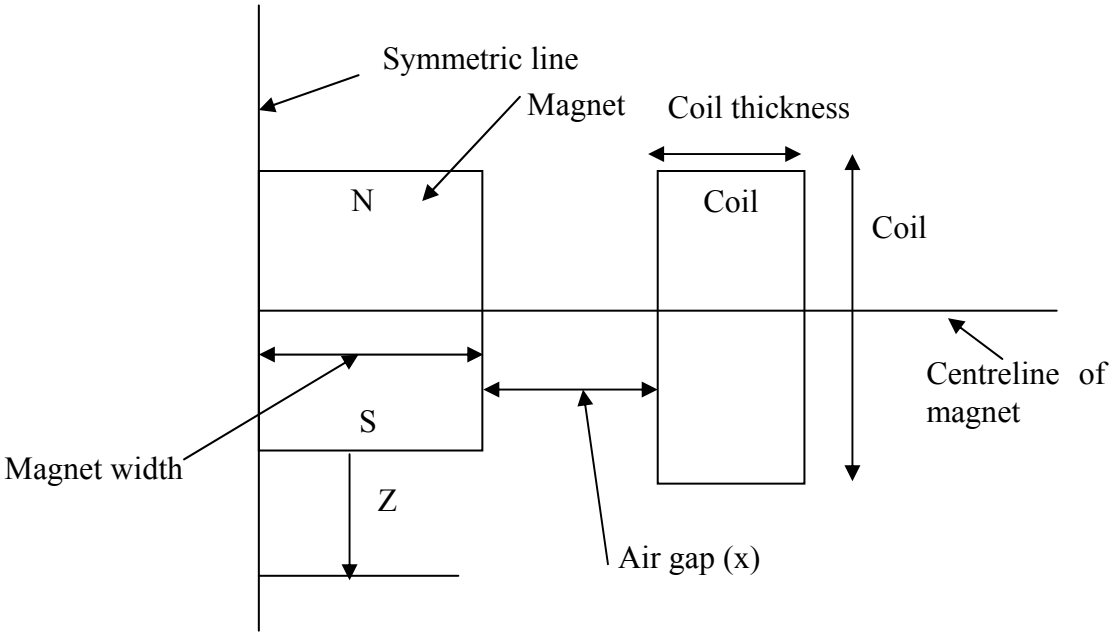

Fig.5.3 The FEA model: Schematic diagram of the magnet and the coil of the microgenerator

5.3 ANSYS magnetic analysis of the microgenerator

Finite element analysis is often used to calculate the magnetic field in devices such as power generators, transformers, video display devices and so forth. FEA package (ANSYS 8.1) is used to analyse the magnetic characteristics of the electromagnetic microgenerator. 2D magnetic static analysis is used to determine the magnetic field caused by the permanent magnet. The aims behind the magnetic analysis are: 1) to determine the magnetic field patterns of the permanent magnet at the initial position, 2) To investigate the distribution of the magnetic flux across the coil. The model comprises of a coil, permanent magnet and the surrounding air.

A two dimensional model is constructed to investigate the optimal configuration. In ANSYS simulation, the 2D element PLANE13 (2D coupled field solid, 4-node with four degree of freedom per node) was applied to all interior regions of the model, including the permanent magnet region, the coil region and considerable region of the surrounding space, while the edge of the whole model is modelled by INFINI 10 element to simulate an infinite extension of the surrounding air. Because the elements are two dimensional, each node has only one vector potential degree of freedom AZ (vector potential in Z direction).The INFINI 10 element has non-linear magnetic capabilities for modelling B-H curves or permanent magnet demagnetization curves. When used in structural analysis it has large deflection, large strain and stress stiffening capabilities.

To build the model of the magnet-coil system as it is shown in Fig.5.4. The outer large area represents infinite boundary. The inner area represents the air surrounding the magnetic field. The permanent magnet and the coil represented by two poles. The magnet coil system is assumed to be axis-symmetric.

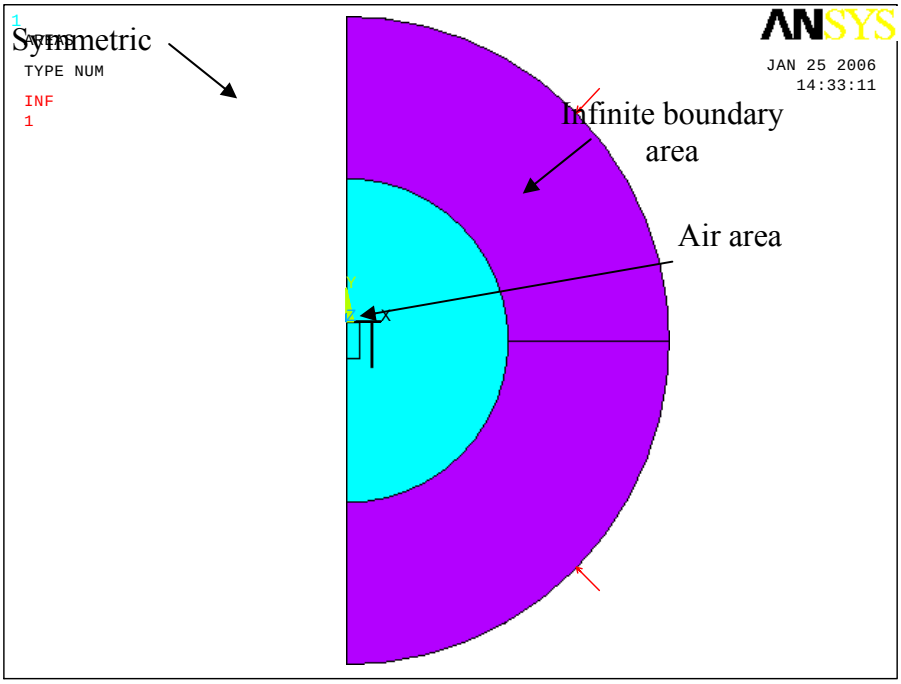

Fig.5.4 2D model used for static analysis

Table 5.3 lists all these properties for the different regions existing within a 2-D magnetic model.

Table 5.3 Material properties in the 2D magnetic model

Air	Relative permeability, $\mu_0 = 4\pi \times 10^{-7} N/A^2$
Permanent magnet	the NdFeB (Neodymium Iron Boron) with density of 7.5g/cm^3 and mass of 5.76mg
coil	relative permeability for copper=1

The permanent magnet Neodymium-iron-boron (NdFeB) has Br=8k Gauss and high corctivity of Hc=5.2KOe are selected to characterize the permanent magnet. The coil is modelled using the relative permeability material of copper as it is selected for its high conductivity. The relative permittivity of air and copper is 1.

ANSYS files with all the static magnetic analysis commands is presented in Appendix A3.

5.4 Effect of FEM meshing size on the result accuracy

Meshing is an important step for finite element analysis. The dimensions of the elements determine the precision of the result. Smaller dimension of the elements yield more precise simulation results, but require a longer time to perform the simulation. Therefore, suitable dimensions of the elements need to be chosen for different models. Before meshing, the physical attributes of material properties have to be assigned to the corresponding areas. In this design, material properties are assigned to the regions of air, copper coil, and permanent magnet.

5.5 Review of results

The flux line distribution of this magnetic system is shown in Fig.5.5. It yields a 2D model of the magnet-coil system and the flux lines of the permanent magnet in two dimensional spaces. The basic assumption for the model is that the magnet and the coil are placed in the same level. The analysis is preformed on the model developed in two steps. The first step is to calculate the magnetic field component of the magnet. The second step is changing the separation distance between the magnet and the coil to determine the magnetic field and flux distribution on the coil nodes.

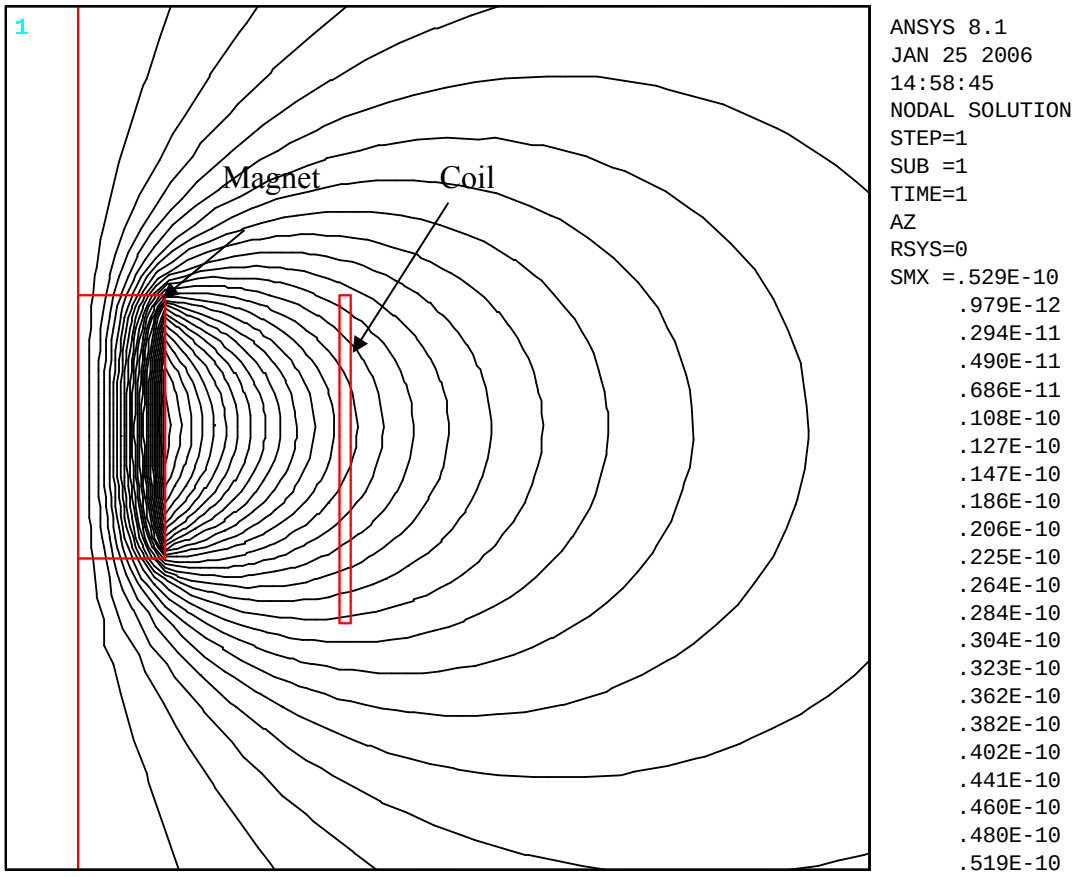

Fig.5.5 Simulation results of magnetic flux distribution of permanent magnet in 2-dimentional space

5.6 Characterization of the permanent magnet

Flux density is an important characteristic in the analysis of electromagnetic devices. By calculating flux densities in different regions of the magnetic circuit, EMF (Electro Motive Force) can be determined and optimum location of the coil can be achieved. A constant magnetic field is provided by the permanent magnet. FEA is used to simulate the magnetic field. Theoretical approach of the permanent magnet was used. The objective of the theoretical analyses was to characterize the permanent magnet and to verify the FEA results. By assuming the magnet to be infinitely long along the z-axis as in Fig.5.6 the problem was reduced to a simpler 2D field problem.

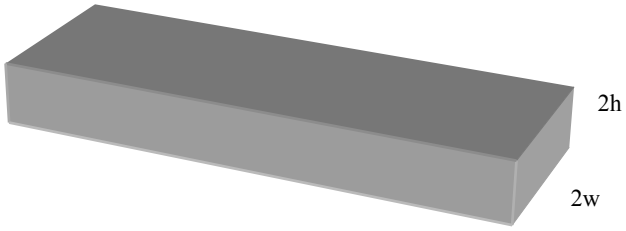

Fig. 5.6 Rectangular magnet of infinite length

The permanent magnet was modelled using the current model [Furlani, 2001]. In this model, the permanent magnet is reduced to a distribution of equivalent currents as shown in Fig.5.7.This is then input into the magnetostatic field equations as a source term, and the field is obtained using standard methods for steady currents.

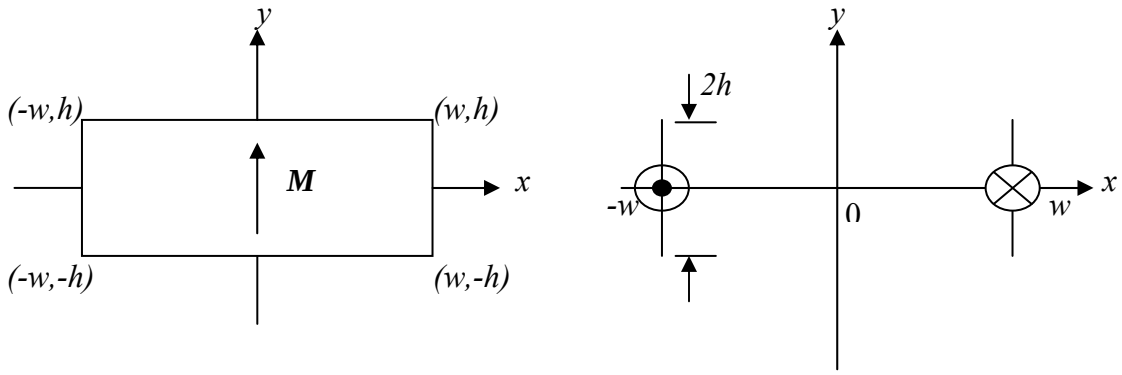

Fig.5.7 Infinitely long rectangular magnet (a) Cross-sectional view, and (b) Equivalent surface current

The components of the magnetic flux density vector of the rectangular magnet at a general point (x, y) outside the magnet are given by the following equations [Furlani, 2001].

$$B_x(x,y) = \frac{\mu_o M_s}{4\pi}\left\{\ln\left[\frac{(x+w)^2+(y-h)^2}{(x+w)^2+(y+h)^2}\right]-\ln\left[\frac{(x-w)^2+(y-h)^2}{(x-w)^2+(y+h)^2}\right]\right\} \quad \text{..... (5.13)}$$

$$B_y(x,y) = \frac{\mu_o M_s}{2\pi}\left\{\tan^{-1}\left[\frac{2h(x+w)}{(x+w)^2+y^2-h^2}\right]-\tan^{-1}\left[\frac{2h(x-w)}{(x-w)^2+y^2-h^2}\right]\right\} \quad \text{..... (5.14)}$$

Numerical results were computed from the above equations for the case of NdFeB permanent magnets with Br = 8k Gauss, Hc = 5.2 × 103 A/m and Ms = 1.83 × 105 A/m, having a volume of 0.8×0.8×1.2 mm^3 and magnetized along the y-axis. The same magnets were simulated in ANSYS to determine their magnetic field patterns. Fig.5.8 shows the magnetic flux pattern of the permanent magnet obtained by FEA simulation within the region defined by the infinite boundary elements.

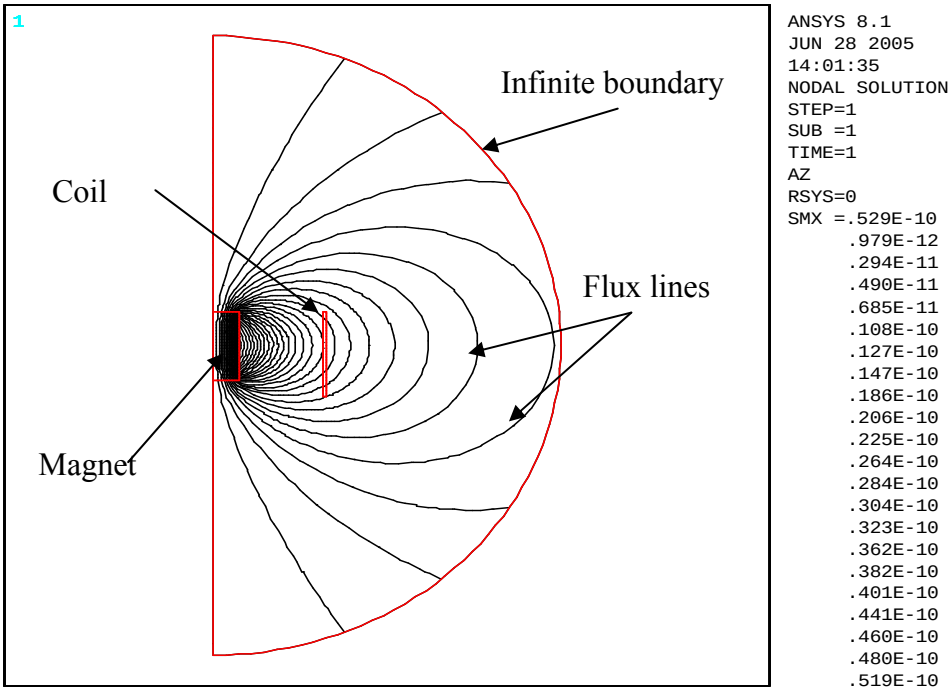

Fig.5.8 Magnetic flux pattern

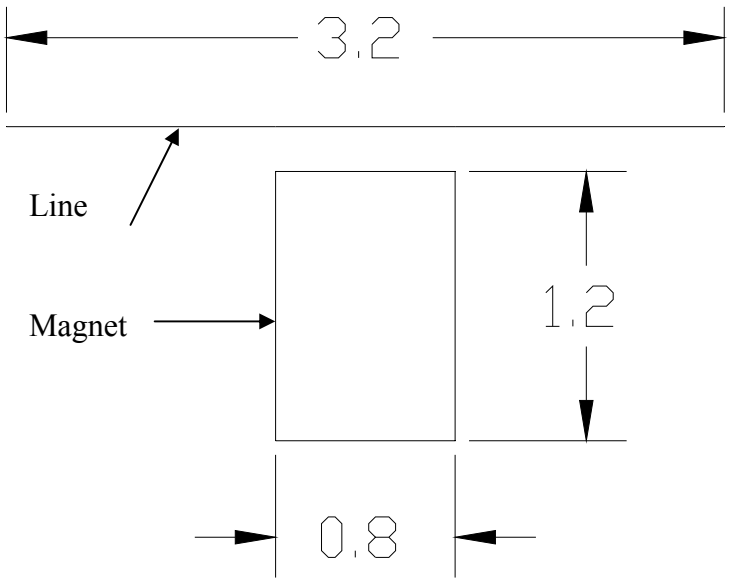

Fig. 5-9 Magnet dimensions in millimetres with a line 0.2 millimetres above the magnet pole.

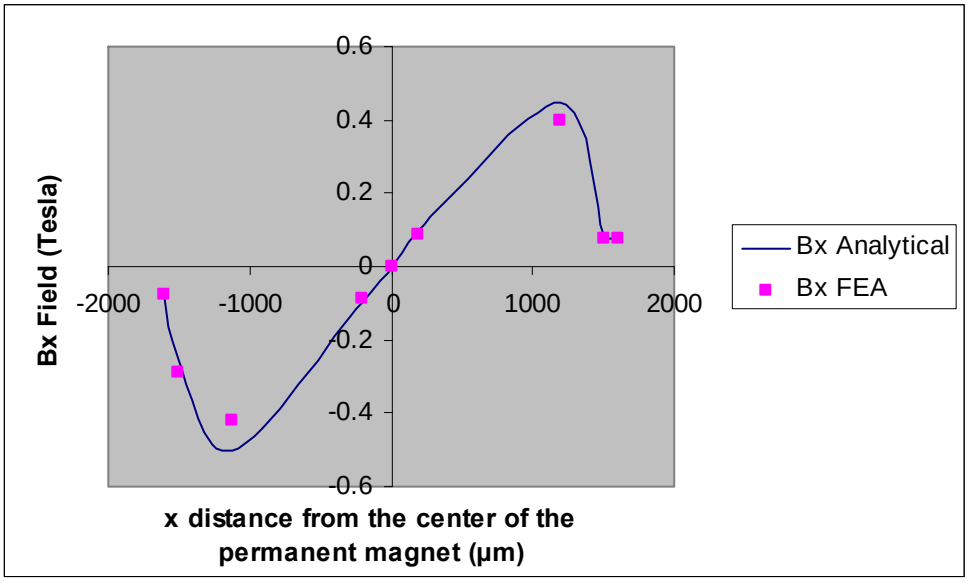

a)

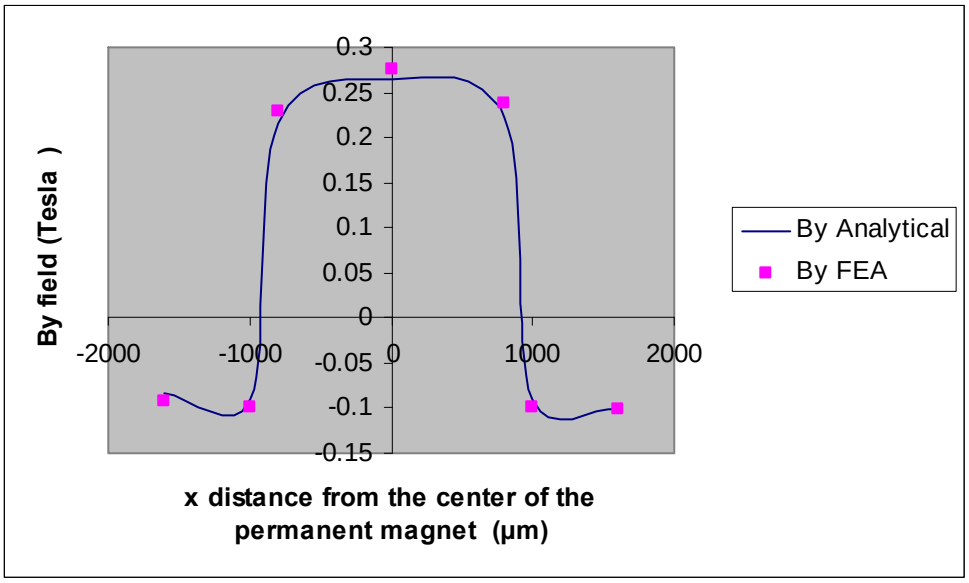

b)

Fig.5.10 The magnetic field components a) Bx and b) By for -2w>x<2w where w is 1600 microns and y is 800 microns

Fig.5.10 shows the magnetic field components at points along a line at a distance of 200 µm above the permanent magnet. There is close agreement between the finite FEA results and the analytical results. Fig.5.10.a shows the that the horizontal component Bx peaks a above the edge of the permanent magnet, while Fig.5.10.b shows BY component reaches its peak value at the point directly above the centre of the top pole face. The BY component is significantly higher in magnitude than the BX component. The reason for this is that near the magnet, the field is predominantly vertical across the entire surface and has a grater magnitude closer the ends of the magnet. However, as you may move away from the magnet, the vertical projection of the field decreases dramatically near the ends of the magnet and this result in a peak value in the centre.

5.7 FEA to calculate the magnet-coil separation

The objective of this analysis is the determination of the optimum position of the electric coil relative to the permanent magnet in the magnetic circuit. The optimum position of the electric coil is meant the position at which the magnetic induction field is at its maximum value. The only limitation of the distance of the coil and the magnet is the spring dimensions as the magnet is attached to it. In ANSYS simulation the applied distance is (x) starts from 200µm to 1000µm. The magnet is at the initial position. The outcome is the magnetic induction field (B) on each node of the coil. Only rectangular permanent magnet is considered with dimensions of 0.8×0.8×1.2 mm^3, while the wound coil was modelled in the FEA by a rectangular area of 1.5×0.005mm.

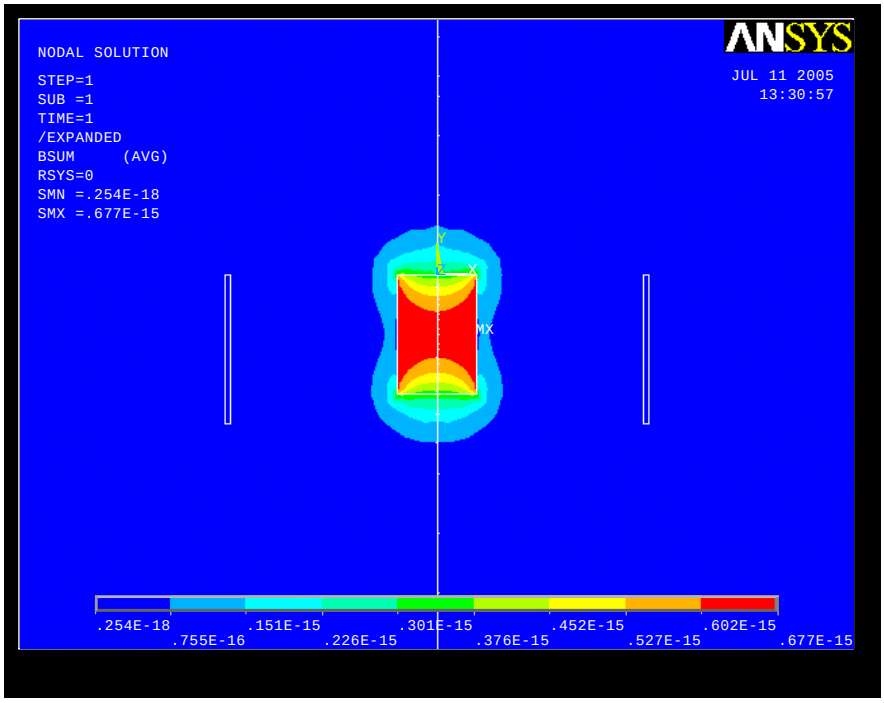

a) X=1000µm

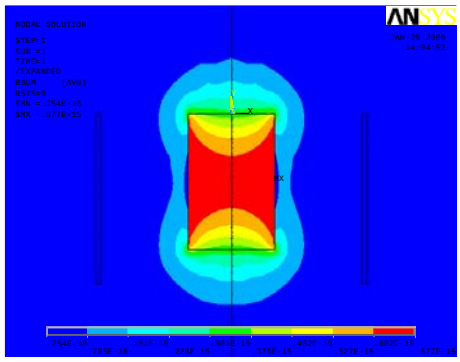

b) X= 800µm

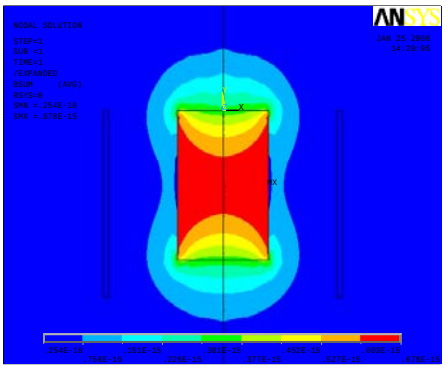

c) X= 600µm

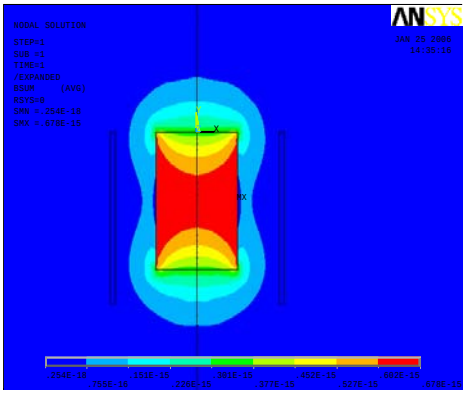

d) X= 400µm

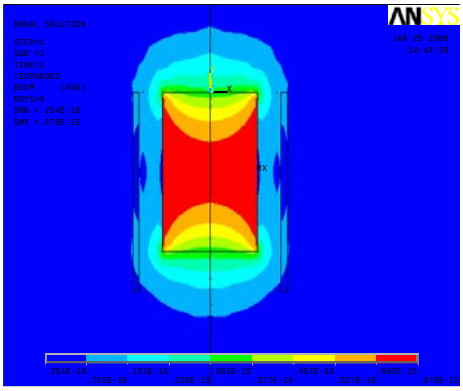

e) X= 200µm

Fig. 5.11 The magnetic induction field B for a range of values of X at initial position

The simulated results of magnetic field density are shown in Fig.5.11 the magnetic field is at maximum values in the middle of the magnet and as the separation distance is reduced the coil pole seems to be much closer to the highest density of the magnetic field.

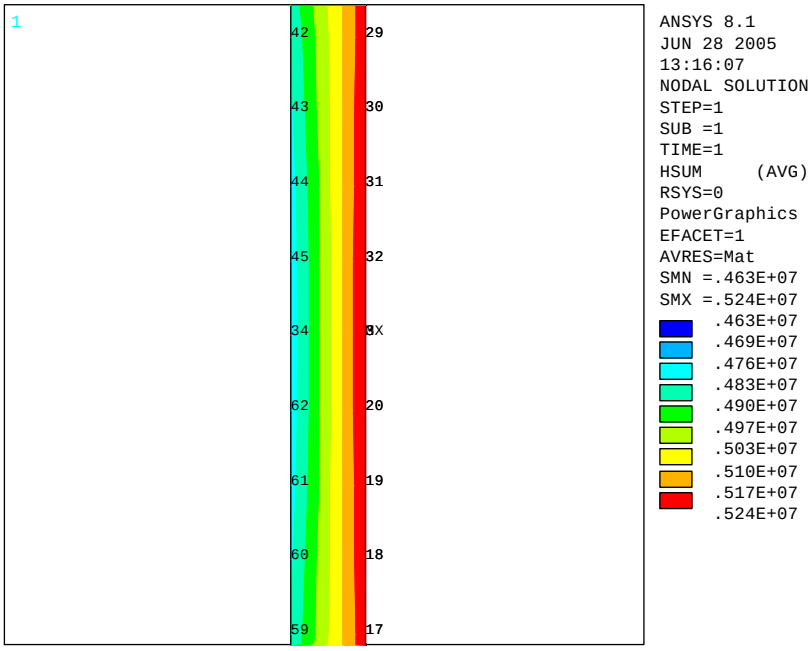

(a)

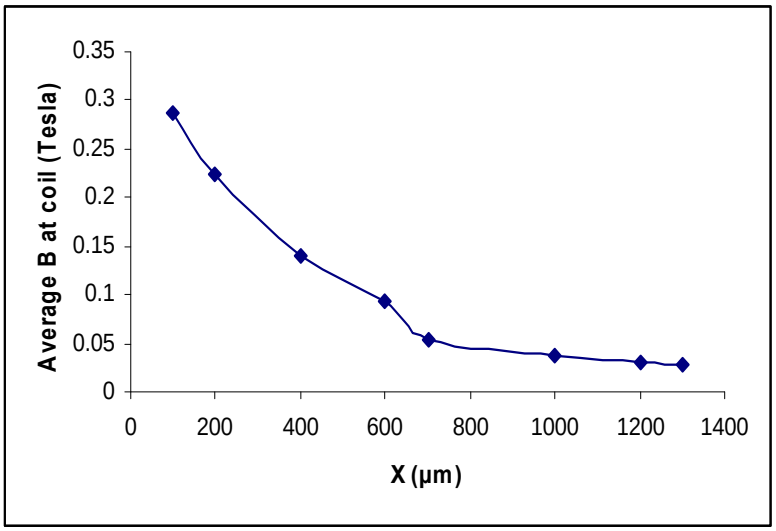

(b)

Fig.5.12 a) ANSYS results of magnetic density B at the coil nods b) average B versus distance between the coil ant the magnet

As shown in Fig.5.12 a and b the magnetic field, *B* on the coil nodes seems to increase with the reduction in the distance between the magnet and the coil. The magnetic field density B in the coil pole is calculated by computing the magnetic field density along a number of nodes and taking the average. The maximum value of the magnetic field is 0.28 Tesla. These results of magnetic field density are close in values to the result obtained by Kulkarni et.al [Kulkarni et.al, 2006]. This indicates that the closer the coil to the magnet, the larger the induced magnetic field on the coil. However, the distance is limited by the spring dimension and the size of the generator. This shows that the magnetic field can be optimized by reducing the distance between the coil and the magnet.

5.8 Estimated Voltage and output power

The voltage and output power generated by the electromagnetic power generator are obtained using the simulation results of the magnetic field from the section 5.7. For maximum power output, the resonance frequency of the electromagnetic power generator should match the frequency of external vibrations. The value of frequency is taken as 13.98 Hz from simulation result of the model analysis of the flat spring in chapter 4. An input velocity is given by equation (3.3). It is also assumed that the generator has a coil with N turns all of the same area *A* (as mentioned in table 5.2) and the magnet is moving in a variable velocity towards the coil. The applied displacements are taken from the structural analyses in chapter 4, table 4.3. Copper material is used for the coil. The calculation results in table 5.2 are used to get the coil resistance of 14.7Ω and estimate the load resistance as 15 Ω to match the coil resistance [Williams et. al., 2001]. The output voltage and power is calculated using equations (3.2) and (3.9) respectively.

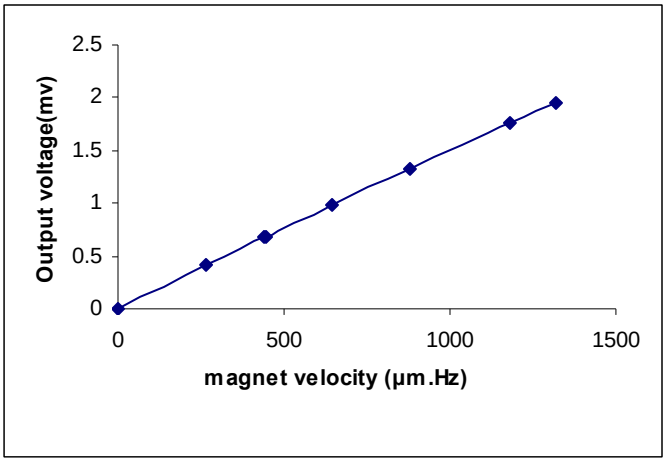

(a)

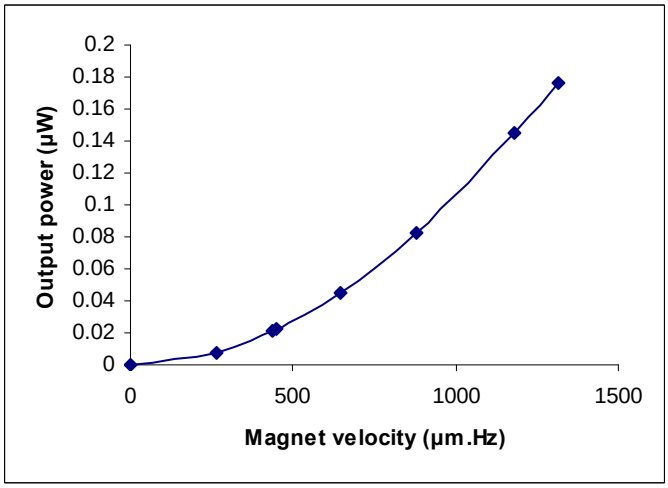

(b)

Fig.5.13 a) The output voltage. b) The output power at different magnet velocity

Fig.5.13 clearly shows that the voltage and the output power are dramatically increased as the magnet velocity gave an increase in the magnetic flux rate ($d\varphi/dt$). It is observed that the

maximum voltage is 1.95 μV and the maximum power is 1.76μW when the magnet velocity reaches 1316.9 μm.Hz.

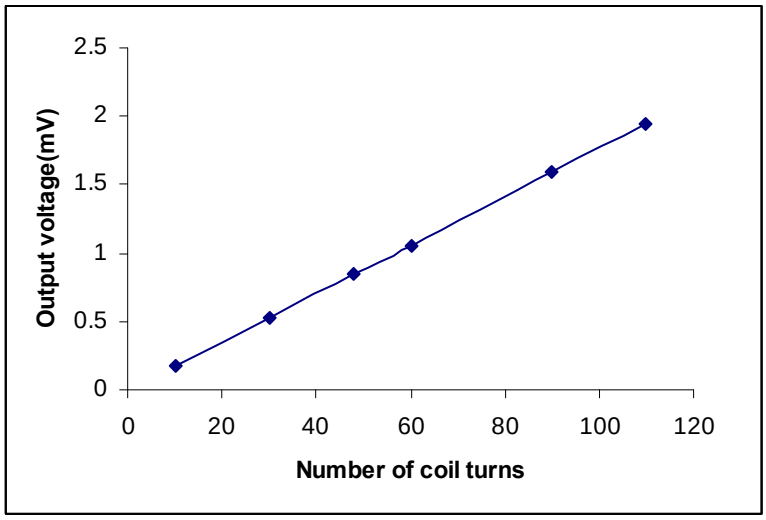

(a)

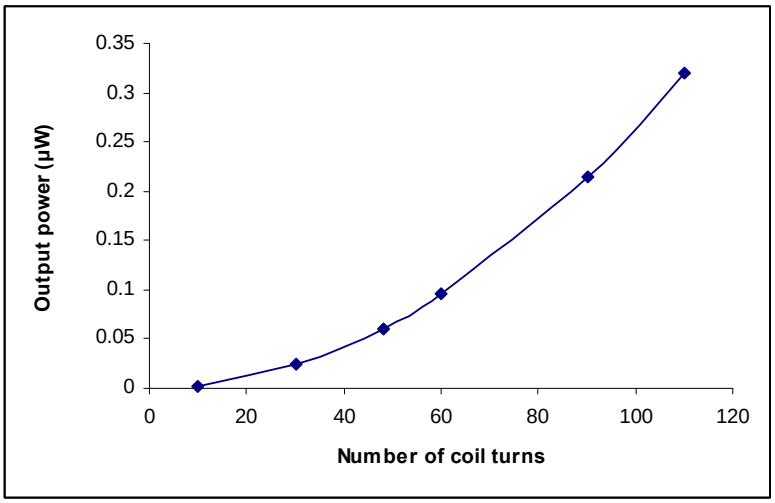

(b)

Fig 5.14 a), b) output voltage and power versus number of coil turns.

In Fig 5.14a,b, the output voltage and output power increase with number of coil turns. The maximum output voltage is 1.9mV while the output power shows a maximum value of 0.32 μW with a coil of 110 turns and a load resistance of 15Ω. From equation 3.2 and Fig.5.14a it is clear that an increase in the number of turns lead to an increase in the generated voltage. In the same time the increase in the number of turns leads to an increase in the coil resistance. The value of load resistance has to be varied to keep the damping factor constant for the flat spring to resonate at 13.43μm. The maximum values for voltage and power are close in values to the result published by Huang et.al. [Huang et.al.,2007].

5.9 Design evaluation

100 Hz is assumed to be the natural frequency of the generator to prove the design principal based on a practical amount of vibration out of a 1hp motor. The dimensions of the spring, coil and magnet were based on the over all size of the generator without specifying the material for each one. Also, the displacement of the generator is based on the proposed model in section 3.3. While, 13.89Hz is resulted from the FEM analyses and comes from selecting the dimension of the spring and its material properties. The classical formulae describing the dependence of mechanical resonance frequency on geometrical and material properties are valid for all modelled designs using finite element analysis.($f = \frac{1}{2\pi}\sqrt{\frac{k}{m}}$ ……..4.5).

Table 5.4 Maximum out put voltage and power of the electromagnetic generator

Electromagnetic microgenerator	Frequency	Voltage output	Power output	Reference
Analytical equations	100 Hz	150.9 mV	$1.754\times10^{5}\mu W$	Fig .3.14a,b
Simulation	Free Vibration	195 μV	1.76 μW	Fig.5.14a,b

Table 5.4 shows the results of the maximum out put voltage and power of the electromagnetic generator at maximum coil turns. The analytical results show the output power and voltage under force vibration of an electric motor, this study was to maximize the potential applicability of the microgenerator. While the simulation results are under the free vibration (the free vibration term means that the generator is under a gravitational force only**)**. This study was to investigate the performance of the generator under the gravitation force. Both results were for a generator in micro level size. The values of the output voltage and power of the analytical equation are higher than the values of the power and voltage in the simulation and that is due to the fact the generator works better under force vibration.

5.10 Summary

To justify the selection of the NdFeB as a magnetic material for the electromagnetic microgenerator, FEA using ANSYS magnetic analyses was conducting to characterize the permanent magnet at initial position. It is found that the magnetic field of the permanent magnet

in the vertical direction represented by By is higher in magnitude than the magnetic field in the horizontal direction represented by Bx .

FEA was then used to investigate the optimum location of the coil in relation to the permanent magnet. The results showed that the maximum magnetic field of 0.28 Tesla could be obtained on the coil if the coil is as close as 100μm to the magnet. By providing the FEA results and using voltage and output power equations, the effect of varying the coil turns in the output voltage and power has been investigated. The maximum voltage and power are 1.9mV and 0.32 μW, for an input frequency of 13.98Hz.

Chapter 6: Conclusions

A comparison of the various electromagnetic microgenerator designs has been discussed through the literature review of this thesis and power supplies for MEMS devices have been briefly demonstrated. This thesis describes the design of a new electromagnetic microgenerator. The analysis of a new flat spring and the selection of a number of coils of the generator are also presented. The electromagnetic generators in the literature can be classified according to: their moving element part, coil and magnet shapes, input vibration and or the device volume. The general guide lines for efficient electromagnetic microgenerator design have been concluded. Theses guide lines was undertaken for further study the generator model through analytical investigations and parametric study. A brief review about the springs design was also presented. It was focusing on the improving of the beam deflection of the spring from first design with one cantilever beam to the design of a spring with a platform and four cantilever beams.

The proposed electromagnetic generator was modelled and analysed under force vibration (vibration out the motor cover) to prove the design principal and increase the applicability of the generator.

The first key component of the electromagnetic microgenerator is a flat spring. The main contribution of this thesis is the new modelling and simulation of a flexible flat spring with a platform and beams. Different beam configuration and different spring materials has been investigated. This analysis was performed using the commercially available FEA software tool - ANSYS. The main goal was the investigation of the design parameters in order to achieve the largest possible spring deflection. The simulation results of four flat springs with different type of beam configuration indicated that a flat spring with L-shaped beams could produce more

deflection under free vibration compared to the other shapes of the flat springs. The improvements in deflection may be attributed to the reduced stiffness and increased beam length. Model analysis was conducted to characterize the vibration behaviour of the spring and to choose the desirable mode of vibration. It was found that the motion of the spring mass system has three different resonant vibrations. The first resonance modes where the spring and the mass move in vertical direction while rotate in the second and third mode and have movement in horizontal direction. That leads to make the generator have more movements and then it produces more power.

FEA using ANSYS magnetic analyses was conducting to characterize the permanent magnet at initial position. It is found that the magnetic field of the permanent magnet in the vertical direction is higher in magnitude than the magnetic field in the horizontal direction. FEA was then used to investigate the magnetic forces acting on the coil. The results showed that the maximum magnetic field could be obtained if the coil is as close as 100μm to the magnet.

6.1 Comparison study of the electromagnetic microgenerator

A comparison study between the electromagnetic generator in the literature and the electromagnetic generator in this thesis concluded that the generator presented in this thesis aims to generate significant power from low frequency.

Table 6.1 Comparison between the reported electromagnetic generators based on moving magnet.

Ref.(Year)	Resonance frequency (Hz)	Power (μw)	Voltage	Device volume	
Shearwood et.al, (1997)	440	0.3		$5\times5\times1$ mm^3	Measured
Ching et.al. (2002)	110	830		1 cm^3	Measured
Kulah and Najafi (2004)	25, 11000	2.5, 4nw		4 cm^3, 2 cm^3	Simulated/Measured
Glynne-Jones et.al .(2004)	322	180		0.84 cm^3	Measured
Pan et.al.(2006)	60	100		0.45 cm^3	Measured
Wang et. al.(2007)	121.25		60mV		Measured
Serre et. .al (2008)	360	200nw			Measured
Kulkarni et.al. (2008)	60	584nw		150 mm^3	Measured
The electromagnetic generator of this thesis	13.98	1.76	195 μV	$5\times5\times2$ mm^3	Simulated

Table 6.1 shows a comparison between the reported electromagnetic generators based on moving magnet. The comparison based on the resonance frequency, output power, output voltage and the volume of the generators. This table also shows that the output power and voltage of this thesis

electromagnetic generator does not show the best performance compared to other generators. This is due to the majority of the reported generators have resonant frequencies of tens of Hz whereas the generator of this thesis has frequency of 13.98. The average of the generated electrical power from vibration generators is related to frequency cubed [Williams et.al., 2001] and the frequency of all reported prototype generators are more than 25 Hz. The generator presented in this thesis aims to generate significant power from low frequency.

An electromagnetic microgenerator published by Wang et.al. [Wang et.al., 2007] was selected for closer and detailed comparison with this thesis generator. This selection was due to the similarity in the design of the resonator spring of both generators.

Table 6.2 Comparison between of the electromagnetic microgenerator of this thesis and the microgenerator published by Wang et.al. [Wang et.al., 2007].

Dimensions	**Electromagnetic generator of this thesis**	**Wang et.al. [**Wang et.al., 2007**]**
Spring	(2600x2600 x10)μ m^3	(950x950x20) μ m^3
Magnet	(0.8x0.8x1.2) mm^3	(2x2x1) mm^3
Coil	48 turns	30 turns
Platform size	(1000x1000x10) μ m^3	(3000x3000x20) μ m^3
Natural frequencies (simulated results)	13.98Hz, 17.79Hz, 18.56Hz	48.586 Hz, 146.72Hz, 146.89Hz
Output voltage and power	1.76 μw, 195 μV (simulated)	60mV (measured)

Table 6.1 shows a comparison of the dimensions, the o/p power and voltage between the electromagnetic microgenerator of this thesis and the microgenerator published by Wang et.al. [Wang et.al., 2007].

The dimension of the flat spring and coil size are larger than one designed by Wang et.al., while the magnet and the platform are smaller in size.

The natural frequency of the flat spring in this thesis is less than the natural frequency of the spring designed by Wang et.al. However both springs have second and third mode of vibration close in values.

The spring beam in Wang et.al. generator was design with circular spring corner instead of right angle corner to reduce the stress intensity of the spring. The spring was fabricated by copper electroplating technique in a silicon substrate instead of silicon spring. That was because the copper has lower young's modulus than that of silicon. Although copper's yield strength is lower than that of silicon so they need extra care when designing the spring to make the maximum stress of copper spring below its yield strength.

The 2-layer coil was fabricated by copper electroplating on a glass substrate, while the coil in this thesis is winding coil to get maximum number of turns.

Finally, the Wang et.al. Generator was assembled by attaching the magnet in the centre of the spring and the two substrates were glued. The generator was tested and the out put voltage was 60mV. This generator also has three resonance frequency and they are comparatively match with simulated resonance frequencies. The voltage result of Wang et.al. is higher than the output voltage results of the generator in this thesis.

6.2 Suggestions for Future Work

Electromagnetic microgenerator represents an ideal power solution for MEMS applications because of its potential to power MEMS devices indefinitely. However, more work need to be done in the field of vibration to electricity conversion. A few issues that can be an extension of this research are presented below.

Only limited numbers of design configurations have been evaluated in this study. Other design configurations that have better mechanical characteristics, and potentially higher power outputs should be evaluated. More effort needs to be done to improve the electromagnetic microgenerator design for example the flat spring could be designed with holes on the beams to allow vacuum operation or consider using different spring materials.

A more detailed simulation study of the spring deflection would help to improve its stiffness further in achieving high deflection. More comprehensive work is required in modelling and fabrication of the springs and studying their effects on the output power. Work is needed to consider the spring behaviour under other environmental vibrations.

Detailed electromagnetic simulation studies of the coil and the magnet are needed such as:

(i) changing the magnet size and calculate the B_x and B_y and also B at the coil node (ii) changing the coil size and calculate the B at the coil nodes. (iv) Adding a core made of ferromagnetic material to the coil and do more simulation work to calculate the B. (v) from the coil theoretical model we can vary the coil parameters and get different length and thickness of the coil to apply it to the ANSYS analysis.

The most challenging aspect of any MEMS project is the design of the processing steps that are required to batch-fabricate the device. Many problems that are not foreseen during the design phase are very likely to crop up when attempting to fabricate the device. Only by fabrication and evaluation of a number of prototype electromagnetic microgenerators, the proof of concept of the electromagnetic microgenerator could be established. Experimental results can be used to validate the FEA results.

Appendix A

A1 ANSYS Input File: Mechanical Analyses

```
/TITLE, STRUCTURAL ANLYSIS OF THE FLAT SPRING DEFLECTION
/UNITS, mks
! objective: to investigate the large displacement of the flat spring.
!          Initialise variables
!
*DIM,E,Array,4,1,1
E(1,1)=190000,110000,75000,3000
*DIM,L,Array,4,1,1
L(1,1)=2600,2800,2900,3000
*DIM,b,Array,4,1,1
b(1,1)=10,15,20,25
*DIM,g,Array,4,1,1
g(1,1)=50,100,150,200
*DIM,w,Array,4,1,1
w(1,1)=100,150,200,250
*DIM,P,Array,4,1,1
P(1,1)=0.22,0.35,0.31,0.22
*SET,c,1000
```

```
!    **********************
!        OPEN OUTPUT FILE
!    **********************
*CFOPEN,L_Shaped.all.2,out,D:\L_Shaped2,
*VWRITE,'E','p','L','b','g','W','uz_max'
 ('No.      ',A1,'         ',A1,'        ',A1,'      ',A1,'    ',A1,'    ',A1,'        ',A6)
 *CFCLOS
count =0
/PREP7

!    ****************************************************
!         SELECT ELEMENT TYPE AND MATERIAL PROPERTIES
!       ****************************************************
*DO,E_num,1,4,1
*DO,l_num,1,4,1
*DO,b_num,1,4,1
*DO,g_num,1,4,1
*DO,w_num,1,4,1
E_Val= E(E_Num)
l_Val= l(l_Num)
B_Val= b(b_Num)
g_val= g(g_Num)
w_Val= w(w_Num)
P_val=p(E_Num)
```

```
/PREP7
ET,1,SOLID92
KEYOPT,1,5,2
KEYOPT,1,6,0
MPTEMP,,,,,,,,
MPTEMP,1,0
MPDATA,EX,1,,E_Val
MPDATA,PRXY,1,,P_val
!      **********************************
!       CREATE THE FLAT SPRING MODEL
!    ************************************
RECTNG,g_val,g_val+w_Val,0,l_Val-2*g_val-w_Val
RECTNG,0,l_Val-2*g_val-w_Val,l_Val-g_val-w_Val,l_Val-g_val
RECTNG,l_Val-g_val-w_Val,l_Val-g_val,2*g_val+w_Val,l_Val
RECTNG,2*g_val+w_Val,l_Val,g_val,g_val+w_Val
RECTNG,g_val+w_Val,l_Val-2*g_val-2*w_Val-(l_Val-4*g_val-4*w_Val-c)/2,l_Val-2*g_val-
2*w_Val,l_Val-2*g_val-w_Val
RECTNG,l_Val-2*g_val-2*w_Val,l_Val-2*g_val-w_Val,2*g_val+2*w_Val+(l_Val-4*g_val-
4*w_Val-c)/2,l_Val-g_val-w_Val
RECTNG,2*g_val+2*w_Val+(l_Val-4*g_val-4*w_Val-c)/2,l_Val-g_val-
w_Val,2*g_val+w_Val,2*g_val+2*w_Val
RECTNG,2*g_val+w_Val,2*g_val+2*w_Val,g_val+w_Val,l_Val-2*g_val-2*w_Val-(l_Val-
4*g_val-4*w_Val-c)/2
```

```
RECTNG,l_Val-2*g_val-3*w_Val-(l_Val-4*g_val-4*w_Val-c)/2,l_Val-2*g_val-2*w_Val-
(l_Val-4*g_val-4*w_Val-c)/2,l_Val-2*g_val-2*w_Val,l_Val-2*g_val-2*w_Val-(l_Val-4*g_val-
4*w_Val-c)/2
RECTNG,l_Val-2*g_val-2*w_Val,l_Val-2*g_val-2*w_Val-(l_Val-4*g_val-4*w_Val-
c)/2,2*g_val+2*w_Val+(l_Val-4*g_val-4*w_Val-c)/2,2*g_val+3*w_Val+(l_Val-4*g_val-
4*w_Val-c)/2
RECTNG,2*g_val+2*w_Val+(l_Val-4*g_val-4*w_Val-c)/2,2*g_val+3*w_Val+(l_Val-4*g_val-
4*w_Val-c)/2,2*g_val+2*w_Val,2*g_val+2*w_Val+(l_Val-4*g_val-4*w_Val-c)/2
RECTNG,2*g_val+2*w_Val,2*g_val+2*w_Val+(l_Val-4*g_val-4*w_Val-c)/2,l_Val-2*g_val-
3*w_Val-(l_Val-4*g_val-4*w_Val-c)/2,l_Val-2*g_val-2*w_Val-(l_Val-4*g_val-4*w_Val-c)/2
RECTNG,2*g_val+2*w_Val+(l_Val-4*g_val-4*w_Val-c)/2,l_Val-2*g_val-2*w_Val-(l_Val-
4*g_val-4*w_Val-c)/2,2*g_val+2*w_Val+(l_Val-4*g_val-4*w_Val-c)/2,l_Val-2*g_val-
2*w_Val-(l_Val-4*g_val-4*w_Val-c)/2
!    ********************
!    ADDING THE AREAS
!   **********************
AADD,2,6,10
AADD,1,5,9
AADD,4,8,12
AADD,3,7,11

!   *******************************
!    CREATE THE INNER RECTANGLE
!   *******************************
```

```
RECTNG,l_Val/2-400,l_Val/2+400,l_Val/2-400,l_Val/2+400
ASBA,      13,     3
RECTNG,l_Val/2-400,l_Val/2+400,l_Val/2-400,l_Val/2+400
!    ********************
!       GLUE ALL AREAS
!     ********************
FLST,2,6,5,ORDE,3
FITEM,2,1
FITEM,2,-5
FITEM,2,14
AGLUE,P51X
!      ************************
!       EXTRUDE THE MODEL
!      ************************
VOFFST,1,B_Val, ,
VOFFST,2,B_Val , ,
VOFFST,4,B_Val, ,
VOFFST,3,1200+B_Val, ,
VOFFST,6,B_Val, ,
VOFFST,7,B_Val, ,

!        *************************
!       APPLYING DISPLACEMENT
!      ***************************
```

```
FLST,2,4,5,ORDE,4
FITEM,2,47
FITEM,2,27
FITEM,2,37
FITEM,2,16
DA,P51X,ALL,0
!    ************************************
!       APPLYING PRESSURE (Pre=8.979E-5MPa)
!     ************************************
FLST,2,1,5,ORDE,1
FITEM,2,3
SFA,P51X,1,PRES,0.00008979
!   *************************
!       MESH THE MODEL
!     *************************
ALLSEL,ALL
MSHAPE,1,3D
MSHKEY,0
VMESH,ALL
FINISH
!   *************
!     SOLUTION
!   *************
/SOLU
```

```
/STATUS,SOLU
SOLVE
!     **********************
!       REVIEW THE RESULTS
!    ************************
/POST1
 /EFACE,1
 AVPRIN,0,0,
 PLNSOL,U,Z,0,1
 *get,UZ_MAX,PLNSOL,,MAX
 FINISH
!    **********************
!     SAVE THE GRAPHS
!   ************************
/ui,copy,save,jpeg,graph,color,reverse,portrait
 count=count+1
 *CFOPEN,L_Shaped.all.2,out,D:\L_Shaped2,append !
  *VWRITE,count,E_Val,P_Val,l_Val,B_Val,g_Val,w_Val,UZ_MAX
  (F4.0,'   ',F9.0,'  ',F15.5,'  ',F6.0,'  ',F4.0,'  ',F4.0,'  ',F4.0,' ',F15.4,)
  *CFCLOS
!     ******************************
!       CLEAR THE PREVIOUS DATA
!     ******************************
  PARSAV,ALL,Parameters,txt,
```

```
 /CLEAR,NOSTART
 PARRES,NEW,Parameters,txt,
*ENDDO
*ENDDO
*ENDDO
*ENDDO
*ENDDO
```

A2 ANSYS input file for Analysis of the frequency modes

```
/TITLE, FREQUENCY ANALYSIS OF THE FLAT SPRING
 /UNITS, mks
! Objective: To investigate the first desired mode of vibration
!          Initialize variables
!
*DIM,E,Array,4,1,1
E(1,1)=190000,110000,75000,3000   !Young's modulus
*SET,g_val,100              !Gap
*SET,l_val,2600             !Spring length
*SET,w_val,200              !Beam width
*DIM,P,Array,4,1,1          !poisson's ratio
P(1,1)=0.22,0.35,0.31,0.22
*DIM,D,Array,4,1,1
D(1,1)=2.3e-15,8.94e-15,5.3e-15,1.19E-15
*set,EXX,152000
```

```
*DIM,Dx,Array,4,1,1

Dx(1,1)=5.783e-13,5.849e-13,5.813e-13,5.7719E-13


*SET,b_val,10              !Beam thickness

*SET,c,1000                !constant

!    ******************

!    OPEN OUTPUT FILE

!     ********************

*CFOPEN,L-Shaped.Mat.1.1,out,D:\

*VWRITE, LIST

*CFCLOS

count =0

!    *****************

!        DO LOOP

!    *****************

*DO,E_num,1,4,1

E_Val= E(E_Num)

P_val=p(E_Num)

D_val=D(E_Num)

 Dx_val=Dx(E_Num)

  !   ****************************************************

  !     SELECT ELEMENT TYPE AND MATERIAL PROPERTIES

  !   ****************************************************

  /PREP7
```

```
ET,1,SOLID92
KEYOPT,1,5,2
KEYOPT,1,6,0
MPTEMP,,,,,,,,
MPTEMP,1,0
MPDATA,EX,1,,E_val
MPDATA,PRXY,1,,P_val
MPDATA,DENS,1,,D_val
MPDATA,DENS,2,,Dx_val
MPDATA,EX,2,,EXX
!    ************************************
!       CREATE THE FLAT SPRING MODEL
!     ************************************
RECTNG,g_Val,g_Val+w_Val,0,l_Val-2*g_Val-w_Val
RECTNG,0,l_Val-2*g_Val-w_Val,l_Val-g_Val-w_Val,l_Val-g_Val
RECTNG,l_Val-g_Val-w_Val,l_Val-g_Val,l_Val,2*g_Val+w_Val
RECTNG,2*g_Val+w_Val,l_Val,g_Val+w_Val,g_Val
RECTNG,g_Val+w_Val,l_Val/2+w_Val/2,l_Val-2*g_Val-2*w_Val,l_Val-2*g_Val-   w_Val
RECTNG,l_Val-2*g_Val-2*w_Val,l_Val-2*g_Val-w_Val,l_Val/2-w_Val/2,l_Val-g_Val-
w_Val
RECTNG,l_Val-g_Val-w_Val,l_Val/2-w_Val/2,2*g_Val+w_Val,2*g_Val+2*w_Val
RECTNG,2*g_Val+w_Val,2*g_Val+2*w_Val,g_Val+w_Val,l_Val/2+w_Val/2
RECTNG,l_Val/2+w_Val/2,l_Val/2-w_Val/2,l_Val-2*g_Val-2*w_Val,l_Val-2*g_Val-
2*w_Val-(l_val-4*g_val-4*w_val-c)/2
```

```
RECTNG,l_Val-2*g_Val-2*w_Val,l_Val-2*g_Val-2*w_Val-(l_val-4*g_val-4*w_val-
c)/2,l_Val/2+w_Val/2,l_Val/2-w_Val/2
RECTNG,l_Val/2-w_Val/2,l_Val/2+w_Val/2,2*g_Val+2*w_Val,2*g_Val+2*w_Val+(l_val-
4*g_val-4*w_val-c)/2
RECTNG,2*g_Val+2*w_Val,2*g_Val+2*w_Val+(l_val-4*g_val-4*w_val-c)/2,l_Val/2-
w_Val/2,l_Val/2+w_Val/2
RECTNG,2*g_Val+2*w_Val+(l_val-4*g_val-4*w_val-c)/2,l_Val-2*g_Val-2*w_Val-(l_val-
4*g_val-4*w_val-c)/2,2*g_Val+2*w_Val+(l_val-4*g_val-4*w_val-c)/2,l_Val-2*g_Val-
2*w_Val-(l_val-4*g_val-4*w_val-c)/2
!      **********
!        ADDING THE AREAS
!     **********
AADD,2,6,10
AADD,1,5,9
AADD,4,8,12
AADD,3,7,11
!    **********
!      CREATE THE INNER RECTANGLE
!    **********
RECTNG,l_Val/2-400,l_Val/2+400,l_Val/2-400,l_Val/2+400
ASBA,      13,     3
RECTNG,l_Val/2-400,l_Val/2+400,l_Val/2-400,l_Val/2+400
!    **********
!      GLUE ALL AREAS
```

```
!     ******************
FLST,2,6,5,ORDE,3
FITEM,2,1
FITEM,2,-5
FITEM,2,14
AGLUE,P51X
!         ************************
!          EXTRUDE THE MODEL
!         ************************
VOFFST,2,B_Val, ,
VOFFST,1,B_Val, ,
VOFFST,4,B_Val, ,
VOFFST,14,B_Val, ,
VOFFST,3,1200+B_Val, ,
VOFFST,6,B_Val, ,
!         ***************************
!            APPLYING DISPLACEMENT
!         ***************************
FLST,2,4,5,ORDE,4
FITEM,2,16
FITEM,2,27
FITEM,2,37
FITEM,2,42
DA,P51X,ALL,0
```

```
!
!Mesh the model
!
VSEL, , , ,       5
VATT,       2, ,   1,       0
VSEL, , , ,       6
VATT,       2, ,   1,       0
ALLSEL,ALL
MSHAPE,1,3D
MSHKEY,0
VMESH,ALL
FINISH
!   ***************************
!    APPLYING MODAL ANALYSIS
!   ***************************
/SOLU
ANTYPE,2          !Select new analysis
MODOPT,LANB,5     !Analysis Options,  Block Lanczos method
EQSLV,SPAR        !Sparse direct equation solver
MXPAND,5, , ,0    !No. of Modes to Expand
PSTRES,0
MODOPT,LANB,5,0,0, ,OFF, ,2
/STATUS,SOLU
SOLVE
```

```
FINISH
!
!Review The Results
!
/POST1
SET,LIST,2
set,first
PLDISP,0
ANMODE,10,.5E-1
/ui,copy,save,jpeg,graph,color,reverse,portrait
   FINISH
 count=count+1
 *CFOPEN,L-shaped.mat1.1,out,D:\,APPEND!
  *VWRITE,list
    *CFCLOS
!    ******************************
!    CLEAR THE PREVIOUS DATAT
!    ******************************
  PARSAV,ALL,Parameters,txt,
  /CLEAR,NOSTART
  PARRES,NEW,Parameters,txt,
```

A3 ANSYS Input File: Magnetic Analyses

```
/NOPR
```

```
/PMETH,OFF,1
! *****************************************************************
!   MAGNETIC ANALYSIS OF THE ELECTROMAGNETIC MICROGENERATOR
!  *****************************************************************
! objective : is investegate the optimum position of the coil relative to the magnet.
!
KEYW,PR_SET,1
KEYW,PR_ELMAG,1
KEYW,MAGNOD,1
/PREP7
!
!         ****************************
!         CHANGE UNIT TO UMKS UNITS
!         ****************************

EMUNIT,MUZRO,0.125663706144E-23
EMUNIT,EPZRO,0.885399999845E-02
*SET,l_pm, 800
*SET, h_pm, 1200
*SET,x,1300
*SET,y,0
*SET,l_coil1,3000
```

```
*SET,h_coil1,100

*SET,l_coil2,50

*SET,h_coil2,1500

*SET,R_AIR,2*(h_pm+h_coil2)

*SET,R_INFIN,2*R_AIR



 /PREP7

!       ********************************

!         ASSIGN MATERIAL PROPERTIES

!       ********************************

HC=520e6

BR=8000       e-12

MP,MGyy,1,HC        !!!Define pole

MP,MURX,1,1.22

MPTEMP,,,,,,,,

MPTEMP,1,0

MPDATA,MURX,2,,1          !material 2 as air

MPTEMP,,,,,,,,

MPTEMP,1,0

MPDATA,MURX,3,,1          !material 3 as copper
```

```
!       ******************
!       SET ELEMENT TYPE
!       ******************
ET,1,PLANE13
KEYOPT,1,3,1

ET,2,INFIN110
KEYOPT,2,3,1
!       ***************************************************
!       CREATE SURROUNDING AIRGAP & INFINTE BOUNDARY
!       ***************************************************

CYL4,0,-h_pm/2,R_AIR,0,,90
CYL4,0,-h_pm/2,R_AIR,0,,-90
CYL4,0,-h_pm/2,R_INFIN,0,,90
CYL4,0,-h_pm/2,R_INFIN,0,,-90
RECTNG,0,l_pm/2,-y,-h_pm,
RECTNG,l_pm+x,l_pm+x+l_coil2,0,-h_coil2
AOVLAP,ALL
NUMCMP,AREA
aadd,2,3
aadd,4,5
```

```
aadd,7,8

numcmp,area



ASEL, , , ,      1                !select area infinite & assign material 1 and element 2

AATT,      2, ,   2,      0,

ALLSEL,ALL

ASEL, , , ,      4

AATT,      2, ,   2,      0,

ASEL, , , ,      5

AATT,      1, ,   1,      0,       !select pm area and asssign mat. attribute 1

ALLSEL,ALL

ASEL, , , ,      3

AATT,      2, ,   1,      0,       !select air  area and asssign mat. attribute 2

ALLSEL,ALL

ASEL, , , ,      2

AATT,      3, ,   1,      0,       !select coil  area and asssign mat. attribute 3

ALLSEL,ALL

ALLSEL,ALL


!         ********************

!         MESH THE MODEL
```

```
!          ********************

ESIZE,50,0,             !mesh pm and coil
MSHAPE,0,2D
MSHKEY,0
AMESH,2
AMESH,5
ESIZE,200,0,            !mesh air area
MSHAPE,0,2D
MSHKEY,0
AMESh,3
numcmp,line
LSEL,S,LINE,,7          !SELECT LINE OF to mesh one layer
/PREP7
LESIZE,ALL,,,1          !ONE LAYER MESHING
TYPE,2
MSHAPE,0
MSHKEY,1
AMESH,1
AMESH,4
ALLSEL,ALL
/PREP7
```

FLST,2,2,4,ORDE,2

FITEM,2,2

FITEM,2,19

SFL,P51X,INF

/SOL

MAGSOLV,0,3,0.001, ,25,

Appendix B

B1 Fabrication proposal of silicon flat spring

Chapters 4 and 5 discussed the design parameters for a flat spring. This section discusses the fabrication of the silicon flat spring structures. This fabrication method is based on a multiple etching sequence carried out on both front and back surfaces of <100> silicon wafer. A fault in any fabrication stage can lead to an irreversible error that requires restarting the entire process. The important processing techniques for fabricating the flat spring structure are described such as anisotropic etching, etch-stop and photolithographic procedure. The selection of the techniques used in the fabrication process and subsequently the design of the processing sequence are explained. The finalised fabrication flow is proposed.

Fabrication flow design of the flat spring

The fabrication method has been proposed from the early work of Bhansali et.al [Bhansali et.al ,2000]. The following fabrication process differs from that of the Bhansali et.al [Bhansali et.al,

2000] process in that some of the steps in their work is not required for the fabrication of this flat spring. Also the masking layer has been changed to silicon nitride to better suit the anisotropic etching of silicon. The finalised proposed process design for the fabrication of the silicon flat spring is schematically illustrated in Fig.B1.1.

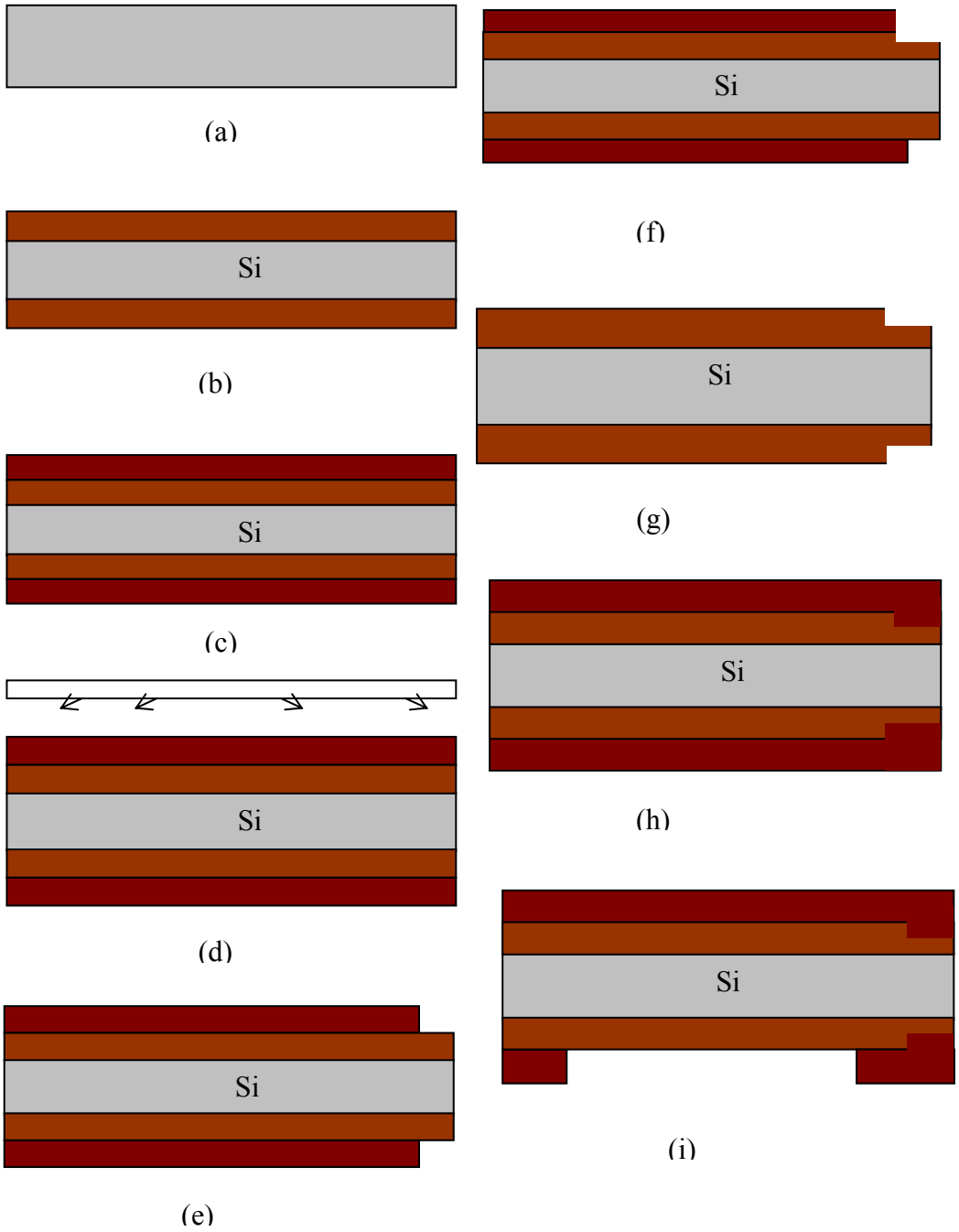

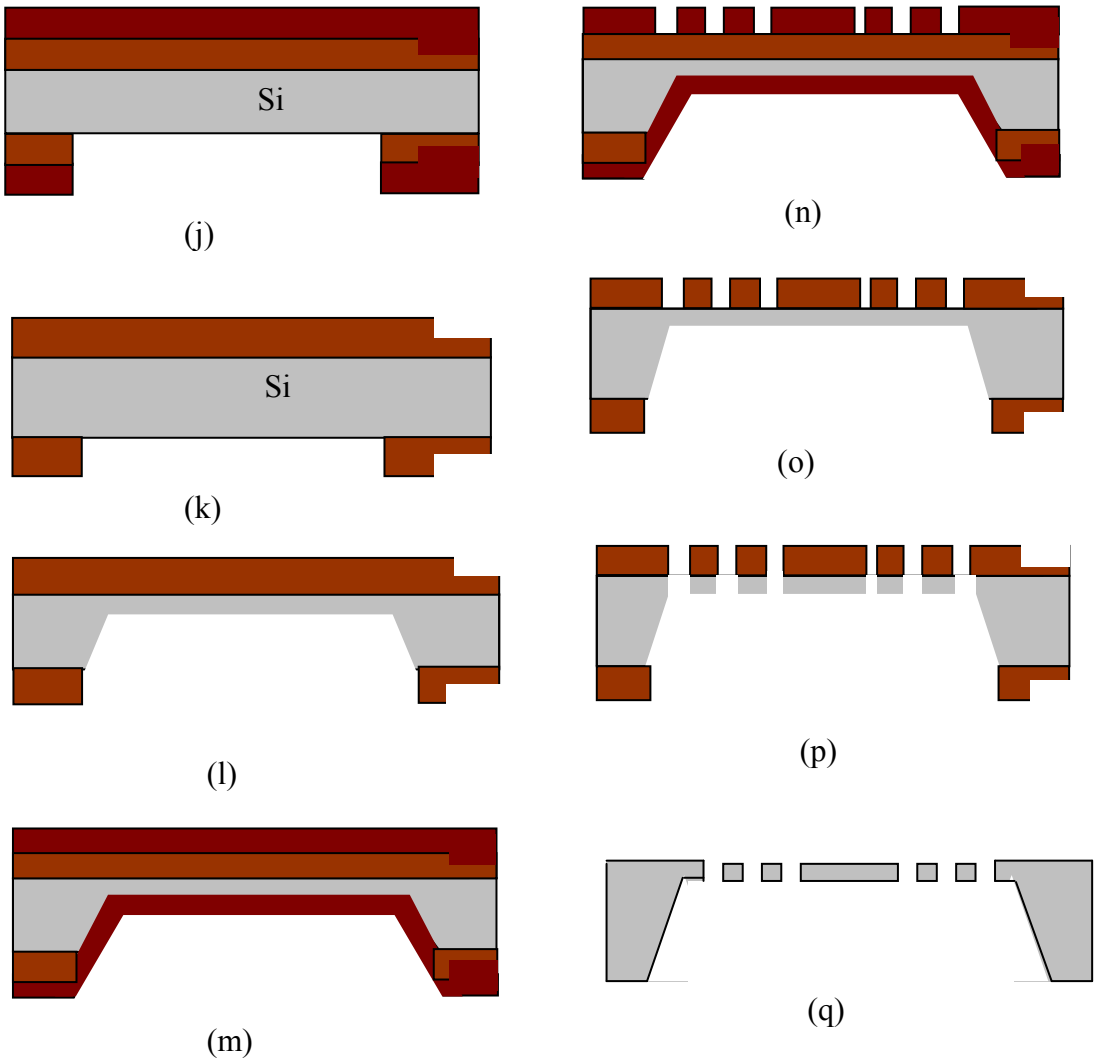

Fig. B1.1 Schematic of the flat spring fabrication process: (a) clean wafer ,(b)oxidize wafer, (c) photoresist coating, (d) UV exposure and registration marks pattering, (e) photoresist developing, (f) isotropic etching, (g) photoresist removing, (h) photoresist coating, (i) pattern backside and UV exposure, (j) develop photoresist, (k) backside oxide etching, (l) backside silicon etching, (m) spin resist, (n) front side UV expose and photoresist developing, (o) front oxide etching and photoresist removing, (p) silicon etching, (q) oxide etching.

Two masks are proposed to be used, the back etching mask is first patterned onto the backside of the wafer to form a thin membrane. Anisotropic wet etching is preformed on the backside and it should be terminated by using time etch stop. Next the front etching mask is patterned on the

front side of the wafer and etched in wet etching. Again a time etch stop terminates the etching process and the flat spring structure is released.

The spring fabrication comprises is proposed to be a four stages for a positive mask: sample preparation, thin-film metal deposition, photoresist patterning, and etching.

Sample Preparation

Double-sided polished 2-inch diameter <100> prime grade silicon wafers is planned to be used for our fabrication process. The thickness of each wafer is measured using a micrometer. The sample cleaning is a vital first stage, which is significant to the final success of the spring fabrication. Any small particle on the substrate will result in a break in spring beams. To obtain reliable adhesion between the thin-film layer silicon nitride (Si_3Ni_4) and the substrate, a thorough cleaning of the bare wafer surface is necessary. The cleaning should be performed in a clean room to avoid dust and small particles. The process is performed under a fume cupboard to allow for safe and fast removal of harmful vapours generated during the process.

The sample cleaning was conducted by an acetone bath in which the surface of the sample was gently rubbing using an extra soft cotton bud. The sample was then rinsed in methanol for 2 minutes followed by deionized water rinsing for 5 minutes. The sample was then dried with high purity nitrogen gas. In order to evaporate the trapped moisture, the sample was heated for half an hour in an oven containing nitrogen gas flow at 80°C.

Thin-Film Deposition

Chemical vapour deposition (CVD) is a versatile technique used to deposit a wide range of materials for microelectronics and MEMS. The process involves a reaction between two introduced gases, leaving the desired film on the substrate and producing other gases as waste

products. For example silicon nitride (Si_3Ni_4) can be formed as a result of a reaction between dichlorosilane (SiH_2Cl_2) and ammonia (NH_3).

A LPCVD is carried out to grow 0.2 μm thick silicon nitride layer on both surfaces of the cleaned wafers. Baking at 140 ^{o} C for one hour to eliminate any moisture in the nitride layer.

Many CVD films have large tensile stresses, which is a problem for some applications. Careful choice of deposition, conditions can reduce film stress. for this reason most CVD is performed under low pressure conditions (LPCVD). In applications where metal layers are already deposited the deposition must be performed at lower temperatures. This is possible with plasma enhanced CVD (PECVD).

Photolithography and chemical etching

The photolithography procedure was conducted in a class 1000 clean room environment. For the etching process, positive resist was employed. Positive resist is described as a material which in exposure to light breaks the polymer bonds so that the exposed resist can be removed by a solvent. After photolithography, the polymer layer stays on the regions which covered with the positive mask and were not exposed to light. The polymer layer protects the silicon nitride (Si_3Ni_4) underneath to be etched away in the etching stage.

To deposit the photoresist layer the spin coating method was employed. In this process, first hexamethyl disilazane (HMDS) was spun onto the wafer at 3000 rpm for 40 seconds to improve the photoresist adherence onto the wafer. Afterwards, AZ-1500 positive photoresist was spun at 3000 rpm for 30 seconds. This rotation speed provided a photoresist layer of approximately 1.15 μm thickness. The sample was then baked in an oven at 90°C for 20 minutes. A contact mask aligner (Karl Suss MJB-3) was employed to align and expose the photoresist-coated wafer. After the alignment of the wafer, an ultra-violet exposure of 10 seconds

was conducted. The exposed wafer was subsequently developed in a mixture of AZ-400 developer and D.I.-water (1:4) for 18 seconds. HMDS adhesion promoter is applied to the wafer surface to improve the sticking of the photo resist. HMDS is spun on the both sides of the wafer for 60 sec at speed of 4000 rpm and baked for 1 min at 90^{o} C for both sides. A positive photoresist AZ1512 is used in the photolithography. AZ 1512 is thin and positive photoresist. It gives better contact between the wafer and the glass mask. The resist is spun on the front side for 30 sec. at a speed of 3000 rpm and acceleration of 500 rpm/ sec, and soft baked for half of the recommended time (10 minutes). Soft bake is used to improve adhesion and remove solvent from the photo resist. Then the resist is spun on the back side. Extra care must be taken to avoid scratching the resist coatings on front surface. A normal soft bake step is carried out at 90°C for 20 minutes to complete this step.

The wafer with resist coatings on both surfaces is sandwiched in the mechanical jig for the front to back side aligned photolithographic procedure (chapter 7 will presents more details about the mechanical jig). The wafer is then exposed under UV light on both sides and developed using AZ 400 developer. A soft bake step at 90°C for 20 minutes is then preformed.

An Si_3Ni_4 etching is carried out in a buffered HF solution to transfer the alignment marks in to the masking layer. The AZ 1512 resist coating is removed using acetone.

Hard bake of the wafer is carried out at 140°C for one and half hours to get rid of the moisture in the Si_3Ni_4 masking layers. Then we apply the resist on the wafer surfaces. The alignment marks are clearly visible through the resist coatings under the microscope on the mask aligner.

The back side of the wafer is patterned on the mask aligner with registration marks on the photo mask being accurately aligned with the alignment marks on the wafer surface. Prior to its development the resist coating on the front surface is visually inspected to make sure it is free

from defects. The development and post bake steps are carried out the same way as described earlier.

The mask pattern is transferred in to the etching mask layer using a buffered HF etching step, and the resist is removed using acetone.

Anisotropic etching is carried out in 45 wt.% KOH at 60ºC to form cavities on the backside of the wafer. The timed etch stop is used to terminate the etching process and produce a grid of 30μm thick silicon membranes. The etched wafer is then rinsed in DI water and oven dried at 140°C for one and half hours.

A handling wafer is secured onto the back side of the processed wafer using foil tape so as to protect the thin membranes from being damaged by the vacuum chuck of the spinner. AZ 1512 is then spun on the front side. After the wafer is prebaked at 75°C for 10 minutes, the handling wafer is removed, and AZ 1512 photoresist is manually applied on the back side using a cotton bud. The wafer then baked at 75°C for 20 minutes.

The beam structure is patterned on the front side of the wafer. The alignment procedure is the same as in the early work. The contact mechanism of the mask aligner is adjusted to allow for extra thickness of the resist coating on the back side. The development and post bake steps are then carried out.

The etching of the Si_3Ni_4 masking layer on the front surface is carried out using buffered HF. However, the etching time is much shorter than the previous two, because the Si_3Ni_4 is etched during the back etching process. The resist coatings are removed using Acetone.The wafer is etched in 45 wt. % KOH at 60°C from the openings on both sides of the wafer. Continuous observation is required to monitor the etching process which is terminated as soon as the beam structures are released.

The wafer is treated with HF dip to remove the remaining nitride films on the surfaces, and is carefully rinsed in DI water. Finally, the wafer with released flat spring structures is oven-dried at 90°C .

B2 Etching mask design

For fabricating silicon flat spring structure, the convex corner undercutting needs to be corrected by incorporating compensation patterns in the etching mask designs. The front to backside aligned lithography technique is presented which is of importance for pattering the etching masks of the flat spring structures. The operating procedure of double sided lithography is discussed. The possible sources which can cause alignment errors are also analysed.

Design rules of the etching mask

This section presents designing a photolithographic mask by considering the Si micromachining aspects. The fabrication of the flat spring requires a set of two photomasks for defining the etching patterns on the front and back surfaces of the wafer. Apart from the structure patterns, each photo mask must also contain two registration marks for the corresponding alignment marks on the wafer. According to the finalised processing flow, the back etching mask is first used to form thin membranes then, with the assistance of the front to back aligned photolithographic procedure, the front etching mask patterns the beam structures on the front side of the wafer. The design parameters are concerned with the processing techniques and conditions such as etchant concentrations, temperatures and etching depth. With respect to each etching mask, the final geometrical shape and size of the structure is dependent upon the anisotropic etching behaviour of the etching system used for the actual fabrication.

Back etching mask

As shown in Fig.7.1 the back etching forms a cavity on the back side of the wafer. The bottom of the cavity creates a thin silicon membrane on the front surface which is subsequently etched through from the front side to cut out the flat spring structures. The photomask for the back etching process therefore form the thin membrane. Since the side walls of the cavity are always <111> planes, the angle between the side walls and the wafer surface is 54.74º [Madou, 1997]. Thus, the relationship between the dimensions of the photomask and that the membrane on the front surface, which is given by

$$W_m = W_o + \sqrt{2}d \quad \text{(B2.1)}$$

Where the W_m, is the dimension of the window opening in the etching mask, W_o is the dimension of the frame and d is the required etching depth.

As shown in equation (B2.1), the etching depth is the only design parameter for the photomask if the dimensions of the final flat spring are chosen. Moreover, when the conditions of the etching process are decided, the design of the corner compensation is also determined by the etching depth.

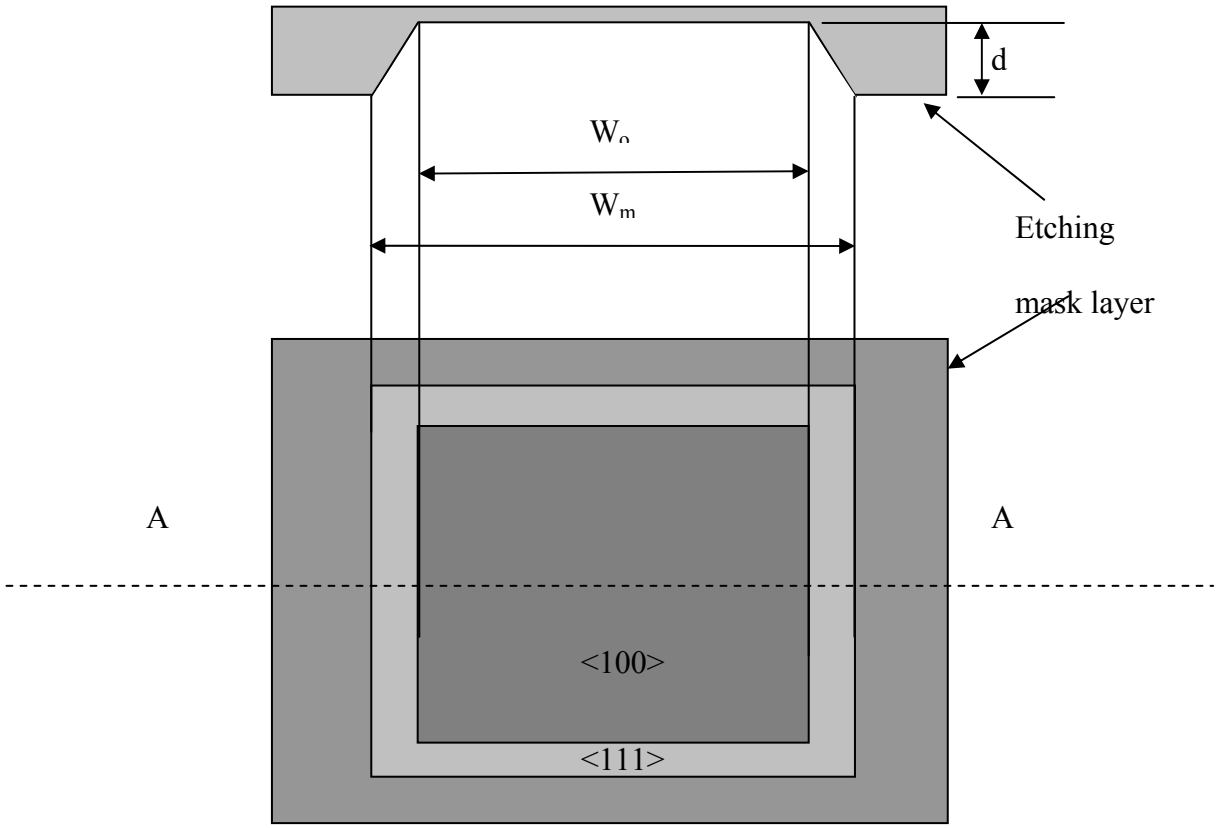

Fig.B2.1 The back etching mask design

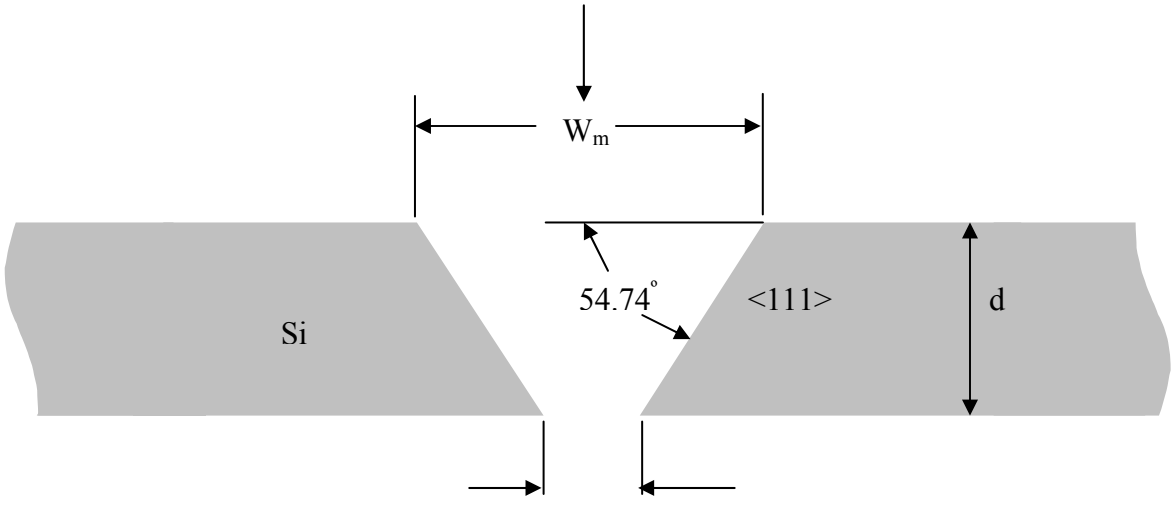

Fig.B2.2 Relation of bottom cavity plane width with mask opening width [Madou,1997]

Front etching mask

The front etching mask defines the pattern of the flat spring structures on the membrane area. The critical design rule for the front etching mask is given by

$$W_{\min} > \sqrt{2}h \quad \text{..... (B2.2)}$$

Where W_{min} is the minimum width of the gaps between the beam patterns on the photomask, and h is the thickness of the final flat spring structures. If this design rule is not observed, V-grooves will be formed in the gaps which will prevent the etching fronts proceeding to the desired depth. As a result, the flat spring structures cannot be released with the thickness of *h.* since the membrane thickness in our design is 30μm, the width of the gaps has to be greater than 42 μm.

Mask designs with corner compensation structures

The flat spring with the four different beam configurations, discussed in chapter 4, were patterned for the front etching mask. In all of those designs the width of the gaps between the beams was 60 μm, therefore the design rule of equation (B2.2) was satisfied. In order to simplify the process of attaching a permanent magnet onto the top of the silicon mass, 1.0mmx 1.0mm channel was designed to be etched in the centre of the platform in the front etching process. The depth of the channel would be the same as the thickness of the beams. Fig.B2.3 shows the designs of the front etching masks which consists of four beam configurations. The back etching mask was designed according to the dimensions of the front etching mask and the required etching depth obeying the design rules of equation (B2.1). Fig. B2.4, shows the transferring of the front etching mask features from the paper mask to the photoemulsion glass mask.

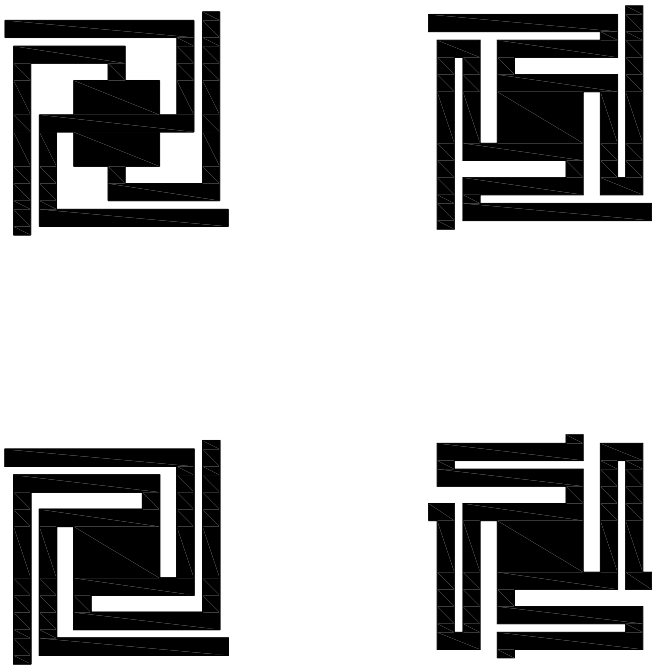

Fig. B2.3 Four springs with different beam configuration

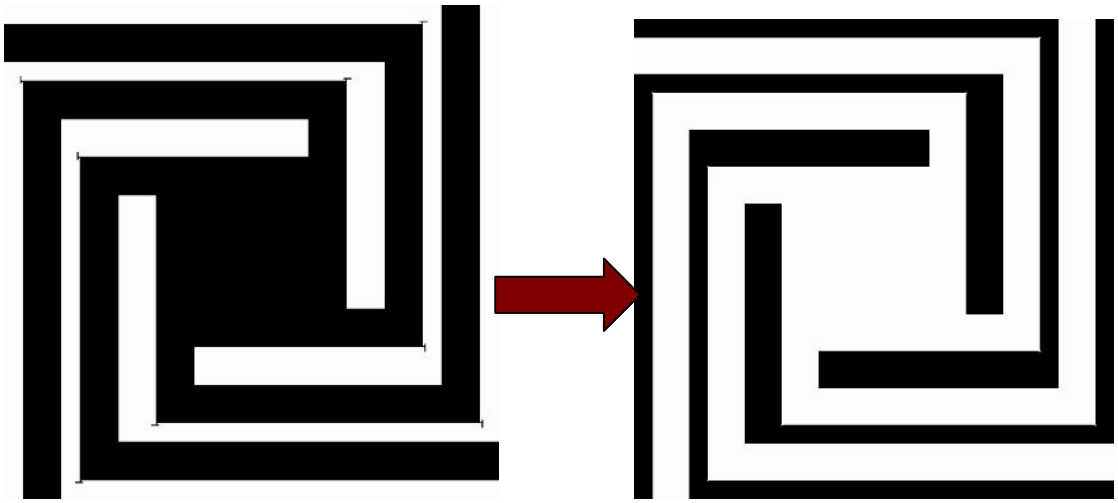

a) b)

Fig. B2.4 Etching mask a) paper mask b) photoemulsion glass mask

Mask layout

The final mask layout is shown in Fig.B2.5 the overall dimension of the layout was chosen to be 40mmx 40mm since the diameter of silicon wafers was 2 inch (=50mm). A set of registration marks was included in the layout for the front to backside aligned lithography. Since the alignment marks occupied two 5mm wide perpendicular tracks from the edge of the wafer, the mask patterns were arranged in 6x6 grids with a stepping distance of 5mm.

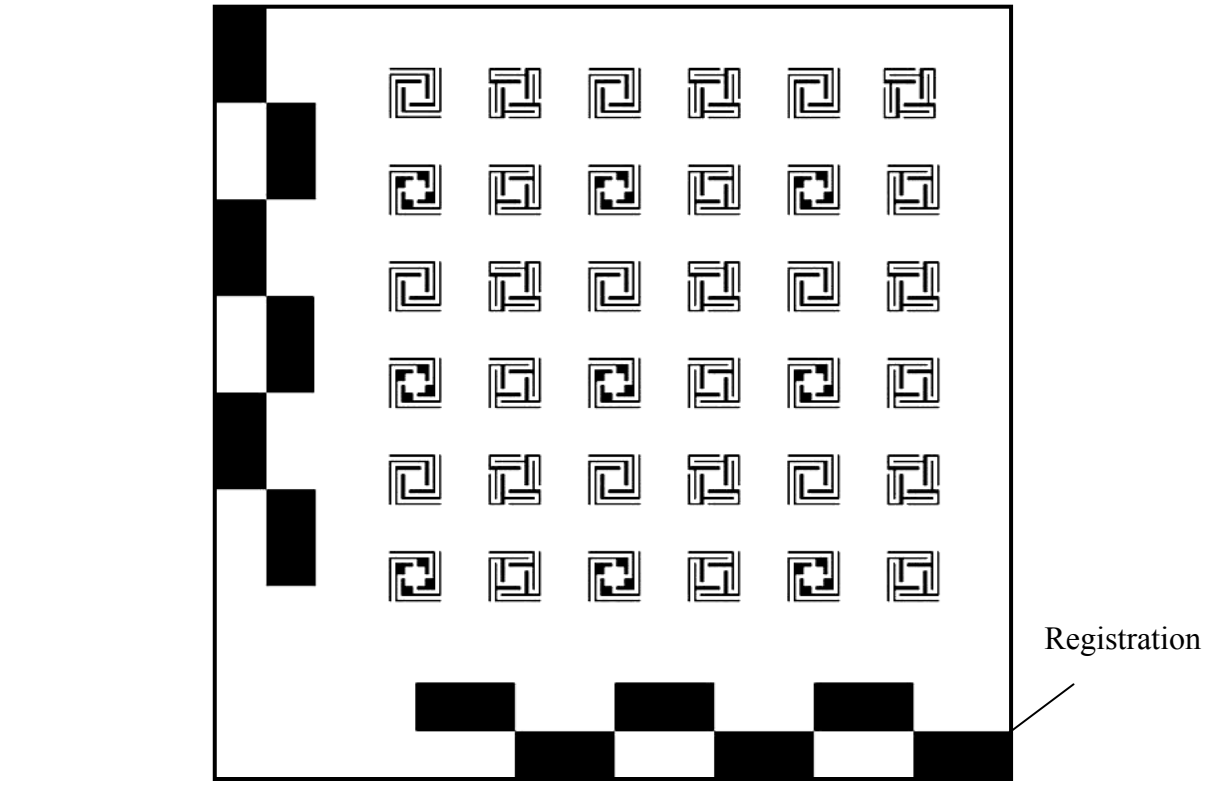

a)

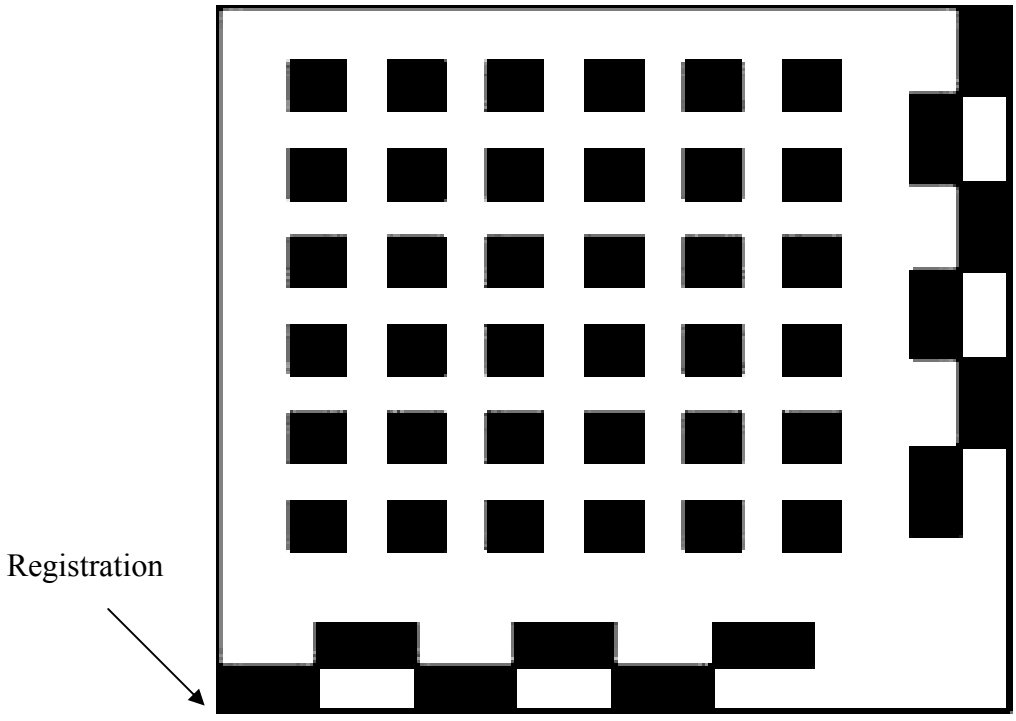

b)

Fig.B2.5 the negative mask layout for the a) front and b) back etching processes.(imported from AutoCAD)

Photolithographic Mask

The photolithographic masks for the flat spring were designed for a 3×3 inch photo emulsion glass plate. The designs were implemented using a computer aided design (CAD)system(AutoCAD).The design of files exported as standard Encapsulated Post script file format. The mask is ready now to be transferred to the film mask by using the step and repeat camera and the developing machine. As shown in Fig.B2.6, the emulsion glass plate should be over the film mask with the emulsion side face down and in contact with the emulsion side of the film. To transfer the mask patterns from the film to the emulsion layer the glass mask.

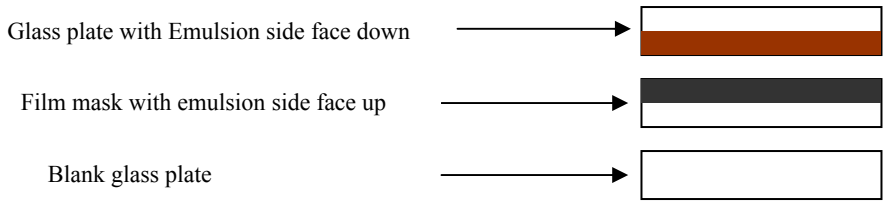

Fig.B2. 6 transferring of the spring patterns from the film to the glass mask.

The emulsion plate is now ready to be developed by the Developer, Fixer and Cleaner solutions. Table B2.1 shows the four solutions with their ratio and time that are suitable to develop the glass mask.

Table B2.1 developing solutions

Solutions	Ratio	Time(min)
Developer	1 to 4 water	4
Fixture	1 to 4 water	3-5
Cleaner	8 to 1 water	1
Water	Full the baker	1

Bibliography

1. (Amirtharajah and Chandrakasan,1998) Amirtharajah R. and Chandrakasan A.P., Self-powered signal processing using vibration-based power generation. Solid-State Circuits, IEEE Journal of, 1998. 33(5): p. 687-695.
2. (Amirtharajah et.al.,2000) Amirtharajah R.,Meninger S.,Mur-Miranda J.O.,Chandrakasan A.,Lang J., Micro power programmable DSP powered using a MEMS-based Vibration-to-Electricity Energy converter. In IEEE International Solid State Circuits Conference. 2000:p.362-363.
3. (Amirtharajah,1999) Amirtharajah R., Design of low Power VLSI Systems Powered by Ambient Mechanical Vibration. PhD thesis, June, 1999, Massachusetts Institute of technology, Department of Electrical Engineering.
4. (Arnold,2003) Arnold, Soft Magnetics Application Guide-Basics of Magnetics. The magnetic product group of SPS technologies, 2003: p. www.arnold.com.
5. (Awaja et.al.,2005) Awaja N., Sood D. K. , Vinay T., Modeling and simulation of a flat spring for use in an electromagnetic microgenerator, Smart Structures, Devices, and Systems II, Proceedings of SPIE ,2005. 5649 , p.361-372 .
6. (Beeby et.al.,2005) Beeby S. P., Tudor M. J., Koukharenko E., White N. M.,O'Donnell T., Saha C., Kulkarni S. and Roy S., Micromachined silicon generator for harvesting power from vibration. in Proc. Transducers 2005. (Seoul, Korea).
7. (Bhansali et.al.,2000) Bhansali S., Zhang A.L. , Zmood, R.B., Jones P.E., and Sood D.K., Prototype feedback-controlled bidirectional actuation system for MEMS applications. Microelectromechanical Systems, Journal of, 2000. 9(2): p. 245-251.

8. (Bhushan and Agrawal,2003) Bhushan B. and Agrawal G.B., Finite element analysis of nanostructures with roughness and scratches. Ultramicroscopy, 2003. 97(1-4): p. 495-507.

9. (Blevins ,1979)Blevins R. D. , Formulas for natural frequency and mode shape, New York : Van Nostrand Reinhold Co.,1979.

10. (Bryzek et.al.,1994) Bryzek J.,Petersen K.,and McCulley W., Micromachines on the march. IEEE Spectrum, 1994(May): p. 20-31.

11. (Burrer et.al.,1993) Burrer Chr.,Esteve J.,Plaza J.A.,Bao M.,Ruiz O., and Samitier J.,Fabrication and characterization of twin-mass accelerometer. in the 7th International Conference on Solid-state Sensors and Actuators. 1993. Yokohama,Japan.

12. (Castano et.al.,1997) Castano E.,Revuelto E.,Martin M. C.,Garcia-Alonso A., and Gracia F. J., Metallic thin-film thermocouple for thermoelectric microgenerators. Sensors and Actuators A: Physical, 1997. 60(1-3): p. 65-67.

13. (Ching et.al.,2002) Ching N. N. H., Wong H.Y., Li W. J., Leong P.H.W., and Wen Z., A laser-micromachined multi-modal resonating power transducer for wireless sensing systems. Sensors and Actuators, 2002. A 3327: p. 1-6.

14. (El-hami et.al.,2001) El-hami M., Glynne-Jones P., White N.M., Hill M., Beeby S.P., James E., Brown A.D. , and Ross J.N., Design and fabrication of a new vibration-based electromechanical power generator. Sensors and Actuators A, 2001. 92: p.335-342.

15. (Furlani,2001) Furlani E. P., Permanent Magnet and Electromechanical Devices: Materials, Analysis, and Applications. 2001, San Diego: California Academic.

16. (Gendron,1997) Gendron G., A review of four PC packages for FE structural analysis. Finite elements in analysis and design, 1997. 28: p. 105-114.

17. (Glynne-jones et.al.,2001) Glynne-jones P., Beeby S.P., and White N.M., Towards a piezoelectric vibration-powered microgenerator. IEE proceedings, 2001. 148.

18. (Glynne-Jones et.al., 2004) Glynne-Jones P., Tudor M.J. , Beeby S.P., White N.M., An electromagnetic, vibration-powered generator for intelligent sensor systems, Sensors and Actuators A , 2004 ,110 , p. 344–349.

19. (Grant et.al.,2001) Grant S.C., Murphy L.A.,Magin R.L., and Friedman G., Analysis of multilayer radio frequency microcoils for nuclear magnetic resonance spectroscopy. Magnetics, IEEE Transactions on, 2001. 37(4): p. 2989-2998.

20. (Hayakawa,1991) Hayakawa M., Electronic Wristwatch with Generator. 1991: US patent.

21. (Holmes et.al.,2005) Holmes A.S., Hong G., and Pullen K.R., Axial-flux permanent magnet machines for micropower generation. Microelectromechanical Systems, Journal of, 2005. 14(1): p. 54-62.

22. (Huang et.al.,2003) Huang W. S., Tzeng K .E., Cheng M. C. and Huang R. S., Design and fabrication of a vibrational micro-generator for wearable MEMS. in Proc. Eurosensors XVII. 2003. (Guimaraes,Portugal).

23. (Huang et.al.,2007) Huang W. S., Tzeng K .E., Cheng M. C. and Huang R. S., A silicon MEMS micropower generator for wearable micro devices., Journal of the Chinese Institute of Engineers, 2007, 30(1), p. 133-140.

24. (Jacquot et.al.,2002) Jacquot A., Liu W.L., Chen G., Fleurial J.P., Dauscher A., and Lenoir B., Improvements of on-membrane method for thin-film thermal conductivity

and emissivity measurements. Twenty-First International Conferences in Thermoelectrics, 2002. Proceedings ICT '02.p. 353-356.

25. (Koukharenk et.al., 2006) Koukharenko E. , Beeby S. P. , Tudor M. J.,White N. M. ,O'Donnell T. , Saha C., Kulkarni S. , Roy S.,Microelectromechanical systems vibration powered electromagnetic generator for wireless sensor applications, Microsyst Technol , 2006, 12,p.1071–1077.

26. (Kruusing,2002) Kruusing A., Actuators with permanent magnets having variable in space orientation of magnetization. Sensors and Actuators, A: Physical, 2002. 101(1-2): p. 168-174.

27. (Kulah and Najafi,2004) Kulah H., and Najafi K., An electromagnetic micro power generator for low-frequency enviromental vibrations. in Micro Electro Mechanical Systems-17th IEEE conf on MEMS. 2004.

28. (Kulkarni et.al.,2006) Kulkarni S., Roy S., and O'Donnell T.,Vibration based electromagnetic micropower generator on silicon. journal of applied physics, 2006. 99(511).

29. (Kulkarni et.al., 2008) Kulkarni S., Koukharenko E., Torah R., Tudor J., Beeby S., O'Donnell T., Roy S., Design, fabrication and test of integrated micro-scale vibration-based electromagnetic generator, Sensors and Actuators A , 2008, 145–146 , p.336–342.

30. (Lee and White, 1995) Lee, S.S., and White, R.M., Self-excited Piezoelectric Cantilever Oscillators. Proc. Transducers 95/Eurosensors IX, 1995, p. 41 – 45.

31. (Lee, 2001) Lee S. H., Development of high-efficiency silicon solar cells for commercialization. Journal of the Korean Physical Society, Aug. 2001. 39(2): p.369-73.

32. (Li et.al.,2003)Li J.F., Tanaka S., Umeki T.,Sugimoto S., Esashi M., and Watanabe R., Microfabrication of thermoelectric materials by silicon molding process. Sensors and Actuators A: Physical, 2003. 108(1-3): p. 97-102.

33. (Li et.al.,2000) Li W.J., Wen Z., Wong P. K., Chan, G.M.H and Leong P.H.W., A micromachined vibration-induced power generator for low power sensors of robotic system. in World Automation Congress:8th International Symposium on Robotics with Applications. 2000. Hawaii.

34. (Madou,1997) Madou, M., Fundamentals of Microfabrication. 1997: CRC Press.

35. (Meninger et.al.,2001) Meninger S., Mur-Miranda j.O., Amirtharajah R., Chandrakasan A. P., and Lang J.H.,Vibration-to-Electric Energy Conversion. IEEE Trans.VLSI Syst, 2001. 9: p. 64-76.

36. (Merlos et.al.,1992) Merlos A., Acero M., Bao M.H., Bausells J. , and Esteve J. , A study of the undercutting characteristics in TMAH/IPA system. j.Micromechining and Microengineering, 1992. 2: p. 181-183.

37. (Middelhoek and Audet, 1989) Middelhoek S. and Audet S., Silicon sensors. Academic press. 1989, London.

38. (Mizuno and Chetwynd, 2003) Mizuno M., and Chetwynd D., Investigation of a resonance microgenerator. Journal of Micromechanics and Microengineering, 2003. 13: p. 209-216.

39. (Moaveni , 1999) Moaveni, S., Finite element analysis : theory and application with ANSYS. 1999: Upper Saddle River, N.J. : Prentice Hall.

40. (Moskowitz, 1995)Moskowitz L.R. ,Permanent magnet design and application handbook, 1995, 2nd ed. Malabar, Fla. : Krieger.

41. (Neagu et.al.,1996) Neagu C.R., Jansen H.V., Smith A., Gardeniers J.G.E., and Elwenspoek M.C., Characterization of a planar microcoil for implantable microsystems. in EUROSENSORS X, 8-11 Sept. 1996.

42. (Ottman et. al., 2002) Ottman G. K., Hofmann H. F., Bhatt A. C., Lesieutre G. A. 2002. Adaptive piezoelectric energy harvesting circuit for wireless remote power supply. IEEE Transactions on Power Electronics, vol.17, no.5, 2002, pp.669-76.

43. (Ottman et.al.,2003) Ottman G.K., Hofmann H.F., and Lesieutre G.A., Optimized piezoelectric energy harvesting circuit using step-down converter in discontinuous conduction mode. in IEEE Transactions on power Electronics. 2003.

44. (P´erez-Rodr´ et.al.,2005) P´erez-Rodr´ A., Serre C., Fondevilla N., Cereceda C.,Morante J. R., Esteve J. and Montserrat J., Design of electromagnetic inertial generators for energy scavenging applications. in Proc. Eurosensors XIX. 2005. (Barcelona, Spain).

45. (Pan et.al.,2006) Pan C.T., Hwang Y.M., Hu H.L., Liu H.C., Fabrication and analysis of a magnetic self-power microgenerator, Journal of Magnetism and Magnetic Materials, 2006, 304, p. 394–396.

46. (Park et.al.,2002) Park S., Lee K., Cho J., and Lee S., Electromagnetic vibration transducer using polyimide elastic body for implantable middle ear hearing aid. Sensors and Actuators A, 2002. 97-98: p. 201-207.

47. (Petersen,1982) Petersen K.E. Silicon as a mechanical Material. in Proc.IEEE. 1982.

48. (Pures and Lapadatu,1994) Pures B. and Lapadatu D., Extremely miniaturized capacitive movement sensors using new suspension systems. Sensors and Actuators A, 1994. 41-42: p. 129-135.

49. (Roundy et.al.,2003) Roundy S., Wright P.K., and Rabaey J., A study of low level vibrations as a power source for wireless sensor nodes. Computer Communications, 2003. 26: p. 1131-1144.

50. (Roylance and Angell,1979) Roylance L.M. and Angell J.B., A batch-fabricated silicon accelerometer. IEEE Trans. Electron Devices, 1979. ED-26(12): p. 1911-1917.

51. (Saha et.al., 2008)Saha C.R., O'Donnell T., Wang N., McCloskey P., Electromagnetic generator for harvesting energy from human motion, Sensors and Actuators A ,2008, 147, p.248–253.

52. (Sari et.al.,2008) Sari I., Balkan T., Kulah H., An electromagnetic micro power generator for wideband environmental vibrations, Sensors and Actuators A ,2008,145–146, p.405–413.

53. (Serre et.al., 2008) Serre C., Pe´rez-Rodrı´guez A., Fondevilla N., Martincic E., Martı´nez S., Morante J., Montserrat J., Esteve J.,Design and implementation of mechanical resonators for optimized inertial electromagnetic microgenerators, Microsyst Technol , 2008, 14,p.653–658.

54. (Scherrer et.al.,2005) Scherrer S., Plumlee D. G. and Moll A. J., Energy scavenging device in LTCC materials. in IEEE Workshop on Microelectronics and Electron Devices,. 2005. WMED '05.

55. (Seidemann et.al.,2002) Seidemann V., Butefisch S., and Bttgenbach S., fabrication and investigation of in plane compliant SU-8 structures for MEMS and their application to micro valves and micro grippers. Sensors and Actuators, 2002. A: p. 457-461.

56. (Shearwood et.al.,1995) Shearwood C., Pate M.A., Affane W., Whitehouse C.R., Woodhead J., and Gibbs M.R.J., Electrostatic and magnetoelastic microactuation of Si3N4 bridges. in Tech.Digest transducer'95. 1995. Stockholm,Sweden.

57. (Shearwood and Yates,1997) Shearwood C. and Yates R.B. , Development of an electromagnetic microgenerator. Electronics Letters, 1997. 33(22): p. 1883-1884.

58. (Shenck and Paradiso,2001) Shenck N.S., and Paradiso J.A., Energy scavenging with shoe-mounted piezoelectrics. IEEE micro, 2001. 21: p. 30-41.

59. (Starner,1996) Starner T., Human-powered wearable computing. IBM Systems Journal, 1996. 35 (3): 618-629.

60. (Strnat,1970) Strnat K.J., the recent development of permanent magnet materials containing rare earth metals. IEEE Transaction on magnetics, 1970. 6: p. 182-190.

61. (Strnat,1987) Strnat K.J., Permanent magnets based on 4f-3d compounds. IEEE Transaction on magnetics, 1987. 23: p. 2094-2099.

62. (Stordeur and Stark,1997) Stordeur M., and Stark I., Low Power Thermoelectric Generator – self-sufficient energy supply for micro systems. 16th International Conference on Thermoelectrics, 1997: p. 575 – 577.

63. (Thomson, 1972), Thomson W.T., Theory of vibration with applications, Prentice-Hall, Englewood Cliffs, 1972.

64. (Timoshenko ,1940) Timoshenko S., Strength of materials, New York : Van Nostrand, 1940, 2nd ed.

65. (Tschan and Rooij,1991) Tschan, T. and Rooij N.D., Characterisation and modelling of silicon piezoresistive accelerometers fabricated by a bipolar-compatible process. Sensors and Actuators A, 1991. 25-27: p. 605-609.

66. (Umeda et.al.,1997) Umeda M., Nakamura K., Ueha S., Energy storage characteristics of a piezo-generator using impact induced vibration. Jpn.J. Applied Physics, 1997. 36: p.3146-3151.

67. (Verardi et. al. ,1997) Verardi P, Craciun F, Dinescu M. , Characterization of PZT thin film transducers obtained by pulsed laser deposition., IEEE Ultrasonics Symposium Proceedings. 1997,1, p.569-72.

68. (Vujanic et.al., 2000) Vujanic A., Adamovic N., Jakovljevic M., Berenner W., Popovic G., and Detter H., Silicon microstructure for precise measurements of mechanical moments. Microelectronics Journal, 2000. 31:p.975-980.

69. (Wagner and Benecke, 1991)Wagner A. and Benecke W., Microfabricated actuator with moving permanent magnet. in IEEE Micro Electro Mechanical Systems'91. 1991: p. P.27-32.

70. (Wang et.al., 2007) Wang P.H, Dai X.H., Fang D.M., and Zhao X.L., Design, fabrication and performance of new vibration-based electromagnetic micro power generator. Microelectronics Journal, 2007. 38: p. 1175-1180.

71. (Williams et.al., 2001) Williams C.B. , Shearwood C., Harradine M. A., Mellor P. H. , Birch T. S., and Yates R. B., Development of an electromagnetic micro-generator. IEE Proc. - Circuits Devices Syst., 2001: p. 337-342.

72. (Williams and Yates, 1995) Williams C.B., and Yates R.B, Analysis of a micro-electric generator for Microsystems. Transducers 95/Eurosensors IX, 1995: p. 369 – 372.

73. (Williams and Yates, 1996) Williams C.B. and Yates R.B, Analysis of a micro-electric generator for microsystems. Sensors and Actuators A: Physical, 1996. 52(1-3): p. 8-11.

74. (Wilson, 1948) Wilson W., The calculation and design of electrical apparatus. 1948: Chapman and Hall LTD.

75. (Zhang, 1997) Zhang L., Silicon micromechanical structures for one degree of freedom suspension, 1997. PhD thesis.